A BOND GRAPH MODEL FOR SIMULATING THE PERFORMANCE OF A FARM TRACTOR

By

Pascal Gitari Kaumbutho

A DISSERTATION

Submitted to
Michigan State University
in partial fulfillment of the requirements
for the degree of

DOCTOR OF PHILOSOPHY

in

Agricultural Engineering

Department of Agricultural Engineering

1987

ABSTRACT

A BOND GRAPH MODEL FOR SIMULATING THE PERFORMANCE OF A FARM TRACTOR

By

Pascal Gitari Kaumbutho

Bond graph models were developed for the simulation of rigid body chassis and drive train motions for a two wheel drive agricultural tractor. Motions of the tractor were constrained to the lateral and longitudinal planes allowing for translatory travel only in the forward direction. The drive train and chassis models were combined as traction and drawbar submodels were incorporated. The resulting integrated model was processed in ENPORT a bond graph and block diagram processor for nonlinear systems. The model was validated by simulating the lugging ability tests for the IH1086 tractor (Test 1247 of Nebraska Tractor Tests Laboratory). The model was demonstrated by simulating a moldboard plowing field-operation. Performance results were compared between radial and bias ply tires, ballasted and non-ballasted operation, and single and dual drive-wheels. The simulation model easily allowed for modifications as would be required by its user to accommodate changes due to

new technologies, or design modifications in the physical system. Terrain variations were accommodated in the model development. Mean power and energy dissipated, transferred or exchanged, could be observed at any point in the model. In its present form the model is an excellent tool for studies of the effects of system component modifications and for sensitivity analysis of the modifications.

Approved: Thomas H Burkhardt

Major Professor

Approved: Donald M Edwards

Department Chairman

To my parents:

Caroline and Felix Kaumbutho

ACKNOWLEDGEMENTS

I would like to express my sincere gratitude to the following:

* Dr. Thomas H. Burkhardt my major professor for his personal and professional guidance, understanding and indebted support throughout the duration of my program.

* My Guidance Committee, Dr. Earl A. Erickson (Professor, Crop and Soil Science), Dr. John B. Gerrish (Associate Professor, Agricultural Engineering), Dr. Ronald C. Rosenberg (Professor, Mechanical Engineering) and Dr. Ajit K. Srivastava (Associate Professor, Agricultural Engineering) for their time, professional counsel and unsurpassed contribution to my professional growth.

* Dr. Ronald C. Rosenberg for creating ENPORT; his assistant Guy Allen and graduate students, Tong Zhou and Zbig Zalewski for their valuable assistance.

* The Netherlands Embassy through the University of Nairobi, Agricultural Engineering-Staff Development Program for their financial support during the duration of my program.

* Suzanne Nesmith for editing and Sun-Young Ahn for typing the manuscript.

* Dr. Kenneth Ebert of the International Students and Scholars Office for his friendship and incomparable sincere support.

* My family and relatives for their love, support and patience during my stay away from home.

* My many friends, with whom I have been gifted; for their love and confidence in me. Special thanks go to Misheck M. Ikirima, Luke Myers, Sera Kariuki, Guegbeh Peal, Yunus Rubanza, Eileen Wilson, Mevin Ndarusigiye and Vincent Chiuswa for adding seasoning-flavor into my everyday life experiences.

TABLE OF CONTENTS

LIST OF TABLES

LIST OF FIGURES

1. INTRODUCTION

The trend toward larger and more productive agricultural tractors will continue to require more studies of the tractor-implement system energy utilization. A tractor's engine and transmission function as a team and the strength of one can offset a shortcoming of the other. A minor deficiency in using the transmission to select a suitable ground speed may receive few complaints when used with an engine having superior torque reserve (Browning, 1978). Tractor owners in North America utilize added tractor power by traveling fast and adding ballast to maximize productivity (Wilkins and Coleman, 1971). This requires good power reserve and speed selection. Vehicles having engines which are slow to respond to load application react best with transmissions that have clutching elements which can tolerate extended slippage and that have infinitely variable speed ratio capability. Many engines have fuel consumption characteristics which would encourage operation at reduced engine speed when vehicle power requirements permit. To exploit this potential it is required that transmission designs have speed steps and conveniently located and easily understood controls (Browning, 1978).

Over the last few decades researchers have put considerable effort into designing transmissions that conserve energy. This is accomplished by utilizing improved control systems. Dual drive wheels, front-wheel-assist, mechanical front-wheel-drive, four-wheel-drive and radial drive tires have been applied in an effort to utilize traction energy more efficiently (Summers, 1983).

While the dynamics of any vehicle are complex and difficult to model accurately, those of off-road vehicles are further complicated by the fact that they operate on rough land surfaces. The evaluation of dynamic motion has been enhanced by computer simulation of tractor performance. Computer simulation allows the field conditions to be controlled. For example, random variables like soil physical properties can be considered in a constrained manner. While computer modeling reduces the evaluation time and cost of new technologies, it also permits alternatives to be quickly compared in specific simulated conditions.

The drive-line of a vehicle is a series of interconnected components for generating, conditioning, and transmitting power. A drive-line design must be evaluated in terms of the efficiency of power transmission, reliability under reasonable overload conditions and the dynamic performance of the drive-line in achieving desired vehicle motion. Since drive-line components have dynamics which are closely coupled, the whole drive-line must be considered as a system. Thus dynamic interactions can be

meaningfully studied. Furthermore, components that are commonly found in drive-line systems often have complex characteristics which may be available only as empirical data (Karnopp and Rosenberg, 1969).

In recent years researchers have tried to develop models that simulate tractor performance. While many have modeled various drive-line components, few have considered the tractor drive-line as a system of component interactions. Differential Equation models of a dynamic system tend to quickly become cumbersome and their physical interpretation suffers (Rosenberg, 1986).

Bond graphs are more readily related to a physical system than are sets of complicated differential equations. They depict the structure and nature of elements even before their characteristics are fully specified. Bond graph methods are of interest to control engineers because of the formulation of state-space system descriptions which are physically interpretable. Bond graph methods are not only superior in ease of intuitive interpretation, but they also suggest instrumentation and filtering techniques for state variable feedback schemes to realize optimal control (Karnopp and Rosenberg, 1970).

1.1 Objectives

The overall objective of this research is to develop a bond graph model for simulation of tractor performance. This development would provide a physically interpretable

"open" model that is useable in the evaluation of new technologies such as improved tractor control systems (geared towards automation), monitors, transmission and traction device configurations. Specific objectives to be fulfilled are:

1. Develop bond graph models describing the general dynamics or dynamic interactions of the agricultural tractor:
   a) rigid body (chassis),
   b) engine and drive train,
   c) tire-ground interface and
   d) implement force effects.
2. Validate the system model by simulating the "lugging ability test", a part of the Nebraska tractor tests.
3. Study the effect (on the chassis and drive-line dynamics) due to varying implement force and terrain characteristics.
4. Demonstrate the model by comparing equally powered two-wheel tractors with single and dual drive-wheels.
5. Observe the effects of tire slippage, forward velocity, energy flow and distribution as influenced by
   a) tire configuration,
   b) terrain characteristics,
   c) ballast (amount and distribution), and
   d) implement drawbar force variation.

2. LITERATURE REVIEW

In order for the agricultural producer to manage in an energy-efficient way, information must be developed to describe the energy required to operate the equipment used in agricultural field operations (Smith et al., 1981). Energy requirements and efficiency have been of interest to both the agricultural producer and the tractor-implement system designer, and in more recent years to the systems control engineer. Energy requirement analysis and measurement is complicated by the many ways in which energy is expended in the tractor-implement system. In an attempt to analyze (by modeling) and measure this energy expenditure, reseachers have concentrated efforts separately in the following main areas: 1) engine, 2) power train components, 3) tire interaction with the soil and 4) implement interaction with the soil.

The efficient use of energy also depends on tractor stability and overall body dynamics as influenced by the operating environment. Research effort has been placed in the areas of chassis dynamics and stability. Also the effects of soil condition, terrain and the operating velocity have been studied.

While the area of tractor wheel dynamics has been investigated, only a few studies have looked at the whole tractor-implement system and none have applied the bond graph technique.

2.1 Chassis Dynamics

With the advent of smaller, lighter tractors, shortly after World War I, long pointed drive-wheel lugs were developed. This resulted in an increase in the drawbar pull to weight ratio. At the same time a need for higher crop clearance was realized. As a result tractor users and engineers alike became acutely conscious of stability criteria. Although tractor engines, transmissions and other components developed, kinematic and dynamic characteristics of wheel-tractors were not explored. In an effort to investigate the subject, McKibben (1927a,b) embarked on what turned out to be a classic investigation of tractor stability. He determined longitudinal stability of a tractor chassis by developing a mathematical model for the equilibrium of a steel-wheeled tractor. The model was derived by summing moments about an axis parallel to the rear axle which intersected points of soil-wheel contact directly below the axle. The torques of the rear wheels and tractor chassis were included.

Expanding upon the work of McKibben, Worthington (1949a) evaluated both lateral and longitudinal stability of steel-wheeled tractors. He went a step further in

developing the stability criteria by including rubber-tired tractors. Rubber tires were found to have a greater slip when compared with steel wheels. On firm ground, rubber tires tended to increase tractor stability. This resulted from the tendency for weight reaction under the tires to be directed at an angle and slightly backwards as opposed to the vertical reaction in the case of steel wheels. The distance component of the instability moment resulting from drawbar pull was also reduced for the rubber tired vehicles. Worthington (1949b) considered the longitudinal stability of rubber-tired tractors when the drive wheels were immobilized.

Sack (1955) developed a new method of evaluating the critical angle of longitudinal stability including a discussion of factors affecting it. He considered the kinematics of the tractor at the instant when the front wheels left the ground.

Tractor models did not differ from the work of McKibben and Worthington until Raney et al. (1961) derived the differential equations of motion for a system with three degrees of freedom to determine the vibrational motions of a tractor. The motivation of Raney et al. was to quantify mass moment of inertia and tire characteristics as dynamic response parameters. Tires were modeled as springs and viscous dampers. After quantifying the mass moments of inertia, spring rates and damping constants were experimentally determined for a tractor. The equations of

motion developed by applying D'Alembert's principle of dynamic equilibrium were solved by analog computer simulation. In comparing analytical and experimental frequency response, good agreement was reported.

Buchele (1962) advanced the land-locomotion theory by introducing soil variables into the existing equations for tractor stability. His analysis avoided differential equations by assuming that the tractor moved with constant acceleration. Thus, his analysis, like those of others before Raney et al. (1961), could not accomodate vibration or tipping of the tractor.

Pershing (1966) simulated an agricultural tractor to determine the transient vibration responses. The tractor model used nine degrees of freedom. This was accomplished by differential equations developed using Lagrange's equation. This approach represented a significant improvement in modeling techniques.

Goering (1965), expanding upon the work of Raney et al., included the rotational motion of the wheels and power train. The power train was represented as an engine, clutch and transmission. A hypothetical flywheel was used to model the engine. The inertial effects of the rotating engine components were included to determine the net torque available at the clutch. The maximum clutch torque was propotional to the normal force on the clutch-face, clutch-face effective radius and the kinetic coefficient of friction of the clutch facing material. The transmission

was treated as a speed reduction and power absorption unit. For an unlocked differential, the torque on the drive wheels was assumed to be equal, and the output torque was determined to be proportional to the angular velocity of the chassis about the transverse axis and the mean angular velocity of the drive wheels. An analog computer was used to simulate a heavily ballasted tractor. During simulation, using the power train previously described, the equations of motion could not be solved due to complexity. The power train model was replaced by empirical torque-time and angular velocity-time relationships in order to complete the simulation.

Goering and Buchele (1967) established the first comprehensive, planar mathematical model which would simulate the tractor rear overturns by allowing for large amplitude vibration and pitch angles. They modeled rear overturns due to rapid and slow clutch engagement with a large drawbar load. This mathematical model was limited to motion in the vertical plane. However, it considered forward travel as well as the bounce and pitch motions. Goering and Buchele treated forward motion as a gross motion as contrasted to a vibratory perturbation around a mean forward travel speed. The engine and drive-wheel rotational speeds were considered as additional degrees of freedom.

Simulation of tractors for predicting field performance was presented by Grecenko (1968). He used a graphical approach. Draft, engine power, wheel slip and a combination

of the tractive and transmission efficiency were plotted to locate the fuel consumption at steady state operation.

Pershing and Yoerger (1969) developed a nine-degree-of-freedom mathematical model to investigate the potential catastrophic failure of a tractor to negotiate bumps on a side slope. The wheeled vehicle was analyzed as six different bodies - four wheels, a main chassis and a front axle. The operator and power train were excluded. Lagrange's equation was used in the simulation. Only oscillatory motions were considered; therefore, in the model formulation, only kinetic energy that was subject to change was included. Comparing the transient responses of the nine degrees of freedom model to that of three degrees of freedom, a considerable difference was realized. In the three degrees of freedom model, the tractor was considered as one body with radial springs and dampers for the tires and only roll and pitch motions were considered.

Wolken (1971) developed a seven degrees of freedom model of a self-propelled vehicle using Lagrange's equation. It was developed to determine the vibration response of the vehicle at the operator's seat. The power train was not included in the simulation. A self-propelled combine and an agricultural tractor were simulated using analysis techniques for random excitation.

Smith et al. (1971) developed a two-part mathematical model to describe the side overturn motion of wide-front-end and tricycle-type wheel tractors. Three dimensional vector

techniques were used to derive differential equations expressing the tractor angular acceleration about a tip axis in terms of tractor geometry, inertial forces, side slopes and ground disturbances. Smith's model was not developed for close prediction of actual overturning motion but rather for the analysis of those factors which influence lateral overturning. Smith and Liljedahl (1972) developed a qualitative mathematical model describing the rearward overturning behavior of a farm tractor. The power train was included to provide theoretical insight into the rearward overturning behavior as influenced by the tractor's engine, clutch and transmission.

Zoz (1972) developed a graphical simulator for the performance of a two-wheel drive tractor. The simulator utilized advertized travel speed, rear weight, engine power, type of hitch and soil condition. From the graph, ratio of drawbar pull to rear tractor weight (traction coefficient) could be determined. The predictor was reported valid only for steady-state performance of two-wheel-drive tractors equipped with single drive wheels.

With the objective of describing tractor overturns more precisely in terms of tractor and terrain characteristics, Davis (1973) developed a ten degrees of freedom model. The equations of motion were developed using dynamic equilibrium and Euler's equations. Realizing the shortcomings of previous research in defining rotational equations of motion and in accurately representing the tire-terrain interface,

Davis modeled the tires as segmented springs with a series of radial spring elements. This would more accurately describe tire deformation as it was moving over the terrain. This was validated by comparing simulated overturn data to that of experimental overturning data of a 1/12 scale model tractor.

Hudson et al. (1973) developed simplified equations for simulating dynamic tractor behavior. The equations of motion were developed for a two degrees of freedom system with a dynamic forcing function for a drawbar load. The simulation was used to predict rearward overturning and it did not include the engine or power train.

Considerable field research work has been devoted to the dynamics of tractor body-implement (or trailer) and implement-soil interactions (Upadhyaya, 1985; Bowers, 1986; Tembo et al., 1986; and Wiedemann et al., 1986). Less has been done in the area of modeling the effect of implements on chassis dynamics. Smith (1974) developed a computer simulation for determining forward motion variations of agricultural tractors subjected to varying drawbar loads. The model included the power train, engine governor and the hydraulic hitch system. The translational frequency-response characteristics of the tractor subjected to a periodic (sinusoidal) drawbar load were studied. Equations of motion were developed using Lagrange's equation. The movement of the tractor was assumed to be confined to the vertical plane of forward motion. The soil surface was undeformable and

structural vibrations were neglected. The power train was modeled as an engine, a torsionally stiff drive shaft between the clutch and transmission (same case for the shaft between the transmission and the differential), a transmission with speed reduction, a differential with speed reduction, two torsional rear tires and torsionally stiff axles. The clutch was modeled as a coulomb friction device with the clutch angular acceleration. A complex model of a flyball governor was included as a means of achieving automatic engine speed control.

Tractor modeling has also dealt with design for rider comfort. In the area of forward motion variation, Smith (1974) pointed out that little was known about braking characteristics of tractor tires. Relating this to rider comfort it was established that the forward motion component of vibration acting on the operator due to pitch of the vehicle varied with the height of the body above the center of gravity of the tractor. The vibration effect was most noticeable at the operator's head. Mathews (1967) investigated the improvement in tractor ride afforded by a flexible front axle. It was found that while a flexible front axle noticeably reduced fore-and-aft vibration due to the pitch effect, its incorporation would not significantly affect the vertical vibration imposed on the operator.

Smith (1977) developed a thirteen degrees of freedom model for determining tractor ride characteristics. Five degrees of freedom were assigned to the tractor chassis with

the roll of the front axle allowed as a sixth degree of freedom. The cab was assigned six degrees of freedom to describe its motion relative to the tractor chassis. The seat suspension was simulated by the rotation of one of its four linkages. Tires were modeled using a segmented tire which was divided into a finite number of radial springs. The spring elements did not rotate relative to the wheel. This research was used to evaluate new designs for ride comfort.

Kim and Hoag (1981) developed a mathematical model for active, semi-active and passive seat suspension systems. Each suspension model was combined with a three degrees of freedom model of the vehicle operator. Information concerning the acceleration levels of the head, body and pelvis were obtained from the simulation. The model was verified by measuring real-time acceleration at the base of the seat suspension of agricultural tractors during the transport and moldboard plowing operations.

The lateral stability of an agricultural tractor towing an unbalanced two-wheel trailer was evaluated by Crolla and Hales (1979). The tractor-trailer combination was modeled as a five degrees of freedom system neglecting the drive train effects. The model was used to investigate the effects of forward velocity and braking on lateral stability.

Takahashi et al. (1981) modeled the motion of rotary tillers attached to agricultural tractors. The rotary-

tiller was assumed to have three degrees of freedom; longitudinal, vertical and pitching. The equations of motion of the rotary tiller were composed of equations for engine power, forward speed of the tractor, coordinate relationships and the force equilibrium of the rotary-tiller body. The forward speed of the tractor was expressed in relation to engine speed and clutch slippage. The external forces on the tractor and tire slip were assumed to be negligible.

The starting behavior of a two-wheel drive agricultural tractor was simulated by Takahashi et al. (1980). With the tractor motion confined to the forward and vertical plane of motion, the tires were modeled as springs and dampers with ground contact at a single point beneath each tire. Dynamic equilibrium was used to develop five equations of motion describing the gross vehicle motions. The engine was described by two differential equations defining the angular acceleration and lag time of torque response to the engine angular acceleration. The transmission was treated only as a speed reduction unit, and the drawbar load was unconsidered.

Another area of interest has been the effect of ballasting and its influence on the location of the center of gravity and tractive performance (reported in the next sub-section). Young and Schafer (1977) discussed the control technology and hardware available which could permit the selection of dynamic load and inflation pressure that

would correspond to optimum tractive efficiency for a particular soil condition. The possibility of an optimum system was the motivation for Burt et al. (1982), Lyne et al. (1982) and Bloome et al. (1982) to undertake field studies to explore potential gains from such a system.

Since conflicting requirements made the location of the center of gravity a matter of compromise, Smith (1986) described an analytical method based on static equilibrium for predicting the required fore-aft center of gravity location of a vehicle in order to optimize performance on a slope. The analysis included differing vehicle design parameters, operating surface conditions and differing power train - steering configurations.

2.2 Power Train Dynamics

Power train modeling has ranged from analysis of specific power train components to that of the entire power train as a system which affects input, transmission and output of energy. Numerous engine models have been developed for predicting transient and steady state response. Whitehouse et al. (1962) based a cyclic thermodynamic analysis of a turbocharged diesel engine on the dual cycle. They showed that the dual cycle more closely approximates the actual engine cycle than the air-standard cycle due to the addition of a constant volume combustion process. An analysis of the effects of the trapped gases in the

clearance volume was included. Cycle calculations were performed 180 times per crankshaft revolution.

Winterbone et al. (1977) used a dual cycle analysis which included the effects of the trapped gases to dynamically model a turbocharged diesel engine. Engine speed changes were evaluated by applying Newton's Second Law to the rotating mass of the engine. The governor was modeled by a first order differential equation describing the movement of the injection pump rack. For calculations during compression, combustion and expansion, a cycle step increament of ten degrees of crankshaft rotation was employed. A cycle step of two degrees of crankshaft rotation was used for the exhaust and intake calculations.

McAulay et al. (1965) developed equations for heat energy transfer and mass flow in a diesel engine. Goyal (1978) used these equations to simulate the transient response of a turbocharged diesel engine. A model of the available fuel burned was included so that when air-fuel ratios were lower than seventeen, only a portion of the available fuel was burned.

Tennant et al. (1979) used regression analysis to model spark ignition engine performance. The dependent variables were engine speed and torque, manifold pressure, air-fuel ratio, exhaust gas recirculation, spark timing, inlet-air temperature, injector pulse width and combustion chamber temperature. The root mean square errors of the fuel, air and torque regressions were less than 7.6 percent.

Engine performance maps have recently been applied in computer simulation to predict tractor performance and fuel efficiency (Strapel, 1980; Jahns and Steinkanf, 1983). They have also been used in developing a basis for engine control using microprocessors for maximum efficiency (Binnervies and Schwanz, 1980). Grogan et al. (1983) and Jahns (1983) used engine performance maps in field tests. They measured two of the three parameters; engine speed, torque and fuel consumption and calculated the third. Jahns et al. (1987) illustrated that diesel engine performance can be predicted with a polynomial of nine coefficients within an accuracy range of 0.6 to 2.5 percent.

Hansen et al. (1986) utilized engine performance maps to establish a basis to calibrate power demand maps which would give the time spent at different levels of tractor engine power. By comparing different tractor operations and operators, the microprocessor-based system developed determined how effectively tractor engines were being managed in the field. With an added ability to measure the area covered during field operations, Meiring et al. (1987) carried out a further quantitative assessment of tractor power utilization by Hansen's system (Hansen et al., 1986).

Pacey and Schrock (1982) revised and discussed the fuel consumption models in ASAE Standard D230.3 (ASAE, 1982). Their concern was that the models over-estimated fuel consumption. Of equations analyzed for potential use in an

updated fuel economy model, the most suitable was a third order polynomial with the zero-order term omitted.

A hard-wired control system was developed by Chancellor and Thai (1984) to test a hypothesis that frequent automatic adjustment of the tractor's transmission ratio might permit a 10% saving in fuel and a 17% increase in the average rate of drawbar work output (Chancellor, 1981). The control system developed had axle-torque and desired forward speed as input signals to control transmission ratio and engine speed for either the most fuel-efficient operating conditons or highest rate of drawbar work. Fuel savings of between 5 and 12 percent were realized in the field tests.

Lyne et al. (1984) carried out field tests to evaluate the specific fuel consumption which resulted from changes in static load, inflation pressure, tire configuration and engine operating point. They found considerable potential for applying automatic controls to improve specific fuel consumption.

Considering fuel consumption characteristics of diesel engines at low loads, Williams and Buck (1985) developed an empirical equation relating fuel consumption to engine speed and power output. They analyzed the input fuel expenditure by internal friction losses, mechanical power output and thermal losses. Each component was individually calculated in terms of its own contributions to overall fuel consumption. A maximum absolute error of less than 7

percent was obtained in comparing experimental to predicted fuel consumption.

Zhang et al. (1985) developed a microprocessor-based control system to improve the operating efficiency of diesel engines. Laboratory tests of this system demonstrated the potential to control engine speed close to the optimum for reduced fuel consumption. Zhang et al. (1986), working on the limitation associated with this control system, established a mathematical model for describing an engine-governor system's dynamics. They developed control algorithms for theoretical simulations and laboratory tests. In order to minimize the complexity of modeling an engine-governor system (which includes complex mechanical and chemical structures), they used the Auto-Regressive Moving-Average (ARMA) method (Franklin and Powel, 1981). The modified control system improved control accuracy significantly.

Wang and Zoerb (1985) developed instrumentation to provide a visual indication of relative operating efficiency of a tractor engine which assisted the operator in gear and throttle setting. During operation the ideal engine speed was compared to the actual speed and the difference was indicated to the operator. Engine speed was measured by a tachometer while engine brake power was measured indirectly by measuring exhaust temperature. Adjustment of the gear selection indicator required mathematical models. This was

determined from fuel consumption maps for the engine and its rated working point setting.

Kolozsi and McCarthy (1974) developed a computer model of tractor performance. They used a torque balance equating engine output torque to transmission losses, motion resistance and output thrust torque (for equivalence in units, motion resistance and thrust force were presented as torques with the torque-arm being the rolling radius of the drive wheel). The torque prediction equation relied upon the measurement of the independent variables in a single gear. A linear relationship between engine speed and transmission losses was assumed. Draft could therefore be predicted in any other gear. The ratio of field speed to engine speed was measured on an asphalt surface before being used as an independent variable.

Some power train research studies have been directed specifically towards clutch dynamics. Goering (1965) used a clutch model where the torque transmitted was proportional to the normal force on the clutch face, the clutch effective radius and the coefficent of friction of the clutch material. The model was adapted from Coulomb's equation where the shearing stress is proportional to the normal force and coefficient of friction. Browning (1978) and Liljedahl et al. (1979) presented the basic clutch model discussed by Barger et al. (1963) with the effective radius of the clutch evaluated in terms of the inner and outer radii of the clutch facing. Takahashi et al. (1980) used a

clutch model with the clutch slippage as a function of the time required to fully engage the clutch. After the clutch was fully engaged, slippage was neglected.

2.3 Tractive Performance

Researchers in vehicle mobility for civil purposes like transportation and forestry are concerned with the challenging economic aspects of determining the effects of the environment on the movement of vehicles. The quest to understand the mechanics of a simple wheel on soft soil has revealed a complex physical phenomenon so that it is difficult to predict what will happen to a wheel in given soil conditions. When all the necessary characteristics of the wheel and soil are known the problem is to determine the relationships between the load on the wheel, the torque, the pull that the wheel can develop and the soil conditions. Wheel-slip plays a major role in traction efficiency because it reduces the distance over which the pull does work. Sinkage must remain smaller than vehicle clearance for mobility to take place (Leflaive, 1966).

The complex nature of soil behavior and its variability has led to limited theorizing of soil-wheel interaction. This has led to experimentation with wheels on soft soils. These have been conducted with actual vehicles, single wheels both rigid and pneumatic, and with scale models. Soils in their natural state, reprocessed soils and artificial soils have been used. Actual vehicles have been

utilized for practical reasons, but they are not convenient for close control and measurement of variables.

A great deal of exploratory field and laboratory traction tests have been conducted. A large quantity of carefully measured data is available. The problem has been to decide in which terms results should be expressed to provide a good description of experimental facts. Confusion arises from the number of parameters and variables playing a part in the phenomenon (Leflaive, 1966).

Predictions of performance of tractive devices from the analysis of certain soil parameters was begun by Bekker (1956, 1960). Barger et al. (1963), Gill and Vanden Berg (1968), Wong (1978) and Yong et al. (1984) presented tractive performance models of a pneumatic tire based on Bekker's pressure-sinkage relationship. Bekker assumed that the terrain reacted radially at all parts of contact on the tire. Soil reaction was assumed to be equal to normal pressure under a horizontal plate. Bekker's pressure-sinkage relationshionship for a homogenous soil was dependent on cohesive and frictional moduli of deformation. The cohesive and frictional moduli were determined from experimental load sinkage relationship for flat plates.

The Bekker approach for prediction of power output for agricultural tractors has not been adopted because it is purely empirical. Furthermore, the model has been adequate only for vehicles operating with small sinkages on clay soils.

Cone penetrometer readings were used in mobility studies as an indication of vehicle trafficability across rough and soft terrain. Freitag (1965) incorporated a single penetrometer reading in a dimensional analysis of tire performance and validated it for dry cohesionless sand and saturated frictionless clay. Based on the analysis of data obtained from laboratory tests, Freitag (1965) derived mobility numbers for tires in clay and sand by consolidating the independent dimensionless terms. Turnage (1972) determined the relative influence of tire parameters and the selection of appropriate tires for specific field requrements.

In developing reaction equations for cohesive-frictional soils, Wismer and Luth (1972) defined a dimensionless wheel numeric similar to that of Freitag's mobility number. The dimensionless term included cone index, tire section width, overall tire diameter and dynamic wheel load. Wismer and Luth (1974) used dimensional analysis to develop a traction prediction equation. The loss associated with towed wheels was determined to be inversely proportional to the wheel numeric. Other parameters were tire rolling radius, towing force, pulling force and slippage. This equation was developed for cohesive-frictional soils of moderate compactibility and for tire inflation pressures producing tire deflections of approximately 20 percent when loaded.

A model was developed for a driving wheel including the towed-wheel loss to account for rolling resistance. A restriction of the tire cross-sectional width to diameter ratio was set at 30 percent. The soil cone index which is measured using a soil cone penetrometer is more readily obtainable than the moduli for Bekker's pressure-sinkage relationship.

A similar set of relationships were developed by Zoz and Brixius (1979) for tires on concrete. They assumed the towed tire motion resistance to be 2 percent of the dynamic load on the tire. A tractive performance prediction model, of the same nonlinear form as the Wismer and Luth (1974) model, was empirically determined for bias ply tires on concrete. The model developed could predict tire pull and efficiency as a function of tire width, diameter, rolling radius, tire load and slippage.

Gee-Clough et al. (1978) modified the tractive performance equation developed by Wismer and Luth (1974) for use in English soil studies. Prediction equations for a moldboard plow draft were combined with the modified tractive performance equation to determine the power required to pull a moldboard plow. The tractor engine speed was calculated from an empirical PTO-power, engine-speed relationship.

Further investigation into the utilization of energy beyond the tire-soil interface or within the interface but relating it to drawbar performance has been modeled. Domier

and Person (1968) compared tractor performance characteristics of tractors with varying tire sizes and weights. Drawbar performance of seven tractors with varying tire sizes, weights and inflation pressures were predicted by relating their performance to that of a `standard' tractor. Accounting for the differences in tire diameter and load factor, it was assumed that : a) the coefficients of front and rear wheel rolling resistance varied inversely with the wheel diameter, and b) the coefficient of net traction of the comparison tractor was less than one-half the relative difference in diameter multiplied by the coefficient of net traction at 30 percent travel reduction. Travel reduction was evaluated on the assumption that engine speed dropped 6 percent from no-drawbar-pull to maximum pull.

Pitts and Goering (1979) used dimensional analysis to model the change of the soil cone index after a driven wheel had passed over it. The predictive equation developed for the change in soil cone index is:

$$CI_A = 1 + 18.09 \left(\frac{W}{CI_B bd}\right)^{0.554} \left(e^{\frac{-0.585x^2}{gb}}\right)$$

where:

CI_A = Soil cone index after traffic

CI_B = soil cone index before traffic

b = tire section width

d = tire diameter

g = gravitational constant

W = tire dynamic load

x = forward velocity of the wheel

Documented attempts to apply the Wismer and Luth (1974) model to field data have pointed out problems in some cases. For example, Macnab (1977) found that the model did not predict satisfactorily on surfaces with heavy grass. In an attempt to force the model to fit field data, research efforts have been centered on the measurement of the soil cone index. Clark (1984) presented a modified Wismer-Luth model. Clark (1985) pointed out the importance of the cone index method of measurement and the soil-depth range in which it was measured. He confirmed that if a soil surface was relatively bare and no excessive sinkage occured, then the average cone index for the 0-15cm depth range is sufficiemt for use in the original model. The prediction of traction for the rear wheel was not as universal as for the front wheel.

Dommel and Race (1964) used instrumented two and four-wheel drive tractors for field studies. They reported up to 50 percent more pull with a four-wheel drive tractor on sod or plowed soil. They also pointed out that under selected conditions the four-wheel drive increased mobility, efficiency and manueverability. In addition it was found that it had better side-hill operation, an increased drive-line life and less soil compaction. Osborne (1971) in a

similar study found that the performance of two and four-wheel drive tractors was similar on hard surfaces. However, the maximum rate of work of the four-wheel drive tractor was as much as 33 percent greater than the two-wheel drive tractor on soft soil. The four-wheel drive tractor also had a higher traction coefficient.

Domier (1971) ran field tests from which it was determined that a two-wheel drive tractor had tractive efficiencies ranging from 55.2 to 69.8 percent. The four-wheel drive tractor had tractive efficiencies ranging from 68.3 to 74.5 percent. Clark (1984) reported a significant increase in drawbar power and ground speed of a four wheel drive tractor, while fuel consumption per hectare decreased.

Jerek and Newendorp (1983) carried out field tests to determine the performance of various tractors and tire combinations with a specific look at fuel efficiency. Fuel efficiency is a combined measure of tractive, engine and mechanical efficiencies. A closed loop draft control system was utilized with which load cycle variations could be specified. The percentage of total static tractor mass on the front axle was 25 percent for the two-wheel drive (2WD) and 40 percent for the mechanical-front-wheel-drive (MFWD). They found radial tires (compared to bias ply tires) caused an increase of up to 10 percent in fuel efficiency. The 2WD tractors showed a higher benefit from radial and dual tires than did MFWD tractors on soft soil. A 19 percent improvement in fuel efficency was reported for the MFWD.

The single rear tires consistently outperformed the 2WD tractors with dual rear tires.

Woerman and Bashford (1983) worked with a four-wheel drive Case 1490 tractor. They found that the tractive efficiency on both concrete and soil surfaces was maximum when approximately 35 to 40 percent of the dynamic weight was on the front axle. They recorded a 3 to 5 percent higher tractive efficiency for the four-wheel drive tractor compared to the front-wheel-assist (FWA) tractor operating in the two-wheel drive mode if both were optimally ballasted. The wheel-speed ratio (ratio of front-wheel to rear-wheel speeds) is important when working with a FWA tractor. Woerman and Bashford (1983) found a wheel speed ratio of 1.01 to 1.03 to be near optimum for most field conditions.

Taylor et al. (1976) compared tractive performances of a radial ply and bias ply tire of the same size and shape in a range of soil conditions. It was concluded that the radial ply tire had its greatest advantages on firm surfaces where most of the soil-tire deformation took place in the tire and not in the soil. Burt et al. (1982) tested radial and bias ply tires with various inflation pressures and static loads in two different soil conditions. On the wetter higher bulk density soil, the bias ply tire attained higher tractive efficiency. The radial ply tire had a greater mean tractive efficiency on the drier less dense soil.

Hausz (1985) stated that the tractive advantages of radial ply tires over bias ply tires resulted from their deflection characteristics. Radial ply tires yielded a larger footprint than the same-size bias ply tire at the same load and inflation pressure. Even when the footprint of the radial ply tire was not significantly greater than that of the bias ply tire, tests showed improved traction for radial ply tires. This is because the lugs on the radial ply tire have a much more uniform pressure distribution and therefore, will bite into the soil more uniformly.

Burt et al. (1979) investigated the role of both dynamic load and slip on tractive performance. The results of this study showed that at low values of slip, large changes in performance occured with small changes in slip. However, at higher slip values, changes in dynamic load had a greater effect on performance than changes in slip. At constant slip, tractive efficiency increased with increases in dynamic load on compacted soil. On uncompacted soil, tractive efficiency decreased with increased dynamic load. Input power increased linearly with respect to dynamic load and nonlinearly with respect to slip. Output power changed in a nonlinear way with respect to changes in either dynamic load or net traction.

Wulfsohn and Upadhyaya (1986) compared tractive performance of radial to bias ply tires. They reported an average tractive efficiency of 27.23 percent for radial ply

tires and 25.37 percent for bias ply tires over the 0 to 30 percent slip range.

Operating efficiency of farm tractors depends on engine, transmission and tractive efficiencies. While most mechanical transmissions have a relatively high efficiency, overall operating efficiency is lowered by the relatively low engine and tractive efficiencies. Several researchers have developed control systems for the improvement of tractive and engine performance. A hitch control system developed by Dodd et al. (1986) tended to improve tractive performance by varying the three point hitch geometry. The variation transfered the weight from the front wheels to the rear wheels for increased traction. Clark and Linde (1986) developed a ballast control system in which liquid ballast was shifted back and forth for an appropriate weight distribution. A major limitation of this system, like others that include the operator within the feedback control loop, was slow response.

Zhang and Perumpral (1987) developed an automatic control system capable of simultaneously improving both engine and tractive efficiencies. Their system maintained engine speed and drive-wheel slip at an optimum for maximum fuel efficiency and maximum tractive efficency. During most field operations the drawbar load on a tractor is much lower than the pull that the tractor can develop, therefore there was no need to compromise tractive efficiency for pull force. The system was then designed to control wheel slip

at an optimum when the tractor was not overloaded and to generate more pull when overloaded. Engine throttle setting, mechanical gear setting and power-shift gear setting were considered as input variables to the control system. Other input variables such as soil cone index, surface slope and drawbar load were considered disturbance input variables. Test results of the control system showed improved operating efficiency and productivity during disk-plowing

2.4 Whole System Simulation

Very few attempts have been made at developing models to simulate tractor performance while considering the whole tractor-implement system. Such models must include the dynamics (or interactions) of the chassis, engine, power train, tire-soil interface and the implement. Summers et al. (1986) developed a mathematical model for determining gross vehicle and drive train motions for two and four-wheel drive agricultural tractors. Chassis motions were constrained to the vertical plane in the forward direction of travel with no allowance for roll, yaw or lateral motions. The chassis motions allowed were forward displacement, vertical displacement (heave), pitch displacement and front axle angular displacement. Drive train motions were described by the engine, clutch, and front and rear wheel angular displacements. Mathematical models were combined into a computer simulation program.

Lagrange's equations of motion, which applied energy relationships within the system, were used to develop the mathematical model.

Assumptions considered in the lumped mass drive train model were:

a. Forces supported on drive-wheels were evenly distributed between the wheels.
b. Angular displacements, velocities and accelerations were equivalent for drive wheels mounted on the same axle.
c. Losses in the transmission and differential resulted from the gear meshes.
d. Drive wheels on each axle developed equivalent tractive efforts.
e. Damping in the axles and drive shafts was negligible.
f. Kinetic energies of the axles, shafts and gears were negligible compared to that of the wheels, clutch and engine.
g. Potential energy stored in the axles and shafts was significant.

Thermodynamic modeling of the engine required 26 thermodynamic relationships. The governor action required two additional differential equations to describe its motion. An engine torque-speed relationship was used in the model for simplicity.

Tractive performance was modeled by use of the equations developed by Zoz and Brixius (1979) and Wismer and

Luth (1974), for tires on concrete and soil. Equations of motion were programmed into a Continuous Modeling Program (CSMP) program for solution. The computer model was validated by simulating the lugging ability data from Nebraska tractor tests. The initial model simulation resulted in large Standard Error of Estimate and required large amounts of computer time. In order to improve the prediction accuracy, the drive train model was revised. It was simplified by a change in assumption 7. Assuming that potential energy stored in the drive train was insignificant gave a much more accurate prediction of engine speed, wheel slip and forward velocity.

2.5 Bond Graph Modeling

The bond graph language was invented by Paynter in 1960 (Rosenberg, 1976). The language supplies a modeling approach that is concise, clear and very broadly applicable. It shows, in simple diagram form, the elements and connections of dynamic systems having a variety of energy types (Rosenberg, 1976). A bond graph can be used to generate a block diagram (or other computing diagrams) of a system from which a state space differential equation representation can be generated for use in control studies.

Bond graphs have had a wide variety of applications ranging from biomedical and medical physics to the technological forecasting and resource policy analysis. They have also been used in thermodynamics, heat transfer,

chemical networks, design, simulation, analysis and control of kinematic systems, vibration studies etc. (See Bos and Breedveld, 1985)

Karnopp and Rosenberg (1970) used bond graphs for the analysis and simulation of vehicle drive-lines. They placed emphasis on the problem of assembling multiport models of system components for a compatible and efficient system description. They demonstrated how state space description for analysis and block diagrams for analog simulation may be obtained systematically from bond graphs. The effect of tire slip characteristics on acceleration was investigated. A physical system representation efficiency comparison was made between bond graphs and block diagrams. They found that bond graphs are more compact than block diagrams, and they are more readily related to the physical system than sets of differential equations.

Rosenberg (1972) considered a multiport approach to problems in mechanics involving large scale motion of rigid bodies in both conservative and nonconservative force fields. A procedure for constructing bond graph models based on key geometric variables and velocity transformations was described. It was observed that bond graph models rendered the structural representation of complicated mechanics problems into a concise and uniform style that was easily communicated between people and to computers. Rosenberg (1972) showed how kinematic variables in the obtained equations could be used in Lagrange's

equations and how bond graphs aided in the interpretation of various dynamic terms.

Martens and Bell (1972) described a suitable mathematical modeling procedure for complex devices. Using a vibratory air pump as the medium of presentation, they derived a step by step procedure for building a bond graph model. It was shown how system properties like energy storage effects, power dissipation and input-output characteristics could be added to the original model. The original model was developed from basic coupling structures and the functional purpose of the system.

Tsai and Wang (1974) analyzed dynamic responses of geared torsional systems with the delay-bond graph technique. Nonlinear elements like varying tooth stiffness, gear-tooth backlash and nonlinear damping were incorporated into the ideal transmission line element. The method of modeling demonstrated that dynamic response can be simulated as torsional waves propagating on a transmission line.

Karnopp (1976) developed a six-port bond graph model for analyzing the stability and control properties of aircrafts, automobiles and ships. He idealized the vehicle as a rigid body and used a body-centered coordinate frame in the study. The effects of simplifying the graph by considering only lateral and longitudinal dynamics were presented. Bond graphs, for stability studies in which the assumption of small perturbations permits linearization,

were shown for elementary models of automobiles and aircraft.

Margolis (1978) used bond graph modeling techniques to represent normal mode dynamic behavior of Bernoulli-Euler beams. Governing state equations were easily procured from the resulting overall system bond graph. These equations were arranged to obtain the normal modes and frequences of the coupled system. The procedure was demonstrated for a vehicle frame structure including primary and secondary suspension dynamics. Modal information was attained with considerable savings in computation time compared to finite element methods.

Gassman (1978) investigated the response and stability of a load sensing cylinder of a tractor hitch system. He compared a conventional method to the bond graph method of analysis. The conventional method was composed of block diagrams and differential equations appropriate for simulation on a digital computer. It was reported that the bond graph method had specific advantages. It could be constructed directly from hardware layout and easily revised if a change in hardware became necessary. Variable causality was readily identifiable from the bond graph and the modeling was suitable for computer simulation without initial derivation of equations.

Hrovat and Tobler (1985) derived a set of four first order nonlinear differential equations describing torque converter dynamics along with the corresponding bond graph

representation. The bond graphs consisted of an inertia-field and modulated gyrators which coupled mechanical and hydraulic ports. Although torque converters had been analyzed for over four decades, Hrovat and Tobler (1985) observed that the bond graph approach disclosed some new aspects of torque converter dynamics. They concluded that bond graphs were an extremely revealing and efficient modeling procedure.

League and Cundiff (1986) studied the dynamics of a hydrostatic drive test stand. They used bond graphs to facilitate the equation development and to understand the system. The resulting first order differential equations composed the mathematical model used for computer simulation. The simulation was implemented using Advanced Continuous Simulation Language (ACSL). The steady-state dynamic performance of the system was recorded experimentally and compared with predicted perfomance of the simulation. The analytical model was found to be in general agreement with the physical device.

Research work involving modeling with bond graphs has increased over the years. Researchers have changed from dwelling on experimenting with the use of bond graphs and increased the number of areas of direct application of the theory as it has been accepted more and more. With the reported efficiency of bond graphs as a means of modeling power and energy flow this study was undertaken with the hope of developing a model with the reported (bond graph)

power of revealing dynamic properties of a system. The farm tractor-implement system was a complex system whose associated research endeavors would benefit considerably from the reported simplifying yet revealing nature of bond graph modeling.

3. MODEL DEVELOPMENT

A general model for analysis and performance prediction of the tractor-implement system could be divided into four major parts; the chassis motions, the power train dynamics (including engine), soil-tire interaction and chassis-implement interaction.

The tillage-tractor system model is made up of a power source (the engine) which supplies energy to the rest of the system where it is used, lost or stored. The fundamental problem with this energy is to get most of it to do useful work without wasting it through the power train and at the tire-ground interface. Of the net energy leaving the engine, power train and traction efficiencies determine how much energy is available to translate the chassis and to pull an implement with the drawbar. Power train and engine losses are dependent in part on the engine speed.

The main features considered in the evaluation of tractor field performance are the drawbar pull, speed, drawbar power, tire slippage, specific fuel consumption, tractive efficiency, rate of work, maneuverability, stability and loading of the tires.

In optimizing energy utilization within the tillage-tractor system, one of the most important and analytically

complex energy consumption processes was at the soil-tire interface. The characterization of this consumption is complicated by the unpredictability and variability of soil behavior. In soil-tire interaction the amount of slip and degree of sinkage that occur are factors which depend not only on the stress-strain, strain-rate and compressibility characteristics of the soil but also on the intimate interaction between the soil and wheel. Input energy is obtained by multiplying axle torque by angular velocity. While angular velocity may be specified as completely independent, the applied torque must depend on the resultant interaction between the wheel and soil. Hence, torque is dependent on response soil behavior. In considering the phenomena from a physical viewpoint of tire rolling motion, it is useful to consider energy input and energy dissipation as independent. Evidently both of these factors are influenced by basic parameters controlling rolling motion, and by secondary phenomena that occur when the wheel is in motion such as the effect of sinkage on geometric conditions and variations of soil density due to shear.

3.1. The Tractor-Implement System

The analysis of the performance of a farm tractor requires a basic understanding of the statics and dynamics of the physical system. Figure 3.1 shows the rigid-body physical-system of the farm tractor. The efforts (forces and torques), flows (rotary and translatory velocities),

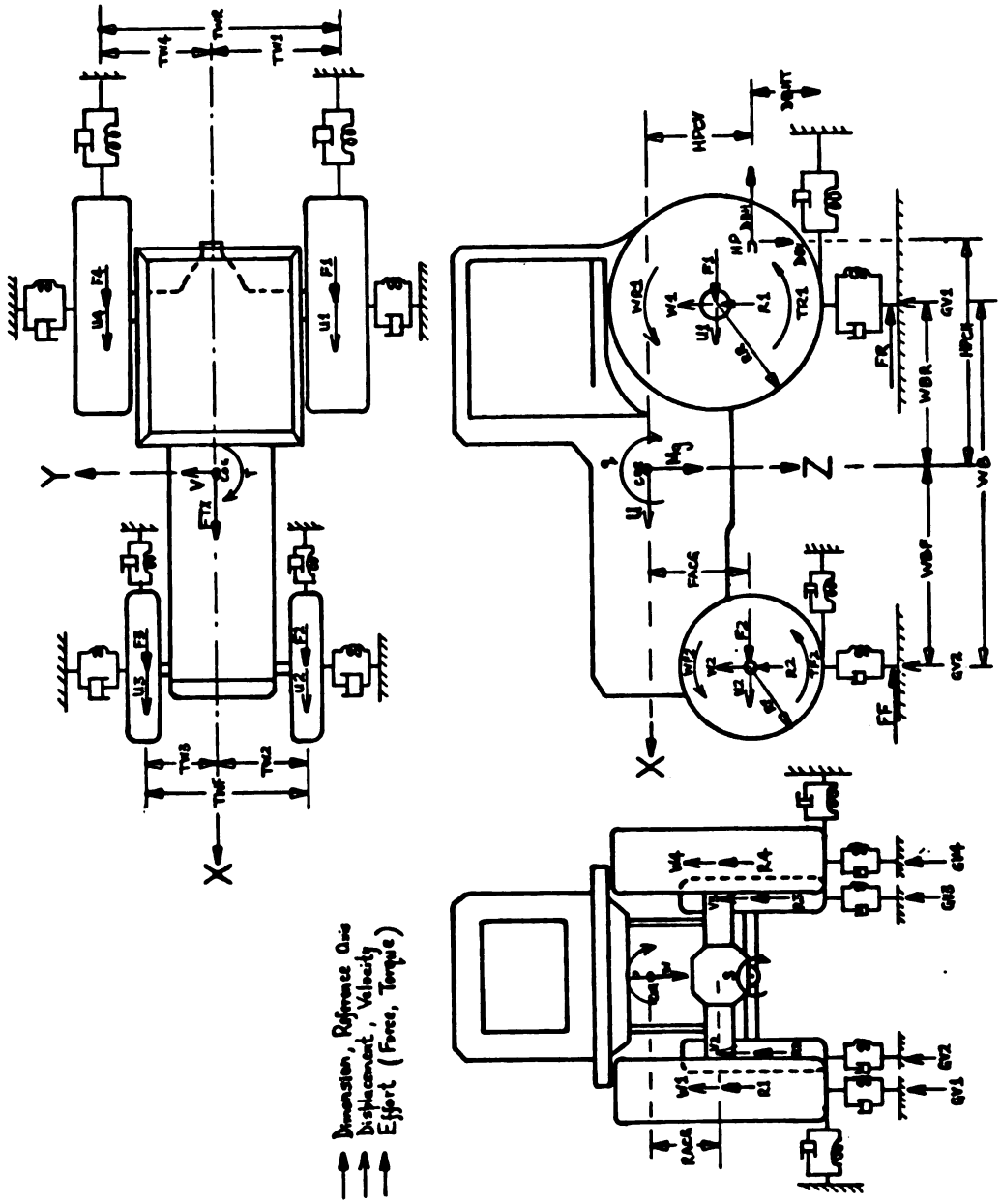

Figure 3.1: Rigid Body Physical System of the Farm Tractor Showing Efforts, Flows and Dimensional References of Its Motions

Table 3.1. Definitions of Labels Used on Figure 3.1

Forces, Torques, Velocities and Axes:

X, Y, Z:	Coordinate axes originating at the center of gravity.
u, v, w:	Linear velocities of the center of gravity in the X, Y, and Z directions respectively.
p, q, r:	Roll, pitch and yaw velocities about the X, Y and Z axes respectively.
s:	Rotary velocity of the front axle about its center.
u1, u2, u3, u4:	Translatory velocities of the left-rear, left-front, right-front and right-rear wheel axles, in the X direction.
w1, w2, w3, w4:	Translatory velocities of the left-rear, left-front, right-front and right-rear axles in the negative z direction.
R1, R2, R3, R4:	Vertical force at the left-rear, left-front, right-front and right-rear axles.
F1, F2, F3, F4:	Thrust forces at the left-rear, left front, right-front and right-rear axles.
GV1, GV2, GV3, GV4:	Ground vertical velocities at the left-rear, left-front, right-front and right-rear wheel.
Mg:	Tractor weight at the (center of gravity).
FTX:	Horizontal force (a sum of forces) at the center of gravity.
FF:	Motion resistance force at the front wheel of the tractor.
FR:	Motion resistance force at the rear wheel of the tractor.
DBV:	Vertical drawbar-force component.
DBH:	Horizontal drawbar-force component.
TF2:	Axle torque at the left front tire.
TR1:	Axle torque at the left rear tire.

Table 3.1 continued

WF2:	Rotary velocity of the left front tire.
WR1:	Rotary velocity of the left rear tire.

Dimensions:

TWF:	Front tread width.
TWR:	Rear tread width
TW1, TW2, TW3, TW4:	Distance between the X axis and the left-rear, left-front, right-front and right-rear wheel centers.
RACG:	Vertical distance between the hitch point and the center of gravity.
FACG:	Vertical distance between the front axle and the center of gravity.
RF:	Radius of the front-left tire.
RR:	Rolling radius of the left rear tire.
HPCG:	Vertical distance between the hitch point and center of gravity.
DBHT:	Vertical distance between the drawbar and the ground.
HPCH:	Horizontal distance between the center of gravity and the hitch point.
WB:	Tractor wheel base.
WBF:	Distance between the center of gravity and the front axle.
WBR:	Distance between the center of gravity and the rear axle.

Others:

COG:	Center of gravity.

dimensions and the scheme for tractor vibratory system are shown. Table 3.1 is a list of definitions of the symbols used in Figure 3.1. The rigid body of the tractor could be represented as attached to a spring and damper setup vertically, laterally and in the fore-aft direction of motion. This vibratory system is a representation of the spring and damping effects of the rubber tires which result during operation. The farm tractor is unsprung, and the only damping and compliance between the rigid body and the ground is in the rubber tires if soil deformation is assumed absent.

For a complete analysis of the dynamics of a tillage-tractor system, it was appropriate to divide the system into subsystems. The subsystems could then be combined for an analysis of the dynamics of the interaction of the subsystems and those of the complete system. The system was divided into three main subsystems for a dynamic analysis: a) the drive train subsystem, b) the tire-soil interface or traction subsystem and c) the rigid-body or chassis subsystem. The subsystems were then combined to form the whole tractor implement system. External sources of excitation were then applied to the entire system model, and observations were made of the component and rigid body interaction dynamics. Further observations of energy exchanges and power distribution at points of interest in the model were conducted.

The external influences applied were terrain variation and implement forces. Of special interest was the tire-soil interface dynamics and energy exchanges. This interface formed the connection between the drive train and chassis rigid-body dynamics. It also is the most important energy exchange station for the energy flow between the engine and the drawbar. Tire-soil interface dynamics determine the amount of energy that is available to pull the implement at the drawbar. Parameters such as the drive-tire spring constant, damping coefficient, slip velocity and interface thrust-force determine the nature of the energy exchange. All of these parameters were affected by the external influences described above.

Figure 3.2 presents a schematic drawing of the drive train of a four-wheel drive tractor. The labels used on Figure 3.2 are defined in Table 3.2. Figure 3.2 displays the components of the drive train and the efforts (torques and forces) and flows (velocities) that determine the nature and the magnitude of the power exchange between them. Two different velocity labels are shown on some of the shafts and drive axles to account for any torsional displacement that would possibly occur under load. With torsional displacement the shafts or axles would have two different velocities at each end, e.g., WR4 and WR41 for the right-rear drive axle.

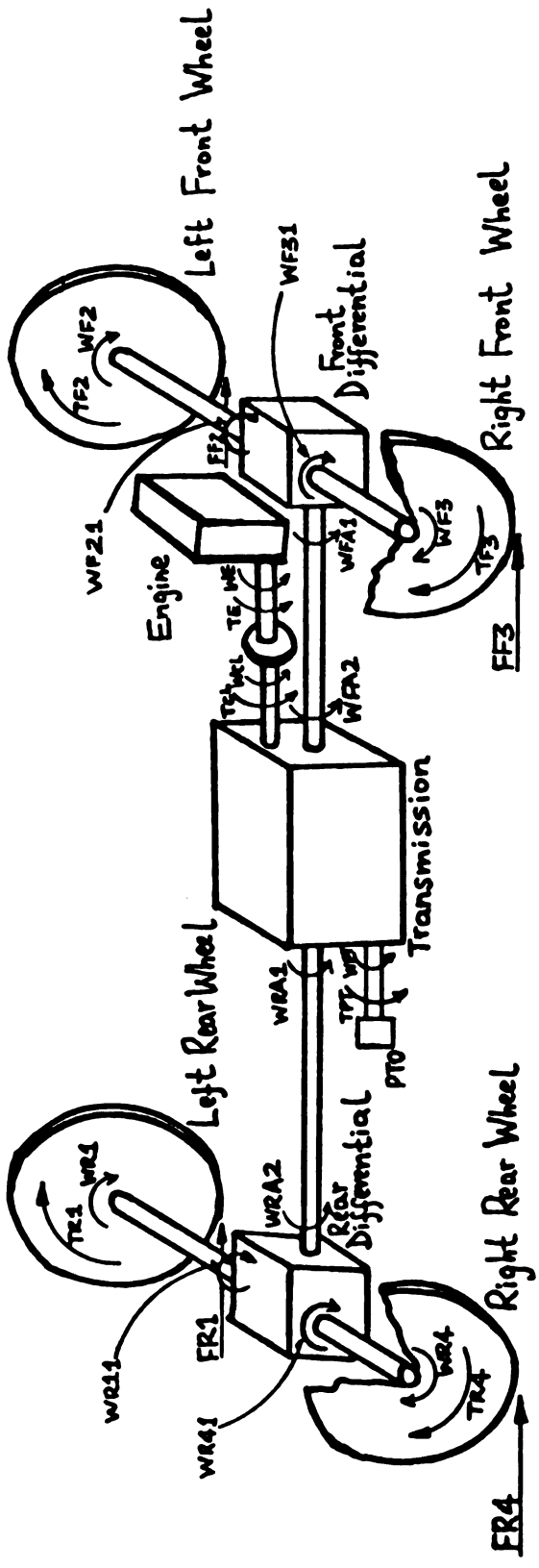

Figure 3.2: The Physical System Schematic for the Drive Train of a Four Wheel Drive Tractor

Table 3.2. Definitions of Labels Used on Figure 3.2

FR1, FR2, FF1: FF2	Thrust forces at the left-rear, left-front right-front and right-rear tires.
WF21, WF31, WR11: WR41	Drive axle velocities at the end connected to the differentials.
TE:	Torque in the engine-shaft (between engine and clutch)
WE:	Engine-shaft angular velocity.
TCL:	Torque in the shaft between the clutch and transmission.
WCL:	Angular velocity of the shaft between the clutch and transmission.
WFA1:	Angular velocity of the front-drive shaft at the end entering and the front differential.
WFA2:	Angular velocity of the front-drive shaft, at the end leaving the transmission.
WRA1:	Angular velocity of the rear-drive shaft at the end leaving the transmission. Angular velocity of the rear-drive shaft at the end entering the rear differential.
TPT:	Torque in the PTO shaft.
WBT:	Angular velocity of the PTO shaft.

Figure 3.3 demonstrates the power exchanges taking place between the components in Figure 3.2. Table 3.3 has the list of symbols used on Figure 3.3 and their definitions. Figure 3.3 shows the final-drives (speed-reducers between the differentials and the tires - FD1, FD2, FD3 and FD4) and the implement schematic. These two are absent on the drive train of Figure 3.2.

Figure 3.3 was the basis of the bond graph model development. It shows power leaving the prime driver (the engine) in the form of a torque (TE) and an angular velocity (WE). The power was transferred to drive a clutch which in turn drove the transmission. The transmission was a four-port component, and it divided the power into three portions to drive the front differential (F DIFF), the rear differential (R DIFF) and power take off (PTO). The rear differential further split the power into two portions to drive the right rear final drive (FD4) and the left-rear final drive (FD1). The front differential also had a similar power division to drive the right-front final drive (FD3) and the left-front final drive (FD2). The power from the final drives then went into the tires labelled 1, 2, 3 and 4 for the left-rear, left-front, right-front and the rear-right tires, respectively. The tires were presented as three port components with output power driving the chassis. Effects of soil tire interaction are considered later.

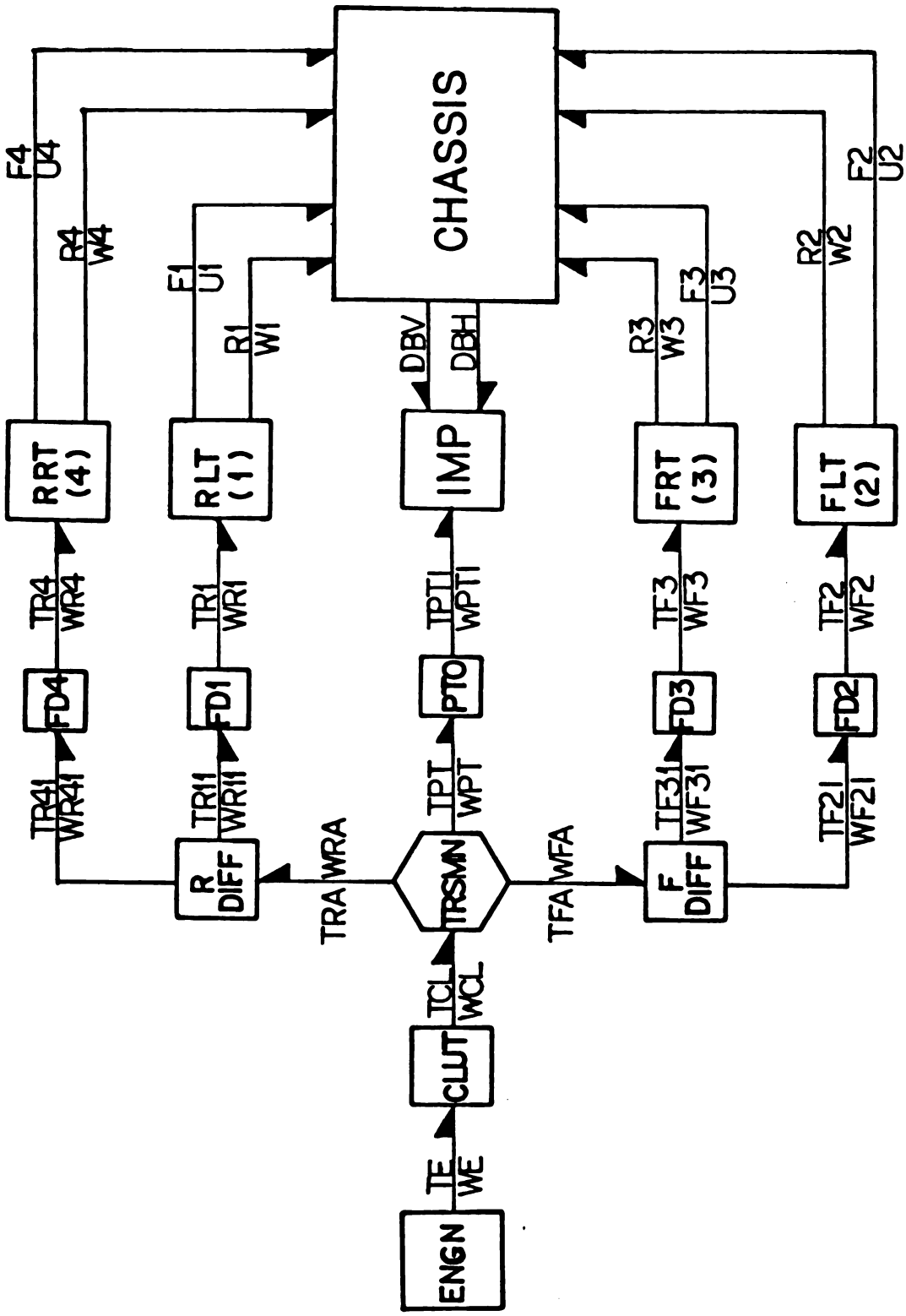

Figure 3.3: The Power Flow Schematic of a Four Wheel Drive Tractor Showing Efforts and Flows that Occur between System Components

Table 3.3. Definitions of the Labels used on Figure 3.3 Components.

Component	
ENGN:	Engine
CLUT:	Clutch
TRSMN:	Transmission
PTO:	Power Take-Off
IMP:	Implement
RRT:	Rear Right Tire
RLT:	Rear Left Tire
FRT:	Front Right Tire
FLT:	Front Left Tire
FD4:	Final Drive #4 (Right Rear)
FD1:	Final Drive #1 (Right Rear)
FD3:	Final Drive #3 (Front Right)
FD2:	Final Drive #2 (Front Left)

Power Bonds	
DBV:	Vertical component of drawbar force.
DBH:	Horizontal component of drawbar force.
All labels beginning with the letter T:	torque delivered between the particular components.
All labels beginning with the letter W:	angular velocities of shafts between the particular components.
Other forces and velocities:	F1, F2, F3, F4; R1, R2, R3, R4; U1, U2, U3, U4 and W1, W2, W3, W4 are defined on Table 3.1.

The tires supplied both a horizontal and vertical force to the chassis. From the tires, four horizontal (thrust) forces F1, F2, F3 and F4 drove the chassis with velocities U1, U2, U3 and U4 respectively. The vertical ground forces R1, R2, R3 and R4 support the chassis. The chassis has the vertical velocities w1, w2, w3 and w4 at these supports. The chassis was further acted upon by two other forces, the horizontal component (DBH) and the vertical component (DBV) of drawbar force. These forces were considered to be within the longitudinal plane of forward travel. All 10 forces acted on the chassis (rigid-body) to determine the amount of fore-aft, yaw, lateral, roll, heave and pitch motions of the chassis while occured.

Figure 3.3 presented the implement as a three port component. It represented a powered implement which received power from the power take-off (PTO). This kind of implement is capable of not only draining power from the chassis system through the power bonds DBV and DBH but also of putting power into the chassis system when the resultant implement force is a push on the chassis. When an implement was non-powered it only retarded the forward motion of the chassis. In such a case, the PTO node and the accompanying power bonds would be absent, making the implement (IMP) node a two-port node.

3.2. Modeling Assumptions and Simplifications

Modeling of the tractor-implement system is generally complex even after many simplification assumptions are made. Assumptions were necessary to make the system model one of a reasonable size and cost and with finite computation time.

The original bond graph subsystem model developed in this study was that of the power train. It included damping and compliance in the axles and drive shafts. Attempts to account for non-mechanical energy losses in the engine, clutch, transmission and the differential were made. The difference in angular displacement between the rim and the tire which allowed for torsional compliance of the tire was considered. Kinetic energies of the axles, drive shafts, gears, engine, clutch and the tires were all considered. With the above considerations, the power-train bond graph model quickly became very large, and the number of state variables increased considerably. Furthermore, the inclusion of all the stated compliance and inertia elements resulted in derivative causality (see appendix A), due to the accompanying statically coupled compliance and intertia elements.

For the sake of keeping the model a reasonable size and at the same time including only the important aspects of the physical system being modeled without oversimplification, the following assumptions were made:

1. The engine was the source of net torque available to the drive train at the crankshaft.

2. Kinetic energies of the axles, shafts and gears were negligible relative to that of the wheels, clutch (flywheel) and engine.
3. Potential energy stored in the axles and drive shafts was insignificant compared with that stored due to tire deflection.
4. Damping in the axles and drive shafts was negligible compared to that of the tires. The damping ratio for steel is about 0.06 percent compared to 3.0 percent for rubber tires (Summers, 1983). Friction in the bearings was neglected.
5. Losses in the transmission and differential resulted from gear meshes only.
6. Under static conditions, forces supported on both rear wheels and both front wheels were assumed equal.
7. The frame and axles of the tractor constituted a rigid body suspended only by the tires. The rigid body had three main degrees of freedom a) heave or the vertical displacement of the center of gravity, b) pitch or the rotation about the transverse axis through the center of gravity and c) roll or the rotation about the longitudinal axis.
8. Tires acted as linear springs with viscous damping and a point contact with the ground. Assuming a constant difference in angular displacement between the rim and the tire, torsional compliance could be considered absent.

9. The rotational inertia of front wheels about their axles was not significant.
10. The tractor differential transmitted equal amounts of torque to both drive wheels on a given axle.
11. The ground surface was rigid enough to be considered non-deformable.
12. Both rear and both front tires were exposed to the same terrain conditions, and rigid body displacements were small enough to allow the center of gravity and all tire centers to have the same forward velocity.
13. No structural vibrations were present. This allowed for a rigid body analysis of the chassis dynamics. The front axle had no rotary motion within the transverse vertical plane and about its support on the chassis.

Assumption 3 basically states that the shaft and axle torsion about their axis of rotation could be considered negligible. For example, considering the rear drive and front drive axles in Figure 3.2 angular velocities WRA1, WRA2, WFA2 and WFA1 could be considered equal.

Assumptions 4 and 5 follow from assumption 3, and they refer to the absence of energy dissipation along the drive shafts and axles. The only energy dissipated by the assumed infinitely stiff shafts and axles is that from the gear meshes.

Assumption 7 is based on the fact that, in the tillage operation, lateral motion and therefore yaw motion, (v and r on Figure 3.1) can be considered absent. Assumptions 7 and

8 together would change the physical system presented in Figure 3.1 by allowing for lateral and longitudinal spring-damper units to be disregarded. In other words, it would only consider the vertical spring-damper units on the tractor - the units directly under the tires (see Figure 3.1).

Assumption 7 was formed on the basis that pitch, heave and roll produced the predominantly excited degrees of freedom. This was because forcing functions in the tractor implement system were considered essentially vertical and horizontal parrallel to the direction of travel. The contribution of the yaw and lateral motions to the overall vibration problem was assumed to be negligible.

3.3 Supporting Models

3.3.1. Tractive Performance

In attempts to characterize the physical phenomenon of tire-soil interaction, researchers have had to use simplifying assumptions in the development of a theoretical basis for the interpretation of the field test results (Yong et al., 1984). Analytical difficulties of a theoretical approach were a result of poor knowledge of the effects of variables such as inflation pressure, tire shape, tire flexibility, tread size and the flow patterns of soil under moving wheels. Mechanical properties of both the soil and the pneumatic tire are complex.

Soil studies have disclosed little about how soil stress and strain are related. Shear tests have addressed stress and displacement; however, this has not given strain distribution within a sample. Stress-strain relations were necessary in reviewing the effect of slip on the theory of rolling motion (Leflaive, 1966). A given slip corresponds to a certain displacement between the wheel and the soil. If this displacement is large enough to mobilize full friction of the soil, coulombs law (which does not consider deformation quantitatively) could be applied. This approach, however, would not provide a basis for the description of the variation of pull and torque with changes in slip. It would also be necessary to determine the soils internal angle of friction. Another difficulty in the theoretical approach is the extensive and rapid soil deformation that can occur under a moving wheel, and the soil properties may differ from those under slowly applied loads in a laboratory. Therefore, while a knowledge of soil mechanics is a necessary guide for a physical understanding of wheel behavior, it does not lead to a direct theoretical solution.

The alternative to theorizing has been to experiment with wheels on soft soils. Graphical representations have been utilized to present the results of these tests and to describe the principles of the analysis technique. Slip as a percentage velocity loss has been used extensively as the reference variable for quantities such as drive axle torque

and wheel dynamic load ratio (Leflaive, 1966). Slippage velocity (the difference between wheel tangential velocity and vehicle forward velocity) has also been used as a reference variable (Yong et al., 1980).

Energy transfer at the tire soil interface could be divided into three main categories. Torque energy (the work done by the axle torque), pull energy and dissipated energy. Dissipated energy is the difference between the torque energy and the pull energy.

$$PE = TE - DE \qquad \ldots (3.1)$$

where:

PE = pull energy

TE = torque energy

DE = dissipated energy

Torque energy is positive in the case of a driving torque or negative for a braking wheel. Pull energy is positive when the wheel is developing a tractive effort and negative when the wheel is towed. Dissipated energy is always positive. Please see further development of empirical and mathematical relationships for the tire-soil interface in Appendix D.

The tractive performance models developed by Wismer and Luth (1974) are recommended for use in ASAE Standards Data: ASAE D230.3 (ASAE 1982a). These models are more useful for quantitative analysis of tractive performance compared to the empirically derived models described in Appendix D. The

latter are only useful for qualitative or specialized studies. The drawbar pull prediction model for agricultural drive tires on cohesive-frictional soils is

$$\frac{P}{W} = 0.75\ (1 - e^{-0.3C_nS}) - (\frac{1.2}{C_n} + 0.04) \quad \ldots \quad (3.2)$$

Where:

P = net drawbar pull

C_n = wheel numeric = (CI)bd/W ... (3.3)

Where:

CI = soil cone index

b = tire section width

d = unloaded tire diameter

W = wheel dynamic load

S = wheel slippage

All other variables are previously defined.

The wheel slippage effects on the drawbar pull to weight ratio, in Figure 3.4, vary significantly in the maximum tractive efficiency range and depend on the wheel numeric value. Tractive efficiency is defined as the ratio of the output power to the input power of the tractive device. Figure 3.5 shows the tractive efficiency relationship with wheel slippage on cohesive-frictional soils. Maximum tractive efficiency occurs between 5 and 20 percent slippage for hard, firm, tilled and soft soils.

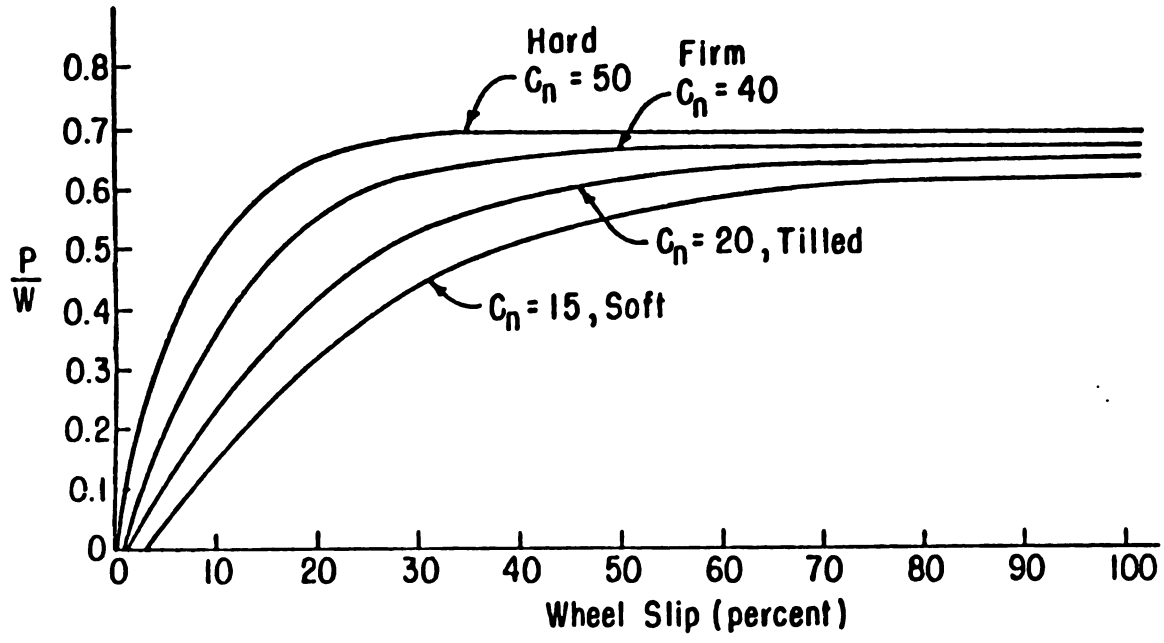

Figure 3.4. Relationship between Wheel Slip and Net Traction to Weight Ratio for Agricultural Drive Tires on Cohesive-Frictional Soils (Summers, 1983).

The wheel numeric can generally be used to classify the condition of the soil. For tires inflated such that the tire deflection is approximately 20 percent of the undeflected section height wheel numeric values of 50, 30, 20 and 15 correspond to hard, firm, tilled and soft soils respectively (ASAE, 1982a).

Zoz and Brixius (1979) presented a tractive performance model for agricultural drive tires on concrete. The drawbar pull to weight ratio model was developed using the same dimensionless ratios as Wismer and Luth (1974). The prediction equation for the pull ratio is:

$$\frac{P}{W} = 1.02 \left(1 - e^{-\left(\frac{kbdS}{W}\right)}\right) \qquad \ldots \quad (3.4)$$

where:

k = 400 kPa

All other variables as previously defined.

The towed tire motion resistance was assumed to be 2 percent of the dynamic load on the tire.

The models above were used in the model development and validation due to their quantitative analysis quality.

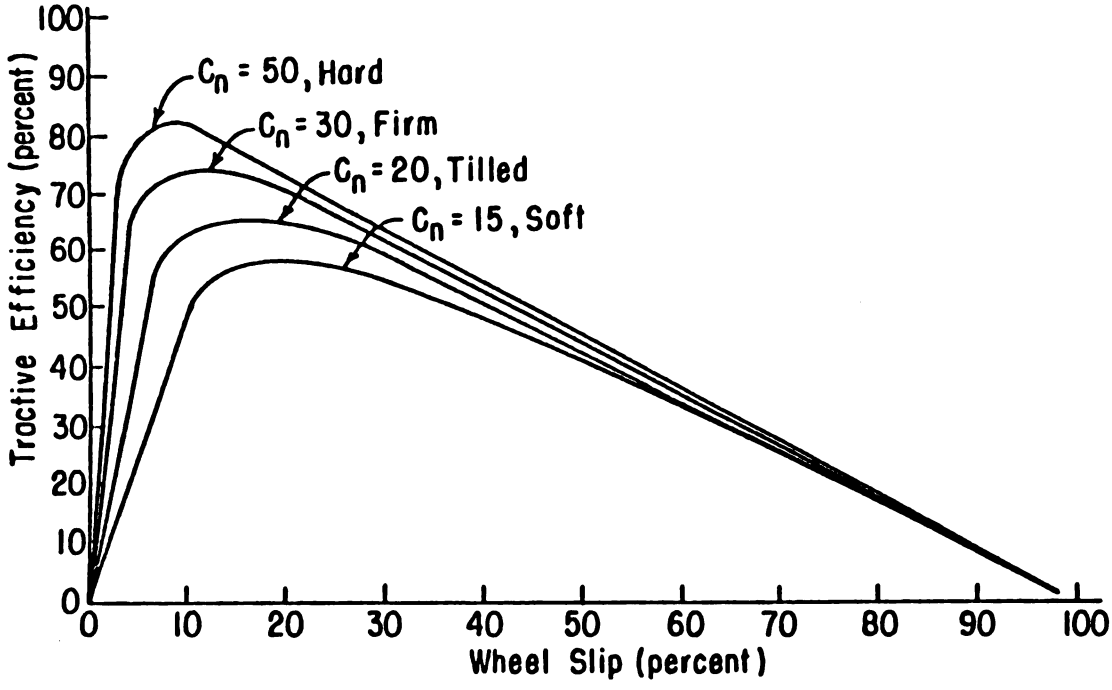

Fig 3.5. Relationship of Wheel Slip and Tractive Efficiency for Agricultural Drive Tires on Cohesive-Frictional Soils (Summers, 1983).

3.3.2. Implement Models

Drawbar loads were applied to a tractor during field operation by implements like the moldboard plow, chisel plow, field cultivator, etc. Kepner et al. (1978) suggested the draft model:

$$D_S = D_O + K\dot{x}^2 \qquad \ldots \quad (3.5)$$

where:

D_s = draft at velocity S

D_o = static component of draft

K = a constant dependent on implement and soil

$\dot{x}$ = forward velocity

This model was based on the concept that acceleration forces vary with the square of the velocity.

Implement draft requirements listed in ASAE data: ASAE D230.3 (ASAE, 1982a) are functions of the implement velocity and its square. Primary tillage implements such as moldboard plows and disk plows have drafts that vary with the square of velocity. Chisel plows and field cultivators are primary, tillage tools which have a velocity dependent draft. A general implement model can be written as:

$$L = A + B\dot{x} + C\dot{x}^2 \qquad \ldots \quad (3.6)$$

where:

L = draft

A = static component of draft

B, C = constants dependent on the implement and soil

Other variables are previously defined.

Drawbar vertical force component relationships have not been as well documented. Kepner et al. (1978) presented draft to vertical force ratios for moldboard plows, chisel-type implements and disk harrows. The moldboard plow varied between 0.1 and 0.3 depending on soil condition, depth of cut, share edge shape and sharpness, while that of harrows ranged from 0.5 to 1.5 depending on blade diameter and disk angle with respect to the direction of travel. Chisel type implements can have a vertical force directed upward or downward depending on the chisel-tool angle and shape. A moldboard plow bottom by itself has a downward-acting vertical component. This component determines the amount of useful soil suction that occurs during operation.

A vertical force-speed relationship for a mold board plow was presented by Summers (1983) as:

$$V = D + E\dot{x} \qquad \ldots \quad (3.7)$$

where:

V = vertical force

D = static component of vertical force

E = a constant dependent on the implement and soil

$\dot{x}$ = forward velocity

The vertical force applied to the tractor drawbar by an implement also depends on the implement hitch type. For implements having support wheels and a hinged hitch, the hitch normally can be adjusted so that the vertical force is negligible. On other types of hitches, the vertical force remains a significant force. A general model for implement vertical force is hard to develop since the vertical force varies significantly with tool shape and orientation, hitch type and the positioning of the support wheel.

3.3.3. ENPORT-7

ENPORT is an interactive computer program that aids in the modeling, simulation and performance assessment of dynamic systems (ROSENCODE, 1987). ENPORT allows for models to be described as combinations of block diagrams and bond graph elements. Power bonds are used to model exchanges of energy, while signals are used to model information flow.

ENPORT-7 is a version of ENPORT currently under development. ENPORT-7 has additional post-processing features for assessment of model performance. It provides the additional capability of displaying a system graph, a graphical display of results and a processed-data listing of effort, flow, momentum, displacement, power, net energy and node energy on bonds. Signals can also be displayed similarly. These data displays include data operation options of absolute mean, root mean square or mean value of the processed data. Linear, logarithmic and rank-ordered

scaling options accompany the system-graph display of processed data.

ENPORT is basically a bond graph and block diagram processor for non-linear systems. ENPORT-7 does not handle systems with elements that have derivative causality (see Appendix A). System bond graphs and block diagrams are input graphically and linearized system matrices and eigenmodes are obtainable from an originally non-linear system. Linearization is conducted at the initial time and state as specified by the user. The linearized system equations are presented in the form

$$\frac{dx}{dt} = A * x(t) + B * u(t) \qquad \ldots \quad (3.8)$$

and

$$y = C * x(t) + D * u(t) \qquad \ldots \quad (3.9)$$

where:

x = local state vector about the global state X

u = local input vector about the global input U

A, B, C and D are matrices of appropriate dimensions

y = local output vector

t = time

ENPORT provides several integrators with both fixed and variable computation step for finding time response of a system. ENPORT has the capability of solving system equations which are algebraically coupled. ENPORT's unique

user-friendly package includes the ability to set trap files and debugging flags for tracking the user's session and for storing additional system processing information.

ENPORT has a large library of element functions readily incorporated. It also has user defined functions which can be linked with the rest of the ENPORT program. The functions provide a link between a node in the system graph and equations defined by a FORTRAN subroutine. Please see ROSENCODE (1987) for more information.

3.4. Subsystem Bond Graph Models

3.4.1. The Drive Train Model

The physical system schematic of the drive train shown on Figure 3.2 was directly modeled into a bond graph. Figure 3.6 shows the two-wheel drive bond graph model reduced according to assumptions 1 through 5 of Section 3.2. Compliance (C), inertia (I) and dissipation (R) elements which represented shaft and axle potential and kinetic and dissipation energies were removed, in accordance with the assumptions.

The power flow within the drive train model was assumed to originate at the engine. It disregarded the fuel combustion process and accounted for heat energy losses within the engine. The engine was therefore modeled as a source of effort (SENG) driving the crank shaft and clutch components with inertia represented by the element IENG and frictional energy dissipation represented by the element

RENG. The torque transfer occured at a common-velocity junction 1ENG (For an understanding of the bond graph modeling procedure and terminology please see Rosenberg and Karnopp, 1983 and Appendix A). The power originated from the engine in the form of a torque (TE) at velocity WE (see Figure 3.2), and it is dispelled by energy dissipating (all elements whose labels begin with the letter R) elements, stored in the energy conservation (the C and I) elements or exchanged in the power conserving (Ø, 1, and TF) elements (see Appendix A).

The clutch was modeled as a constant-effort component with slippage-velocity loss to the RCL element, i.e., the clutch output velocity was less than the input velocity by an amount equal to the slippage velocity and the velocity dissipated by the RCL element. The transmission was modeled as both a power conserving and energy dissipating component. The RTRS element modeled the energy dissipated while the TFT element modeled the power conservation aspect. Across the TFT (transformer) element, velocity was raised or reduced by a transformation modulus (coefficient) while torque was reduced or raised by the same modulus (respectively). The power input and output across the TFT element remains constant. The overall power leaving the transmission entered the differential.

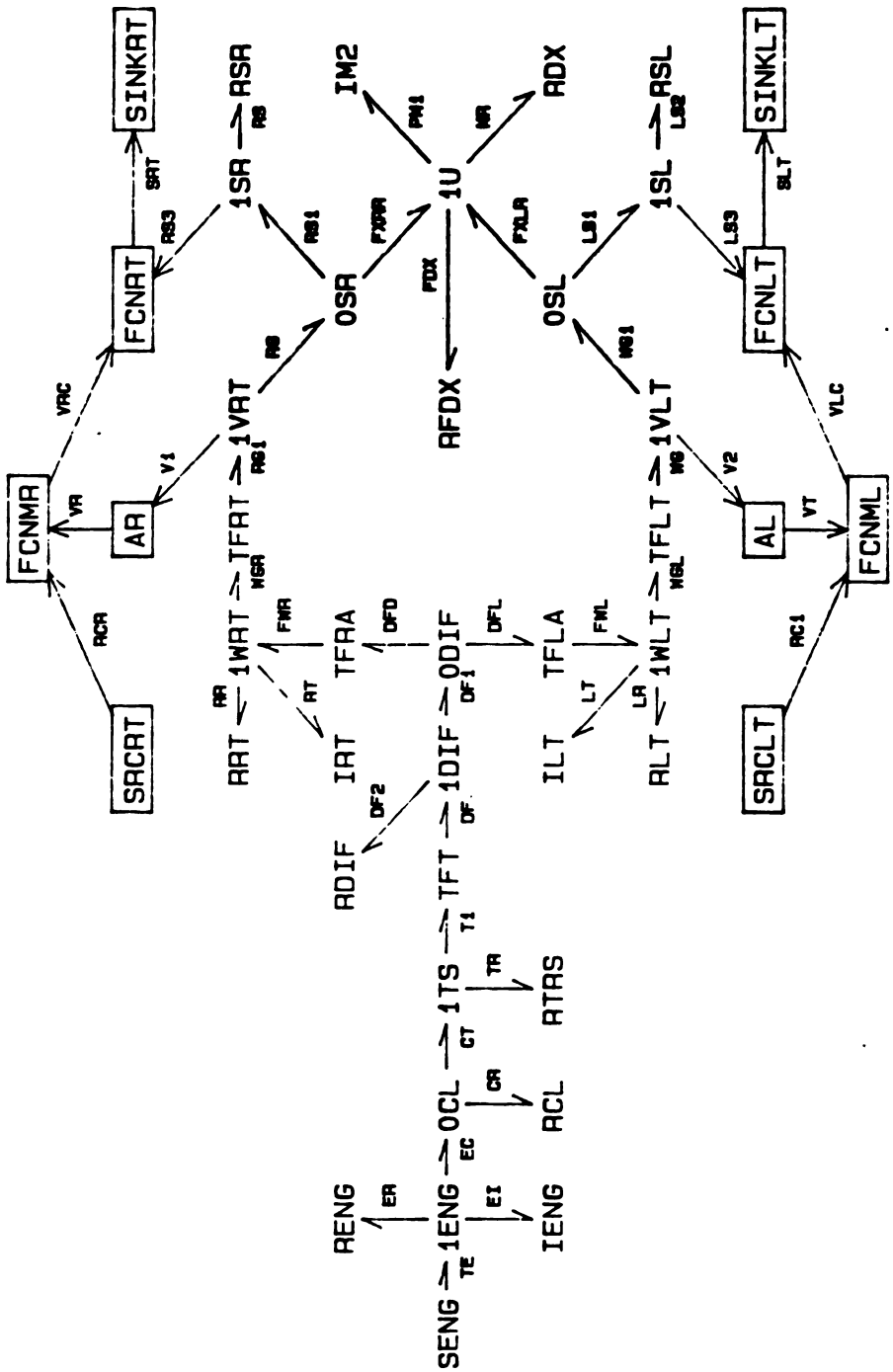

Figure 3.6: The Simplified Power Train Bond Graph Model of a Two Wheel Drive Tractor

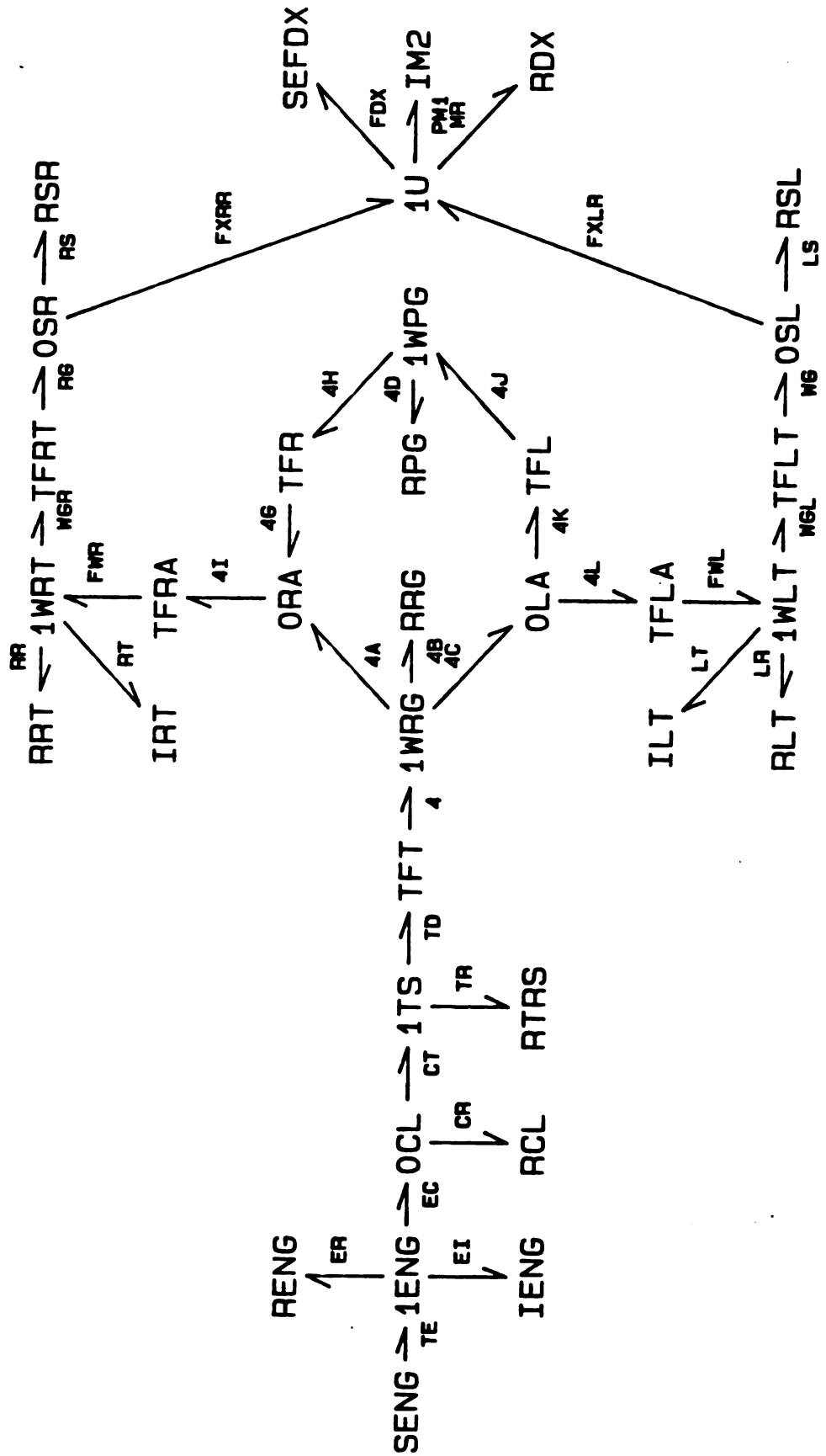

Figure 3.7: The Power Train Bond Graph Model Showing Differential Detail

The differential was modeled as a combination of energy dissipating and power conserving effects. The RDIF element modeled the energy dissipated while the TFLA and TFRA elements modeled the power conserving aspect of the unit. The differential split power at constant torque to the drive axles. The constant torque split was represented by the ØDIF junction. The causality of this junction was such that the drive-axle velocities (carrying equal torque at steady state) depended on the back-effect torque resulting from the tire-ground interface. The differential operation mode is generally used to transfer equal torque to the two drive axles. The velocity of the two axles depends upon the balance between the torque at the differential and the back-effect torque from the tire. When the velocities of the drive axles are different differential action will occur (please see Section 4.1.4 for further discussion of differential action).

Figure 3.7 develops the bond graph model developed to include differential detail, i.e., to allow for differential action dynamics to be observed. The overall effect of this model was to split the torque to the two drive axles. This case accounted for the difference in back-effect torques which caused the motion of the internal gears in the differential. The model in Figure 3.7 would be a necessary part of this study if the internal differential dynamics required explicit analysis.

Power leaving the differential through either drive-axle passed into a transformer element (TFRA or TFLA). This represented the final drive (a gear unit for reducing axle speed while raising torque to drive the tire) of the tractor. The 1WRT or 1WLT port is the constant-flow port representing the wheel velocity. The wheel rotated with some energy dissipation at the bearings (and any other rotation-resisting effect) which was represented by the RRT or RLT elements. The power exerted in the acceleration or deceleration of the wheel was represented by the IRT and ILT elements for the right and left drive-wheels respectively. The power-conserving transformer elements (TFRT and TFLT) have a transformation modulus of magnitude equal to the drive wheel rolling radius. They converted rotary velocity and torque of the wheel to tangential linear velocity and thrust force respectively, at the periphery of the wheel. The thrust force at the tire-soil interface was represented by the common effort junctions (ØSR and ØSL). The slippage velocity loss was set by the defined functions of the dissipation elements (RSR and RSL). This function determined the maximum possible thrust force the tires could generate at the ØSR and ØSL tire-soil interfaces.

Bonds FXRR and FXLR represented the input driving power available to drive the chassis forward. In driving the chassis, the forces available need to overcome the energy dissipating force associated with rolling-resistance element RDX, the energy storage chassis-acceleration element IM2 and

the motion retarding (negative source of effort) RFDX element, which represents the draft force. When the drawbar force was represented by a negative source of effort the force was entered as a function of time. When drawbar force is defined in terms of tractor forward velocity it can be represented as an energy dissipating element.

The models on Figures 3.6 and 3.7 are complete basic representations of the power train energy flow. However as the power train drives the chassis, the dynamic weight on the wheels influences the thrust force generation and motion resistance force at the wheels. This influence was not incorporated in the models of Figures 3.6 and 3.7. Its incorporation is discussed in Section 3.4.3. If the models of Figures 3.6 and 3.7 were to be used in their current form (without the chassis model attached), the dynamic weight would have to be a factor in the function defining the rolling resistance and the thrust force generated. The constitutive equations would look like:

$$E.RS = f(F.RS, W) \quad \ldots \quad (3.10)$$

and

$$E.NR = f(F.NR, W) \quad \ldots \quad (3.11)$$

where:

E.RS = thrust force at tire-soil interface

F.RS = slip velocity

E.NR = total rolling resistance

F.NR = tractor forward velocity

W = wheel dynamic load

These relationships are incorporated into the traction model of Section 3.4.3. The model of Figure 3.6 was tried as a simulation model in this simple form.

3.4.2. The Rigid Body Chassis Model

The behavior of a tractor while traversing a general terrain requires the theory of rigid body dynamics for its description. The complete chassis motions of a four-wheel vehicle without suspension are described by six degrees of freedom for the rigid body chassis (see Figures 3.1. and 3.8), one degree of freedom allowing the front axle to roll relative to the pivot attaching it to the chassis and one degree of freedom for the rotation of each independently driven wheel. The six coordinates describing the motion of the chassis are forward displacement, vertical displacement (heave), lateral displacement, pitch displacement (angular displacement about the lateral axis), roll displacement (angular displacement about the longitudinal axis) and yaw displacement (angular displacement about the vertical axis). The motions of the driver wheels are coupled through the differential and are equivalent when differential motion does not occur.

Figure 3.8 is a schematic of the rigid body chassis. External forces acting on the body and the six-degrees of freedom linear and angular displacements (velocities) are represented. At the end of each axle (FA - the front axle

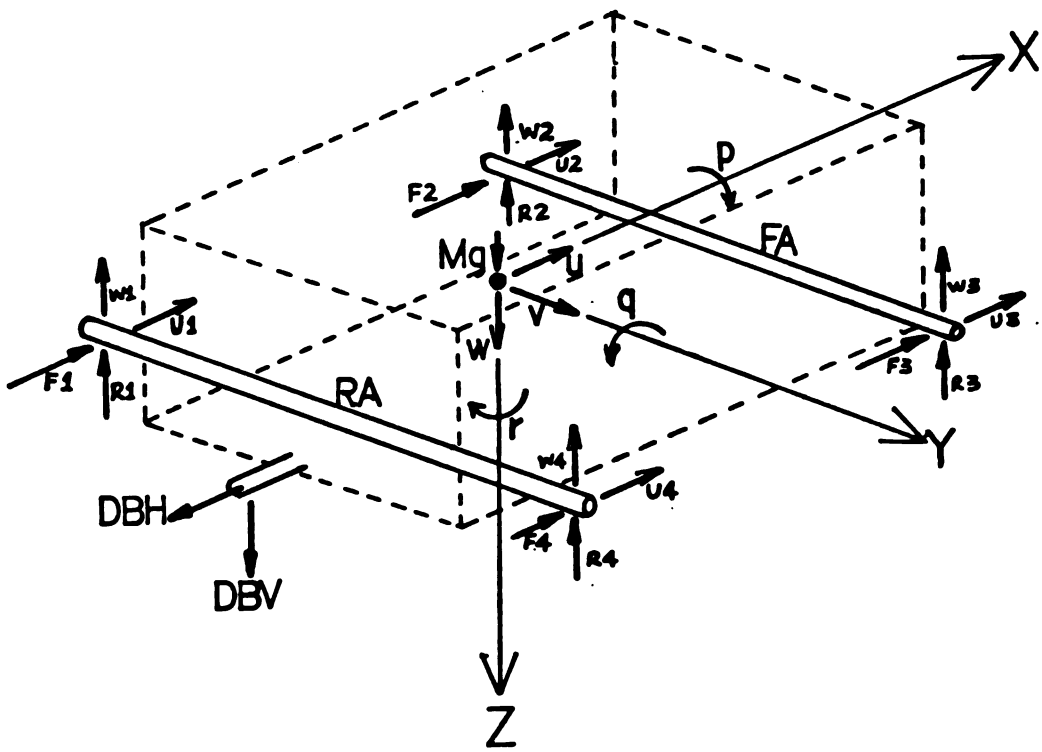

Figure 3.8: A Schematic Drawing of Forces and Velocities of the Rigid Body of a Farm Tractor

and RA - the rear axle), the vertical and horizontal components of axle-end forces and velocities are also shown. All labels were previously defined in Table 3.1.

The performance of agricultural tractors subjected to drawbar loading during normal field operation is dependent on the drawbar loading in the horizontal and vertical directions. These are shown as DBH and DBV on Figure 3.8. Since lateral forces on the tractor are relatively less significant, the motion of the tractor can be considered as constrained to a vertical plane in the direction of forward travel. The necessary coordinates to describe this motion are forward displacement, vertical displacement, pitch displacement and angular displacement of the rear wheels as shown on Figure 3.1 and 3.8. These displacements are associated with velocities u, w, q, WR1 and WR2. The directions of motion in Figures 3.1 and 3.8 are consistent with the right hand system of rotation used for vectors and the forward motion of a tractor during normal field operation. In this system pitch motion was positive backwards and heave motion was positive downwards. All velocities and accelerations were assumed to be positive in the same directions as the displacements.

The rigid body dynamics were considered about a body centered coordinate frame where the coordinate center is located at the tractor's center of mass. Chassis motions were considered small (see Assumption 12 in section 3.2). For example - if pitch displacement occurred in the chassis

of the tractor, it was assumed that it would not affect the rotary motion of the front tires. The pitch displacement and wheel rotation were assumed to be independent, and therefore they did not need to be vectorially added to obtain absolute wheel displacements.

To develop the bond graph model for the chassis rigid body motions, 8 velocities were considered. These corresponded to the heave, roll, pitch and forward displacements of the rigid body at and about the center of gravity, plus the four displacements of the four axles at the wheel centers associated with velocities w1, w2, w3 and w4. The forward velocity (u) of the center of mass was assumed equal to the forward velocity at the wheel centers i.e. $u = u_1 = u_2 = u_3 = u_4$. This velocity however resulted from combined effect of forces F1, F2, F3 and F4 (see Figure 3.8) the thrust forces of the wheels at the ground. As far as rigid body motions were concerned the velocity (u) was therefore considered as generated at the ground and was therefore incorporated into the traction model of Section 3.3.3.

The rigid body motions modeling procedure was conducted as follows: Common-velocity 1-junctions were established for the pitch, roll, heave and four wheel-center axle vertical velocities. Common-effort Ø-junctions were established for the wheel-center vertical forces. To each of the pitch, roll and heave velocities, inertia elements IJQ, IJP and IM1 were added (see Figure 3.9). The tractor

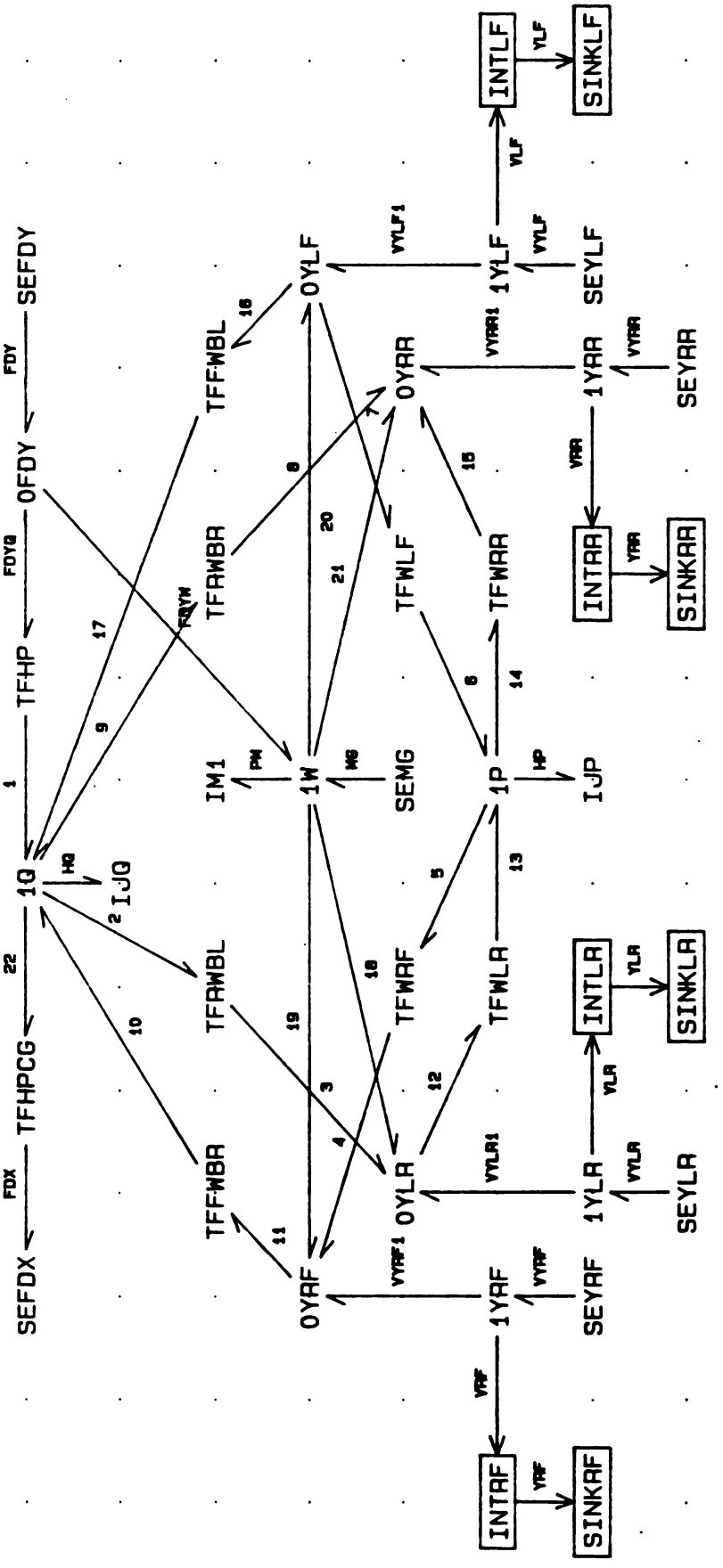

Figure 3.9: A Rigid Body Bond Graph Model of the Tractor Chassis

weight was accounted for by a heave-motion-enhancing source of effort shown as element SEMG on Figure 3.9.

Taking moments about the center of gravity and summing forces at 1-junctions and velocities at 0-junctions the following mathematical relationships were established:

$$\Sigma\ V(LRA):\quad w1 = -w - q * (WBR) + p * (TW1) \quad ... \quad (3.12)$$

$$\Sigma\ V(LFA):\quad w2 = -w + q * (WBF) + p * (TW2) \quad ... \quad (3.13)$$

$$\Sigma\ V(RFA):\quad w3 = -w + q * (WBF) - p * (TW3) \quad ... \quad (3.14)$$

$$\Sigma\ V(RRA):\quad w4 = -w - q * (WBR) - p * (TW4) \quad ... \quad (3.15)$$

$$\Sigma\ M\ (1q):\quad \dot{H}_q = R2 * (WBF) + R3 * (WBF) - R1 * (WBR) - R4 * (WBR) + DBH * (HPCH) - DBV * (HPCV) \quad ... \quad (3.16)$$

$$\Sigma\ F\ (1w):\quad \dot{P}_m = Mg - R1 - R3 - R2 - R4 + DBV \quad ... \quad (3.17)$$

$$\Sigma\ M\ (1p):\quad \dot{H}_p = R1 * (TW1) + R2 * (TW2) - R3 * (TW3) - R4 * (TW4) \quad ... \quad (3.18)$$

where:

Σ V(LRA) = sum of velocities at the left rear axle (wheel) center

Σ V(LFA) = sum of velocities at the left front axle (wheel) center, etc.

Σ M(1q) = sum of moments about the common-velocity 1q junction

Σ F(1w) = sum of forces at the common-velocity 1w junction

Σ M (lp) = sum of moments about the common-velocity lp junction

H_q = angular momentum due to q (pitch velocity)

P_m = linear momentum due to w (heave velocity)

H_p = angular momentum due to p (roll velocity)

All other variables are as previously defined on Table 3.1 and shown on Figure 3.1

These equations were used to draw the rigid-support, rigid-body (chassis) bond graph model on Figure 3.9. The distances in the parenthesis of the equations make the transformer-element moduli on the bond graph. Notice that at this point the model assumes stiff (no compliance or energy dissipation) supports at the wheels, hence, the modeling of the supports (elements SEYRF, SEYLR, SEYRR, SEYLF) as sources of effort. To make it possible to observe instantaneous displacements at the axles the vertical velocities were integrated (functions INTLF and INTRF), and the results were received in SINK-function elements (SINKRF and SINKLF). Elements SEFDX and SEFDY are the source of effort elements representing the horizontal and vertical components of drawbar force (DBH and DBV). All element labels beginning with TF represent the power conserving moduli relating the flows and efforts on their two sides.

The tractor chassis was considered as a mass sprung only by the elastic characteristics of the pneumatic tires. Tire forces were supported by the soil with the weight of the tractor being the only other vertical force acting on

the tractor. Assuming the rigid body of the chassis had negligible damping, the only other source of damping was the tires. The dissipating velocities associated with the tire deflections were represented by the difference in velocities between the axle and the ground velocity. The stiffness of the tire determined the magnitude of the deflection of the tire spring components.

Figure 3.10 shows the same chassis model as Figure 3.9 but expanded with tires added to the supports. Tire motion compliance and energy dissipation are represented by the elements CRRT, CLRT, CRFT and CLFT and RRRT, RLRT, RRFT and RLFT respectively. The ground was modeled as a source of flow (velocity). Elements 1YRR and 1YLR still represent the axle-displacement velocities. The velocities of bonds 28, 36, 24 and 32 from the common-effort ØLRT, ØLFT, ØRFT and ØRRT velocity summations formed the damping-element dissipation velocities (see Figure 3.10). They were obtained from the equations (see Figure 3.1):

$$\Sigma\ V(LRT):\quad F.28 = GV1 - w1 \qquad \ldots \quad (3.19)$$

$$\Sigma\ V(LFT):\quad F.36 = GV2 - w2 \qquad \ldots \quad (3.20)$$

$$\Sigma\ V(RFT):\quad F.24 = GV3 - w3 \qquad \ldots \quad (3.21)$$

$$\Sigma\ V(RRT):\quad F.32 = GV4 - w4 \qquad \ldots \quad (3.22)$$

where:

Σ V(LRT) = sum of velocities at the left rear tire

Σ V(LFT) = sum of velocities at the left front tire

Σ V(RFT) = sum of velocities at the right front tire

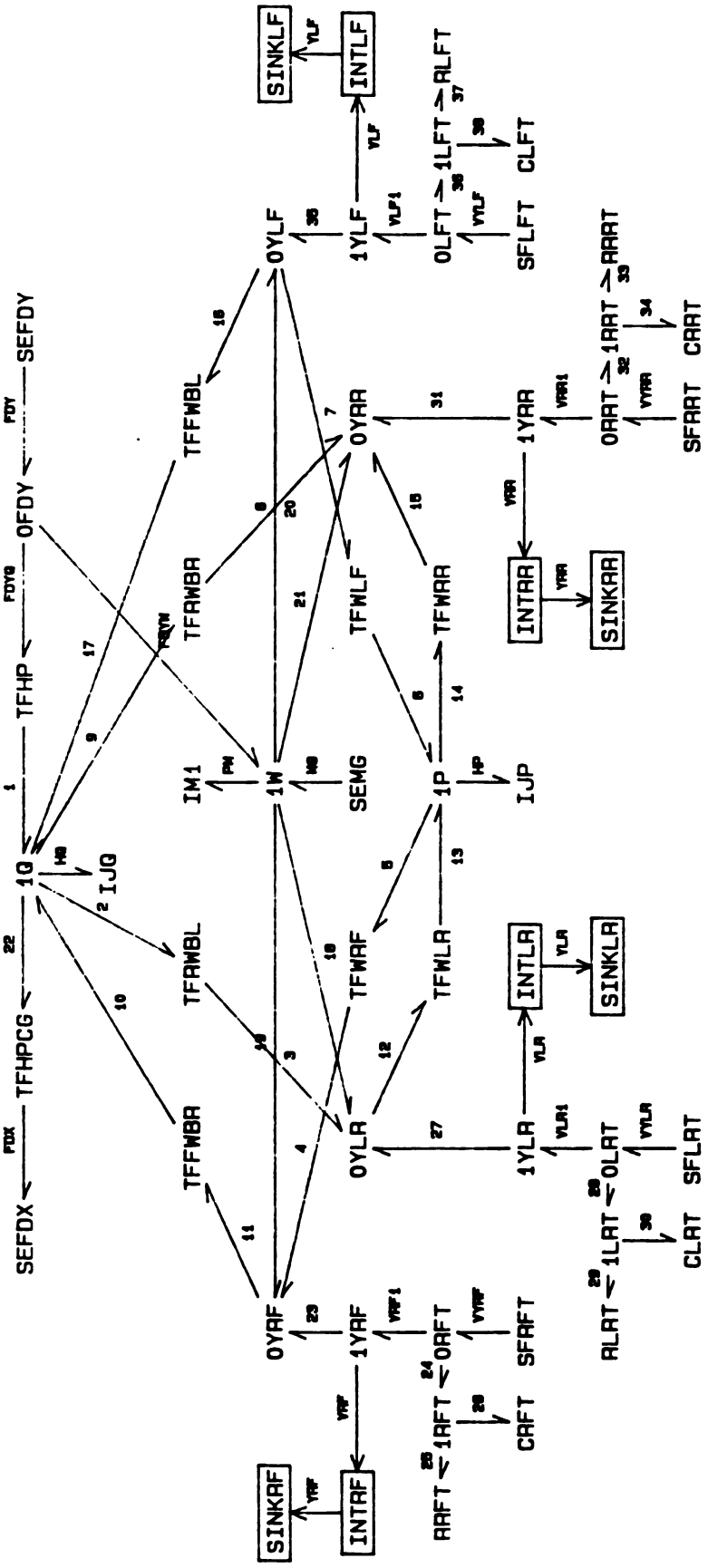

Figure 3.10: A Rigid Body Bond Graph Model of a Tractor Chassis with Tires

Σ V(RRT) = sum of velocities at the right rear tire

F.28 = velocity on bond 28

F.36 = velocity on bond 36

F.24 = velocity on bond 24.

F.32 = velocity on bond 32.

All other variables previously defined on Table 3.1.

While the spring and damper units at each wheel in Figure 3.1 experience different component forces, the velocity experienced by the damper element was the same as that experienced by the spring element. The model of Figure 3.10 represents this physical setup by the common effort junctions ØLRT, ØLFT, ØRFT and ØRRT which carry the force shared by bonds 29 and 30, 37 and 38, 25 and 26 and 33 and 34 respectively .

3.4.3. Traction Model

At the tire-soil interface the ground reaction included rolling resistance, traction and lateral forces in addition to the radial component of the tire force.

In this study, a point contact tire-ground interface model was used. Torsional and lateral compliance and dissipation effects of the wheels were neglected (see section 3.2). Lateral forces on the wheel were insignificant compared with radial and tractive forces when a farm tractor's travel was a straight line. A point contact model was considered as a simplification of a model

that would allow the tire to sense ground conditions at points of the tire contact patch other than the one through which all tire-ground forces acted. For a point-contact model, the ground surface needs to satisfy the following conditions (Davis, 1973): a) the surface in the path of the wheel should have no step changes in elevation and b) the wavelength of the ground surface should be at least 3 times the tire ground contact patch length.

The traction bond graph model was developed to account for the fore-aft motion of the tractor, the tractive forces, the vertical ground velocity and the influence of the dynamic load on the wheel. The dynamic load on the wheel also influenced the traction (thrust) force the wheel was capable of generating. The ground was assumed to be non-deformable although the elevation of the ground surface varied in any selected form along the path of travel of the tractor. Apart from the dynamic load on the wheel, other important factors included the tire-tread configuration and dimensions and the slippage at the tire-soil interface.

Figure 3.11 presents the rigid body chassis model of Figure 3.10 with ground velocity and terrain characteristics incorporated. As shown, the chassis was driven by a force SEFXT. At the forward motion velocity node (1U), there was an inertia element (IMZ) to account for chassis forward-motion acceleration. Node 1U was also connected to the common-effort junction ØFDX through bond FDXU. The effort

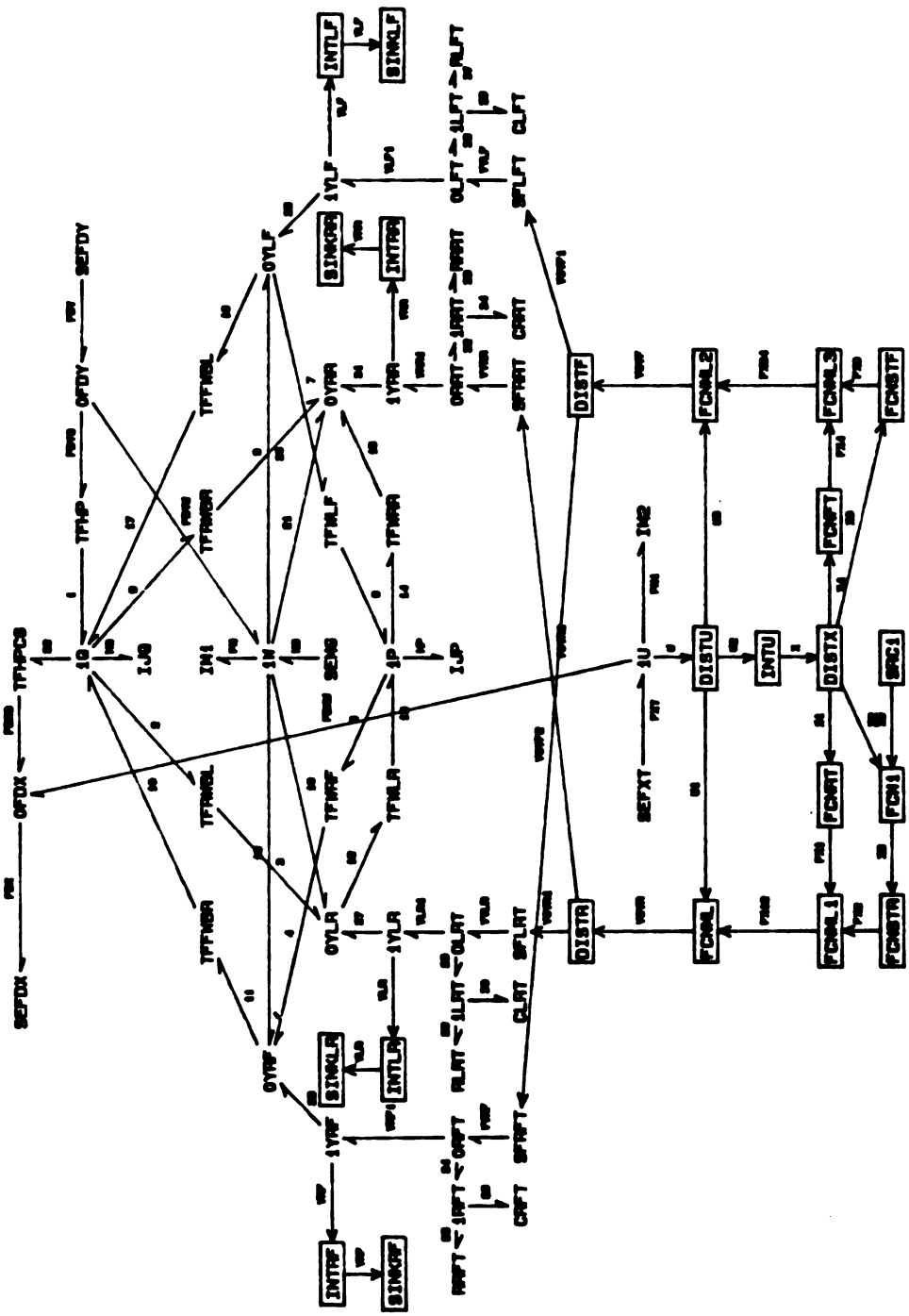

Figure 3.11: A Rigid Body Chassis Model with Ground Velocity and Terrain Variations Incorporated

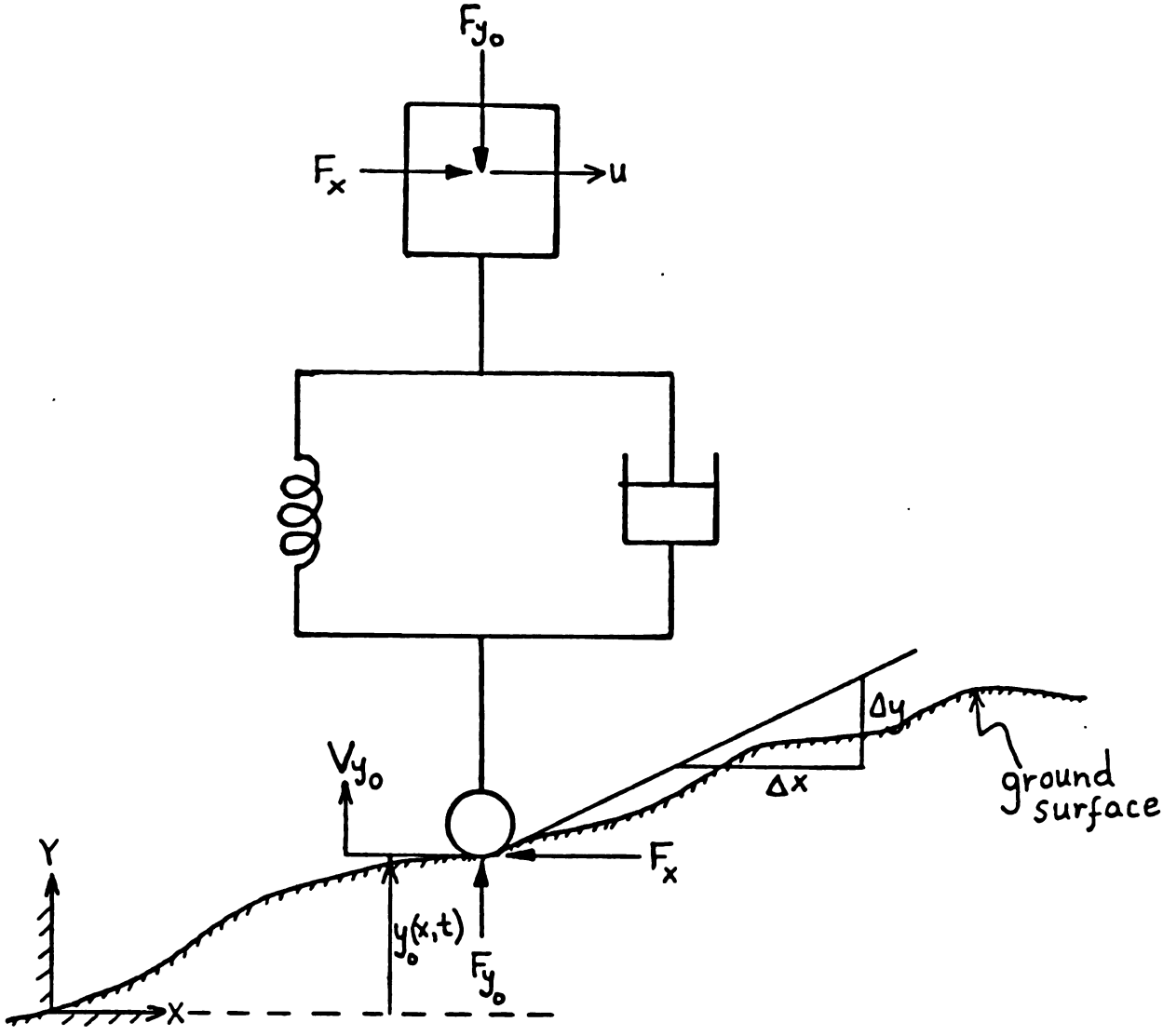

Figure 3.12: A Simplified Schematic Model of The Tractor Tire Traversing a Varying Slope Terrain

at this junction was SEFDX, the horizontal drawbar component force. SEFDX affected the fore-aft motion (1U) as well as the pitch motion of the tractor (1Q) with a moment of magnitude determined by the modulus of the transformer element TFHPCG.

The modeling of the tire-soil interface required the establishment of a relationship between the horizontal thrust force, the accompanying velocity, the vertical wheel load and the accompanying vertical ground velocity.

Figure 3.12 is the schematic of the rigid body mass placed on a tire that is traversing a variable slope terrain with a horizontal velocity (u). The ground elevation (y) varies with displacement (x). Displacement (x) is a function of time to obtain the vertical ground velocity with respect to time, partial derivatives of velocity with respect to displacement (x) and time (t) are required:

$$\frac{dy\ (x)}{dt} = \frac{dy}{dx} \cdot \frac{dx}{dt} \qquad \ldots \quad (3.23)$$

where:

$$\frac{dy\ (x)}{dt} = V_{y0} \quad \text{and} \quad \frac{dx}{dt} = u$$

y(x) = the terrain function

All other variables are as previously defined.

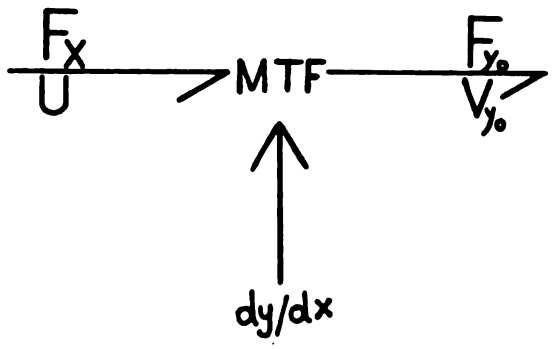

Fig. 3.13: Horizontal and Vertical Tire Force and Velocity Bond Graph Representation

In bond graph form dy/dx could be considered as a modulated transformer (MTF) modulus relating vertical ground velocity (V_{y0}) to the horizontal velocity (u) and the corresponding vertical and horizontal forces at the tire-soil interface (see Figure 3.13).

Figure 3.11 carries the representation of Equation 3.23 in the form of a block diagram. Forward velocity (u) was entered (in form of a signal u) into an integrator block INTU where it was integrated and displacement x obtained. The same velocity (u) (from the distributor element DISTU) is an input for the functions FCML and FCML2. The displacement (x) (from the distributor element DISTX) becomes an input for the functions FCNFT and FCNRT. The y(x) function defined the terrain variation with respect to x. The outputs FX4 and FX1 were multiplied with the outputs

of the unit step functions (FCNSTF and FCNSTR) within blocks FCNML3 and FCNML1 respectively. The multiplication was done as a means of truncating the terrain variation function and to make it possible to introduce a delay between the front and the rear tires. The truncation was a means of allowing the user of the model to select the value of displacement at which variable terrain becomes effective. The blocks FCML and FCNML2 contained the multiplication functions which multiply dy/dx by dx/dt to produce dy/dt. The vertical ground velocities were distributed to the rear and front tires, by elements DISTR and DISTF respectively. The signals VGYR1, VGYR2, VGYF1 and VGYF2 were the vertical ground forces at the tire-ground interface.

Figure 3.14 demonstrates the combination of the drive train model (Figure 3.7) and the rigid body chassis model with terrain (Figure 3.11). The wheel thrust drive forces in bonds FXLR and FXRR (Figure 3.14) replaced the general drive force of bond SEFXT (Figure 3.11).

In Figure 3.14 the terrain model was modified by reducing the number of blocks and by utilizing the user-defined subroutine package available in ENPORT-7 (see Section 3.3.3). Blocks FCN18F and FCN18R now contain the dy/dx computation subroutines (with ground displacement as input) defined as function SUBR18 in Section 4.4 and listed in Appendix A.

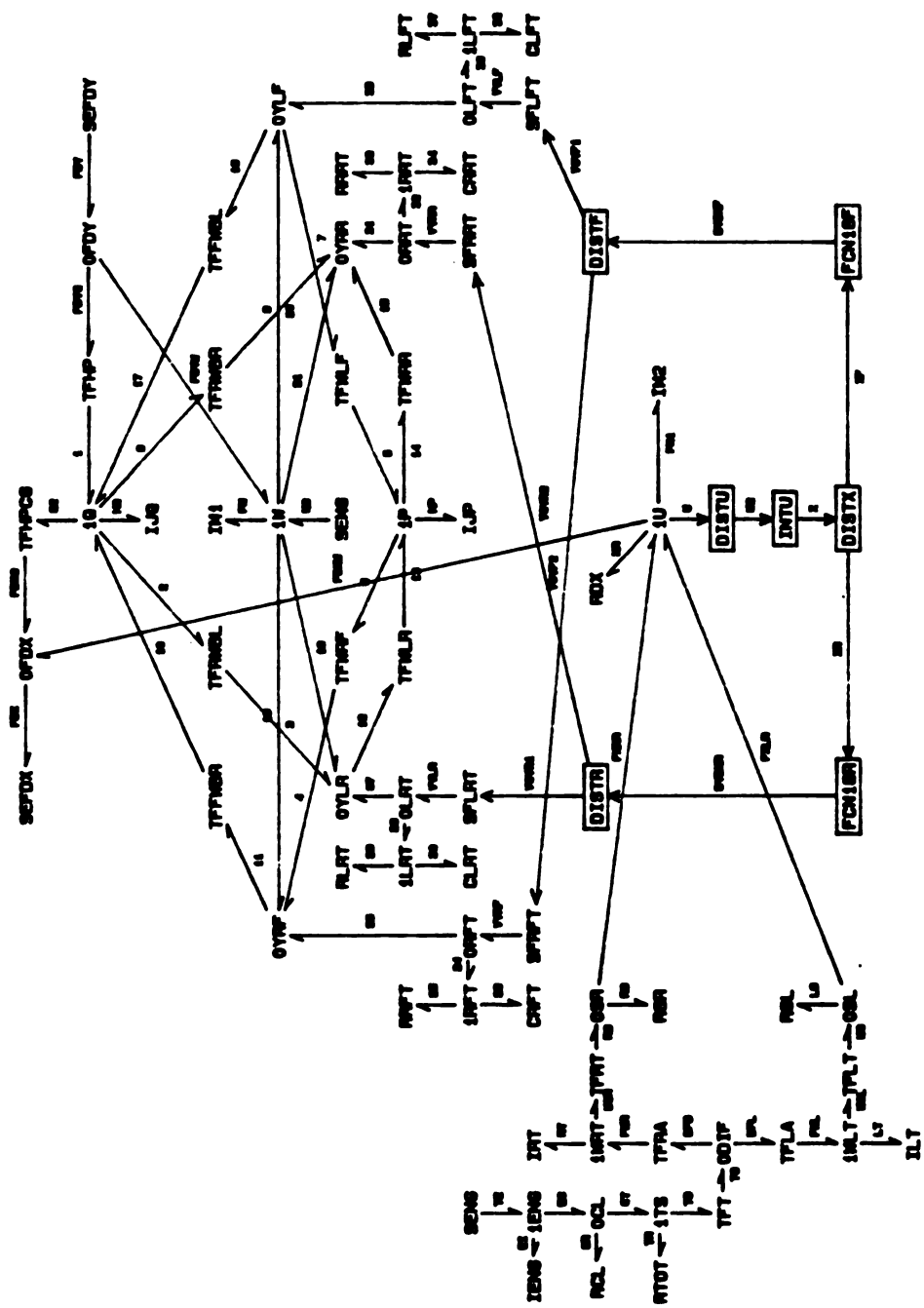

Figure 3.14: The Combined Rigid Body Chassis and Power Train Model of a Two Wheel Drive Tractor

The combined model bond graph of Figure 3.14 simulated the chassis and power train dynamics with limitations. In normal tractor operation both the thrust force developed at the tire-soil interface and the rolling resistance to motion were dependent on the dynamic load on the tire. At high velocities rolling resistance was further dependent on the forward velocity of the tractor (Greenlee et al., 1986). The thrust force developed at the tire-soil interface was also dependent on slippage velocity while both (thrust force and rolling resistance) were dependent on wheel dimensions, tire configuration and soil physical characteristics. In this study, simulated tractor forward velocities were in the range of 0 to 10 km per hour and within this range rolling resistance was assumed to be independent of velocity. Figure 3.15 is a quantitative model usable for relating the thrust force P to slip velocity. This is the LIMITER function used to define the slip velocity elements of the bond graph model, RSR and RSL for the right and left drive tires in the case of a two wheel drive tractor (Figure 3.14). The curves of Figure 3.15 are in accordance with Figures D.4 through D.6 and follow from the work of Yong (1980) (see Appendix D).

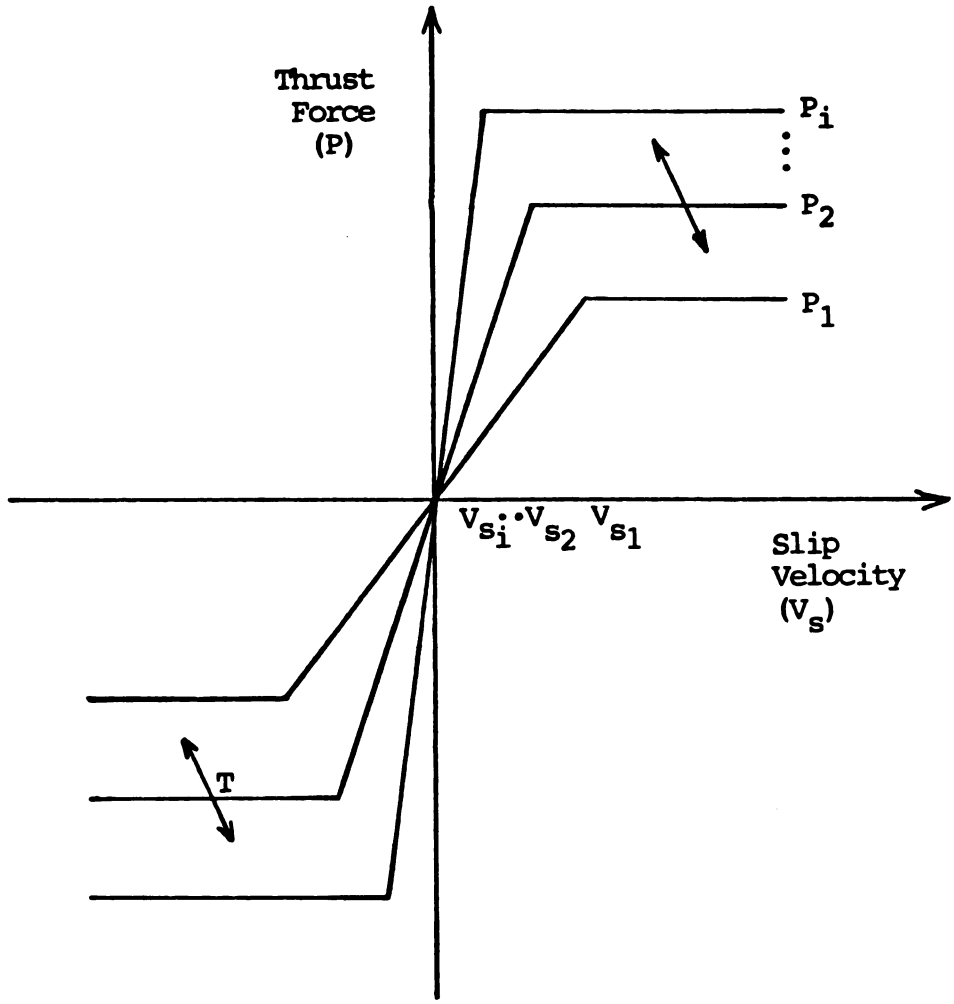

Figure 3.15. A Qualitative Model of Tire-Ground Thrust Force Variation with Slip Velocity

The double arrows marked T on Figure 3.15 describe the general tendency for the thrust force and slip velocity to vary under the influence of varying traction parameters like wheel dynamic load, soil firmness, varying tire configurations or dimensions, and varying tire pressure on frictional soils.

In an attempt to accommodate this wide variety of factors that determine the prevailing thrust force-slip

velocity relationship (hence the selection of the appropriate curve P_i on Figure 3.15), the Wismer and Luth (1974) mathematical model was incorporated into the bond graph model of Figure 3.14. The functions of slip velocity elements RSR and RSL (as Figure 3.15) determined the maximum possible thrust generatable (P_i) and the corresponding threshold slip velocity (V_{si}).

The Wismer and Luth (1974) model (see Section 3.3.1) required slip velocity (as a percentage of theoretical velocity), wheel numeric (C_n) and the dynamic weight as inputs for the computation of thrust force (P). It also required the dynamic weight and wheel numeric as inputs for the computation of rolling resistance force on the wheel.

Figure 3.16 demonstrates the incorporation of the Wismer and Luth mathematical model into the two wheel drive bond graph model of Figure 3.14. For each of the drive wheels a thrust force and a rolling resistance force were computed and used as driving and retarding forces of the forward motion (at node 1u on the bond graph). A rolling resistance force was computed for each of the towed (non-driven) front wheels as well.

The left rear drive tire, whose theoretical forward velocity (peripheral) was represented by node 1VLRT, had an (axle) actual forward velocity represented by node ULR. That was the same velocity as 1U composing signal ULRS1. The left rear drive wheel has a slippage velocity 1SLR. To compute the slip velocity as a percent of the theoretical

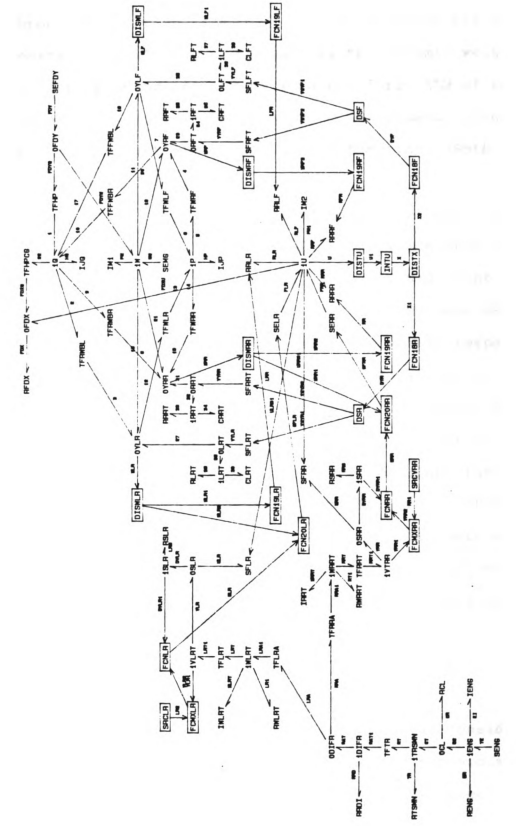

Figure 3.16: The Two Wheel Drive Tractor Bond Graph Model Showing the Incorporation of the Wismer-Luth Model for Thrust Force and Rolling Resistance Computation

velocity the division was done in FCNLR. FCN20LR, a subroutine function, computed the thrust force FLR of element SELR. The second input was the dynamic weight WLRZ. The corresponding rolling resistance (force RLR of element RRLR at node 1U) was computed using the dynamic weight input WLR1 in block FCN19LR, a subroutine function. Both WLR1 and WLR2 equal WLR of element ØYLR.

A similar computation was conducted for the right rear drive wheel to obtain the forces for elements SERR and RRRR. Rolling resistance computations for the towed front wheels were similarly incorporated for elements RRLF and RRRF representing left front and right front wheels respectively.

On Figure 3.17 there is a further expansion of Figure 3.14 which was added for the computation of draft force. In accordance with Equation 3.5 draft is a function of the square of forward velocity (1U). The summation function of block FCNFDX adds the constant input from block SRCFDX to a product of a coefficient and the square of forward velocity (signals U2 and U3). The output is FDX1 a signal making the magnitude of the force in element SEFDX, the horizontal implement force (draft).

3.5. The Complete-System Bond Graph Model

The complete system bond graph model was considered to be that of a four wheel drive tractor. To accommodate the four wheel drive dynamics on the complete two wheel drive model of Figure 3.16, the drive line was expanded at a four

wheel drive transmission. The expansion made drive power available to the front axle of the tractor. Drive-wheel computations similar to the ones described in Section 3.3.3 were incorporated. In other words all four wheels now have both a thrust force component and a rolling resistance component, hence the additional thrust-force elements SELF and SERF are inputing power to further enhance the forward motion.

The four wheel drive split of power occurred at the common-velocity junction 1TRSMN of Figure 3.17. The division of engine torque between the front and the rear axles was dependent on the traction conditions each drive wheel was experiencing. The drive train divides the torque to each axle in proportion to the ratio of the torques resulting from the tractive effort. The dynamics of the front and rear axles were statically similar, with each rear component paired with a front one.

Utilizing the openness of bond graph models, Figure 3.18 demonstrates the additions made at one of the drive tires for the computation of tractive efficiency. This kind of ability makes bond graph theory a favorable choice for energy flow power distribution analytical studies such as this one.

Before the model could be used in the simulation of tractor performance both rigid body chassis, physical system and drive-line data was required. Chapter 4 describes the type and amount of data that was obtained.

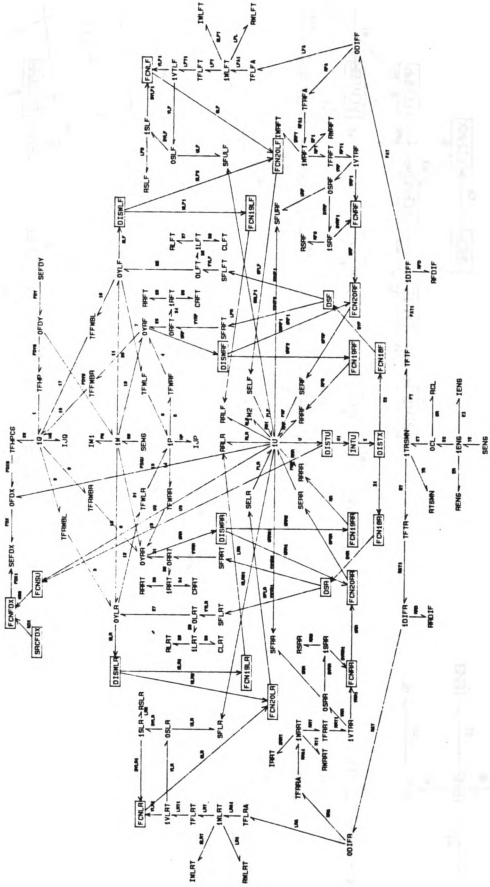

Figure 3.17: The Complete System Bond Graph Model of a Four Wheel Drive Tractor

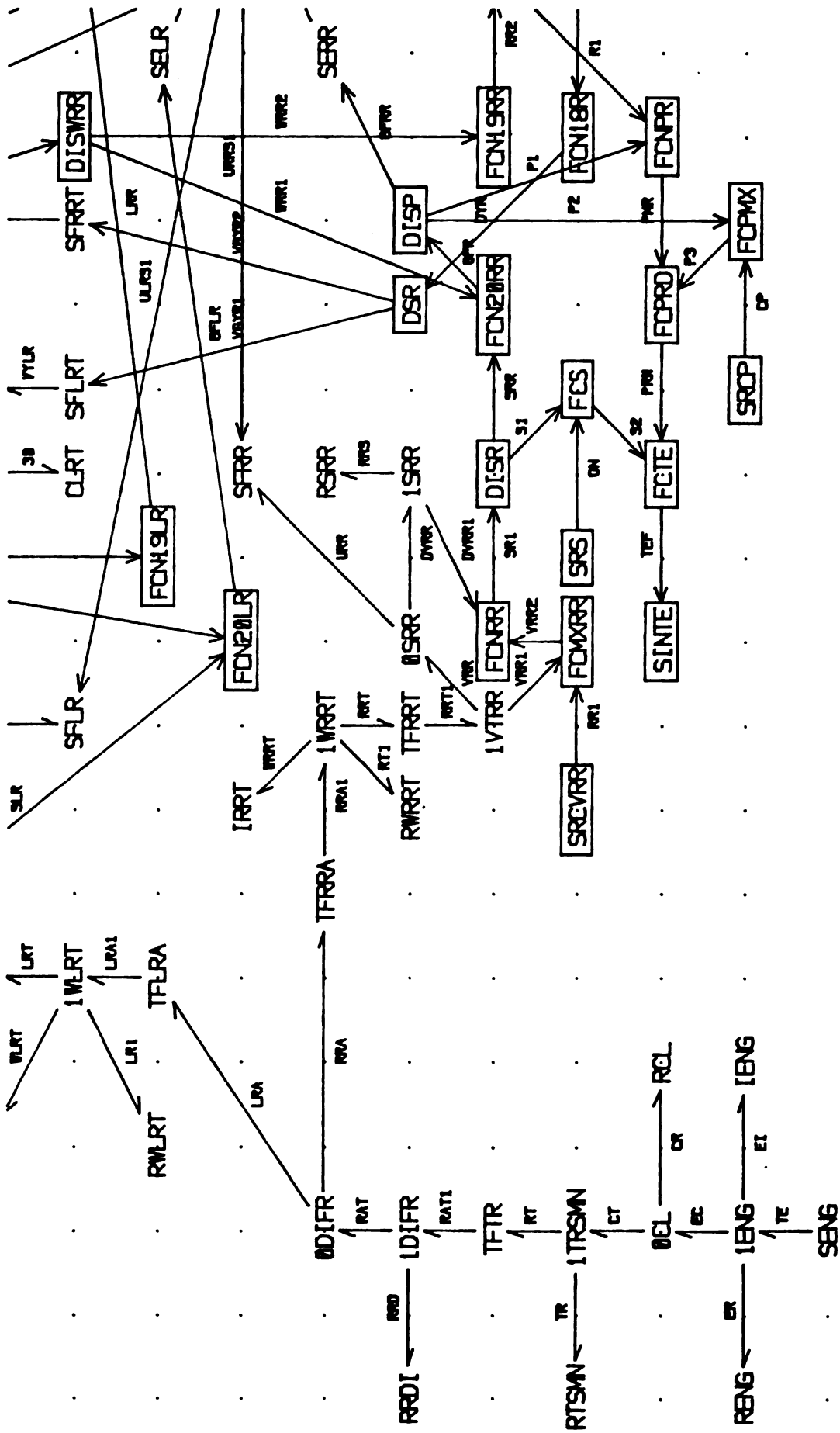

Figure 3.18: A Segment of the Bond Graph Model Showing the Additions for Computation of Tractive Efficiency

4. DATA FOR SIMULATION

Physical data for the simulation of tractor performance was obtained from Nebraska tractor test reports. A large amount of model parameter data was obtained from Summers (1983) and Smith (1974).

4.1. Two-Wheel Drive Tractor With Single Drive Wheel

The two-wheel drive tractor chosen for simulating performance was the International Harvester 1086 diesel tractor. Its actual performance data was reported in Nebraska Tractor Test 1247 (NTTL, 1977). As tested, the tractor was equipped with single 20.8R38 radial ply drive tires. Additional testing was done with 20.8-38 bias ply drive tires. Maximum power ratings at rated engine speed were 97.99 kW at the power-take-off (PTO), 84.29 kW at the drawbar with radial tires and 81.27kW at the drawbar with bias ply tires. The drawbar height was 57 cm.

4.1.1. Gross Vehicle Motions

The pitch mass moment of inertia for the total vehicle can be calculated from the measured period of oscillation of the tractor suspended like a pendulum. A method of estimating the pitch moment of inertia was presented by Rocard (1960). Rocard's analysis of pre-1935 and post-1935

cars yielded the following relationship for the square of the radius of gyration:

$$\rho^2 = (WBF)(WBR) \quad \ldots (4.1)$$

where WBF and WBR are the distances between the center of mass and the front and rear axles, respectively (see Figure 3.3). On pre-1935 automobiles, the front axle was placed at the front of the car and not under the engine as in later models. On a two-wheel drive tractor, the front axle is ahead of, or under the front of the engine. The rear axle is at the rear of the tractor without significant overhang to the rear. These axle locations are similar to the axle locations on pre-1935 cars. The use of Equation 4.1 to estimate the radius of gyration would tend to overestimate the true value. Smith (1974) reported an empirical relationship of:

$$I = 0.4\ m\ (WBF)(WBR) \quad \ldots (4.2)$$

Where:

I = movement of inertia

m = mass of tractor

from the Deere and Company Technical Center. The 0.4 (WBF)(WBR) of Equation 4.2 is the new square of radius of gyration compared to (WBF)(WBR) in Equation 4.1. The inclusion of the 0.4 accounts for the over estimation due to the axle locations.

Nebraska tractor test 1247 supplies the physical data for the International Harvester 1086 tractor. The center of mass of the tractor without the operator or ballast and with the fuel tank filled and the tractor serviced for operation is 75.4 cm forward from the center line of the rear axle. The height of the center of mass above the roadway is 108 cm. With an assumed operator mass of 81.6 kg, the addition of ballast and operator lowers the center of mass approximately 15.7 cm to a height of 91.9 cm above the ground. The wheelbase of the tractor is 2.66 m. The location WBR of the center of mass forward of the rear axle was determined by summing moments about the point of contact (of the rear wheel) with the ground. The center of mass was located 61.7 cm forward of the rear axle for a front axle weight of 16.1 KN and a rear axle weight of 53.4 KN. The center of mass was located 2.04 m behind the front axle. Applying Equation 4.1 the pitch mass moment of inertia was 3580 kgm^2.

Data for the spring and damping rates of the drive tires were obtained from Summers (1983). The 20.8R38 tires on the tested tractor were operated at the 110 kPa. Dimensions associated with the tires are an unloaded outside diameter of 1.85 m, a cross-section width of 55.6 cm and static loaded radius of 89.9 cm at a load of 34.1 kN and inflation pressure of 152 kPa. Load-deflection curves for the tires showed a radial deflection of approximately 8.51 cm for a loading of 26.7 kN (Summers, 1983). For a load of

31.6 kN which is approximately the tire load with a drawbar load of 46.3 kN as determined in the lugging ability test of Nebraska Tractor Test 1247, the radial deflection was approximately 9.53 cm. Assuming a linear load-deflection curve in the above load range the spring rate was 482 kN/m.

The damping ratio for radial tractor drive tires was three percent (Summers, 1983). The damping rate can be approximated by considering one tire supporting its static load. The mathematical model of the tire is:

$$m\ddot{z} + c\dot{z} + kz = 0 \qquad \ldots \quad (4.3)$$

where:

z = generalized coordinate

m = supported mass

c = damping rate

k = spring rate

The critical damping rate is:

$$c_{cr} = \sqrt{4km} \qquad \ldots \quad (4.4)$$

This yields a critical damping rate of 72.5 kN.s/m. Multiplying the critical damping rate by the damping ratio of 3%, a damping rate of 2.17 kN.s/m was determined for each rear wheel.

During testing the drive tires were each ballasted with 653 kg of liquid. ASAE standard: ASAE 5346.1 (ASAE, 1982b) lists a liquid ballast mass of 644 kg for a 20.8-38 tire

containing 419 g of CaCl per liter of water. The mass of a tire filled with liquid at its highest level was 200 kg (B. F. Goodrich, 1977). Assuming the mass of the ballast was evenly distributed around the tire, the mass moment of inertia of the tire with a total mass of 854 kg was calculated for a torus of radius (R), mass (m) and cross section radius (a). Meriam (1971) presented the equation for the mass moment of inertia of a torus as:

$$I = mR^2 + 3/4\ (ma^2) \qquad \ldots \quad (4.5)$$

The mass moment of inertia for each ballasted drive tire about the axle was approximately 702 $kg.m^2$.

The cast iron wheel had a mass of 211 kg with a wheel rim mass of 57.2 kg (Summers, 1983). To calculate the mass moment of inertia of the wheel and rim, each part was considered separately. The mass of the wheel was assumed to be evenly distributed similar to a thin disk with a radius of 48.3 cm. The rim was considered as a circular shell with a radius of 48.3 cm. Adding the mass moment of inertia of 38.1 kgm^2 for the wheel rim to the mass moment of inertia of the ballasted tires, the entire wheel assembly had a combined mass moment of inertia of 740 $kg.m^2$.

The front tires as tested were 10.00-16 tires with a section width of 25.4 cm, unloaded diameter of 89.4 cm and static loaded radius of 40.6 cm. Smith (1974) reported the linearized spring rate for 11.00-16 steering tires as 251 kN/m. Mathews and Talamo (1965) measured a damping ratio of

four percent for 7.50-16 tires. Assuming an insignificant difference between these rates and those of the 10.00-16 tires, the damping rate calculated using Equation 4.4 was 1.15 kN.s/m^2. The effective rolling radius under no drawbar load conditions was 88.9 cm.

4.1.2. Engine

For engines used on tractors, International Harvester develops engine performance maps for ungoverned engines without accessories. Engine performance data can be determined from the power-take-off and drawbar tests conducted at the Nebraska Tractor Testing Laboratory. Engine torque is directly proportional to the drive axle torque by the ratio of the gear reduction to the power transmission efficiency.

Table 4.1. Engine Torque and Speed Data for the IH 1086 Tractor

Engine Speed (rpm)	Engine Torque (N.m)
1196	450
1143	503
1683	498
1925	476
2070	456
2153	443
2402	384
2490	329
2538	247
2588	164
2638	82
2675	0

Engine torque and speed data computed from Nebraska Tractor Test 1247 are listed in Table 4.1. The data are also plotted on Figure 4.1.

The engine was assumed to operate away from the governor controlled speed range (to the left of A on Figure 4.1). The engine torque used was therefore a constant 471 N.m. This was an average over the speed range 1196 to 2153 rpm.

Smith (1974) reported a combined engine and clutch mass moment of inertia of 2.43 kgm^2 as cited by the manufacturer.

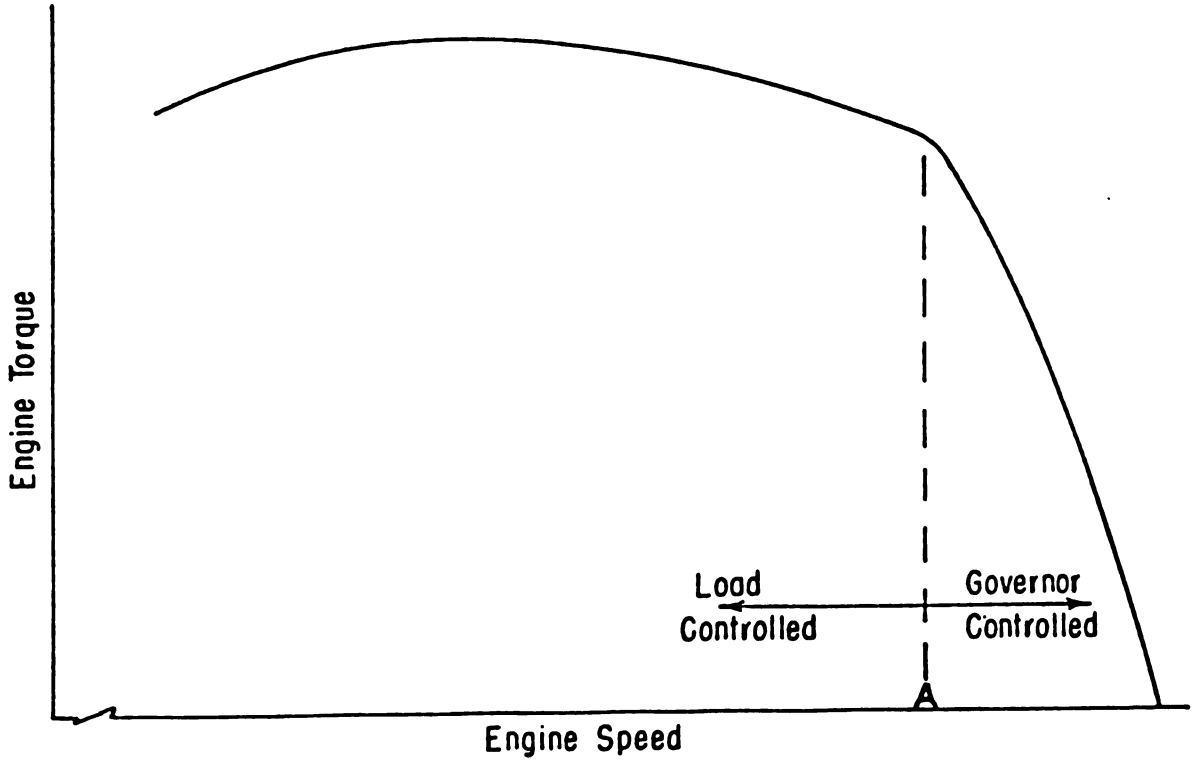

Figure 4.1: Engine Torque vs. Speed for the IH 1086 (Summers, 1983).

4.1.3. Clutch

The clutch was assumed to have an insignificant slippage after engagement. The clutch slippage element on the bond graph (RCL) was assigned a LIMITER function (see Appendix A) relating transmitted torque and slippage velocity (see Figure 4.2). A value of slippage velocity in the order of 0.005 rad/s was allowed at maximum transmittable torque. Browning (1978) specified that a dry clutch should have a torque capacity higher than engine maximum output torque by a service factor of 1.6-3.0. Assuming a service factor of 1.6 the clutch maximum torque was set at 754 N.m.

The clutch could easily have been left out of the model and a stiff shaft assumed between the engine and the transmission, but this was observed to interfere with the causality assignment at the differential. The clutch was therefore included but allowed to have a coupling of very low slippage velocity within the torque range of operation. Under these conditions, the combined mass moment of inertia of the engine and clutch could be used.

Goering (1978) gives the clutch dynamic torque capacity as:

$$T = \frac{1}{4} K_s n F \mu_d (D+d) \qquad \ldots \quad (4.6)$$

where:

T = transmitted torque, N.m

K_s = spline friction factor

n = number of friction surfaces

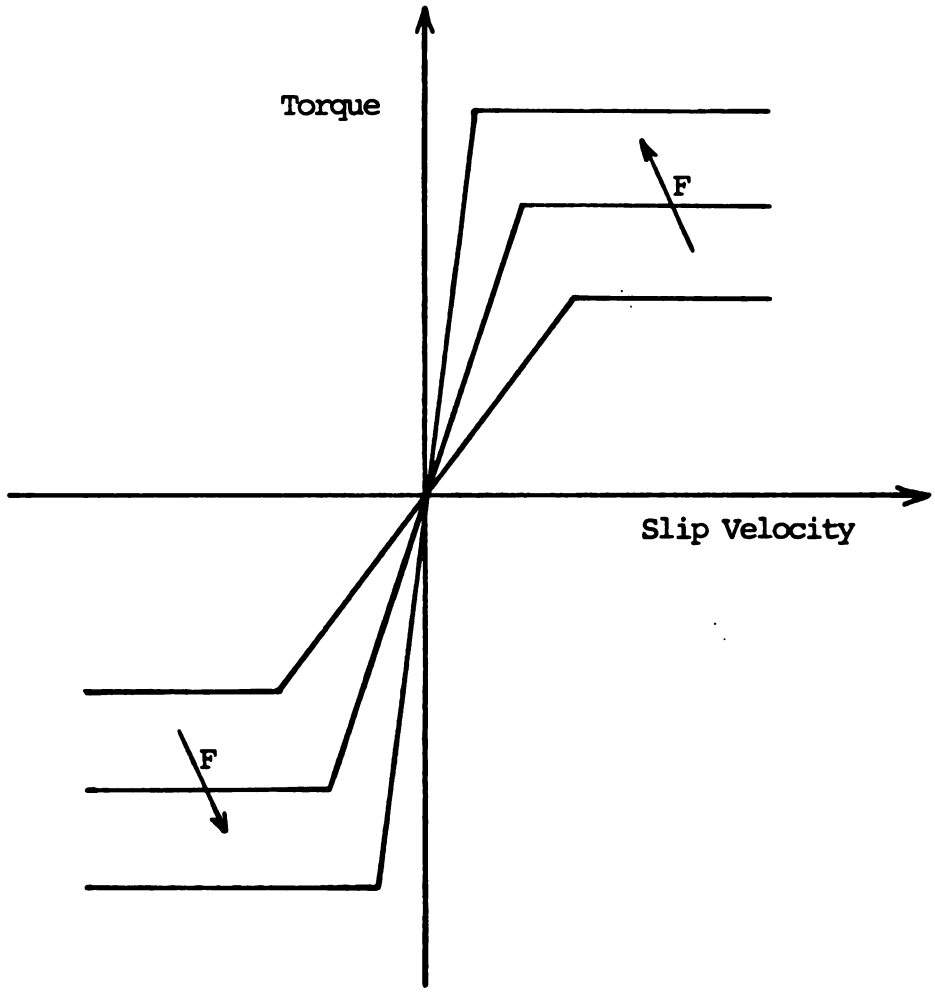

Figure 4.2. Clutch Torque vs. Clutch Slippage Velocity

F = clutch clumping force, N

μ_d = dynamic coefficient of friction

D = outer diameter of the friction disk, m

d = inner diameter of the friction disk, m

Figure 4.2 (arrow F) demonstrates how the clutch torque increases and slippage decreases with increased clutch clamping force. A fixed clutch clamping force (a single curve on Figure 4.2) was assumed.

The IH 1086 tractor was equipped with a single plate dry clutch with two friction surfaces. The friction surfaces were a ceramic-metallic material with a coefficient of friction of 0.2 to 0.5 (Browning, 1978). The clutch disk has six equally spaced trapezoidal shaped pads on each side. The inner and outer radii of the pads are 5.08 cm at the inner radius and 7.62 cm at the outer radius. A spline friction factor (K_s) of 0.3 was listed by Finkin (1968). For bond-graph modeling purposes where the model was based on the physics of the mechanism (and with negligible friction loss assumed) the above clutch data was not used in computational form. The model of Figure 4.2 was used directly.

4.1.4. Drive Train Motions

The drive axles of the IH 1086 tractor are 8.26 cm in diameter and approximately 61 cm long for a tread spacing of 1.63 m. The torsional spring rate (k), given by

$$k = \frac{JG}{L} \qquad \ldots (4.7)$$

where:

J = polar moment of inertia of the axle = $\frac{\pi d^4}{32}$

d = axle diameter

G = modulus of rigidity of the axle = 82.7 GPa

L = length of the axle

The torsional spring rate of the rear axles was approximately 1238 kN.m/radian (Summers, 1983). Torsional spring rates for the shafts connecting the clutch and transmission and the transmission and differential could be assumed to be 302 kN.m/radian and 667 kNm/radian respectively (Smith, 1974). The use of the latter two spring rates was based on the assumption that transmission shaft properties of similar size tractors were not significantly different.

A gear chart for the IH 1086 two-wheel drive tractor was obtained through Summers (1983) from International Harvester Company. This chart lacked adequate information for gear reduction ratios. Gear reduction ratios for the IH 1086 tractor were obtained from the official test file of the Nebraska Tractor Testing Laboratory. The transmission reduction ratios are listed in Table 4.2. The differential reduction ratio (including the final drive) was 0.0454.

Table 4.2. Gear Reduction Ratios for the IH 1086 Tractor

Gear No.	Reduction Ratio	
	Transmission	Differential
1	0.0725	0.0454
2	0.0929	0.0454
3	0.0964	0.0454
4	0.124	0.0454
5	0.167	0.0454
6	0.215	0.0454
7	0.223	0.0454
8	0.253	0.0454
9	0.286	0.0454
10	0.325	0.0454
11	0.337	0.0454
12	0.432	0.0454
13	0.584	0.0454
14	0.749	0.0454
15	0.780	0.0454
16	1.000	0.0454

The transmission and differential efficiencies were computed using gear mesh configurations from the International Harvester gear chart. Gear mesh efficiencies of 0.99 for an internal mesh and 0.985 for an external mesh were used in accordance with the suggestion by Browning (1978).

The transmission efficiency was calculated by successive multiplications of the individual mesh efficiencies. The transmission efficiencies are listed in Table 4.3 for the high gear range of the IH 1086 tractor.

Table 4.3. Transmission Efficiency and Differential Efficiency for the IH 1086 Tractor

Gear No.	Efficiency	
	Transmission	Differential
1	0.941	0.970
2	0.941	0.970
3	0.941	0.970
4	0.941	0.970
5	0.941	0.970
6	0.941	0.970
7	0.941	0.970
8	0.970	0.970
9	0.970	0.970
10	0.970	0.970
11	0.970	0.970
12	0.970	0.970
13	0.970	0.970
14	0.970	0.970
15	0.970	0.970
16	1.000	0.970

The differential consists of a bevel gear mesh between the pinion and ring gear and four bevel gear meshes carried by the ring gear (see Figure 4.3). When differential axle motion occurs, one of the sun gears acts as the sun gear for the planetary set. The gear on the axle with the lesser velocity acts as the ring gear. The efficiency of the differential was evaluated as a planetary gear set for differential motion of the axles. For normal operation of the tractor on a surface where both drive wheels are subjected to similar surface conditions, the axles will rotate without differential motion. The four bevel gears

carried by the ring gear do not rotate relative to their pivot when differential motion does not occur. In this condition the efficiency of the differential is 0.970. This efficiency accounts for the mesh between the pinion and the ring gear in the differential and the gear mesh in the final drives between the differential and wheels.

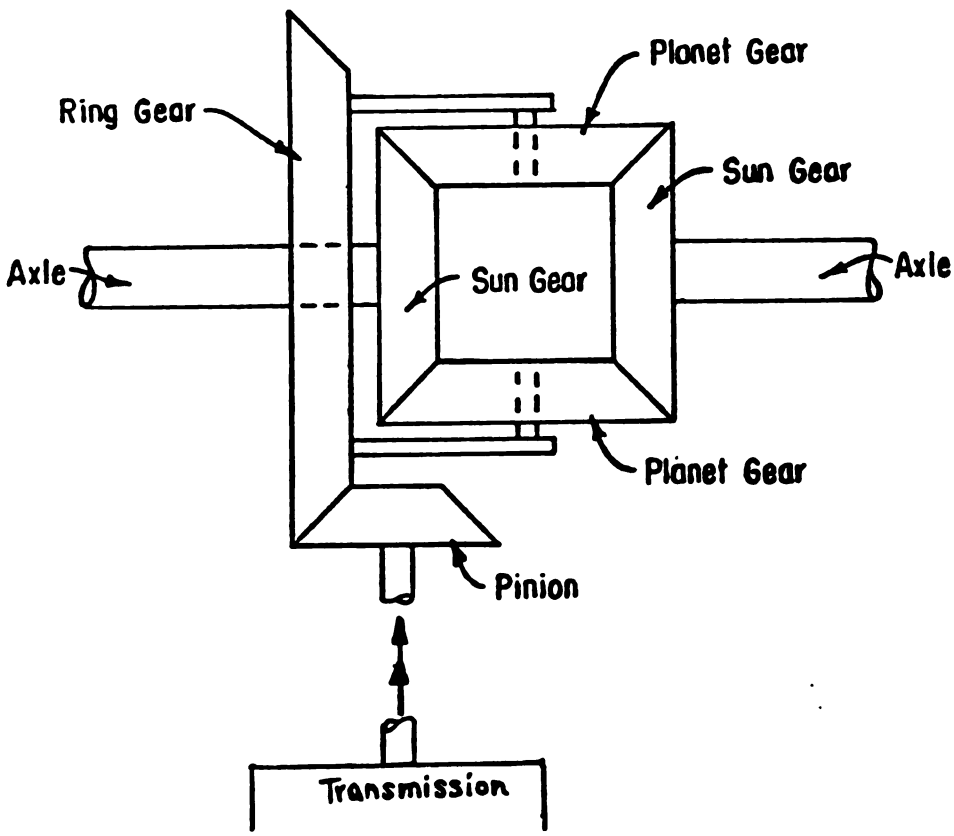

Fig 4.3. Differential Gearing for the IH1086 Tractor

4.2. Two Wheel Drive Tractor With Dual Drive Wheels

The simulation data for the two wheel drive tractor with dual drive wheels was the same except for the gross vehicle motions.

4.2.1. Gross Vehicle Motions

The addition of dual drive wheels to the IH 1086 tractor changed the physical properties of the tractor. Summers (1983) indicated that the steel wheel used for attaching dual wheels to the tractor had a mass of 250 kg. Assuming the mass of the rim portion of the wheel was 57.2 kg, as in the case for the steel rim used with the cast iron wheel, the mass moments of inertia were determined for a thin disk with a radius of 48.3 cm. Adding the two mass moments of inertia, the mass moment of inertia of the entire steel wheel was 35.8 kgm^2. The tire had a mass of 200 kg without ballast. Applying Equation 4.5 again the mass moment of inertia of the tire was 106 kgm^2. The total mass moment of inertia for each added wheel and tire was 142 kgm^2 about the rear axle.

The extra mass of the added wheels and tires shifted the location of the center of mass rearward. Assuming the mass of the tractor without dual wheels is unchanged, the force acting on the rear tire was the sum of 53.4 kN (the original rear axle force) plus the force resulting from the dual wheels and tires. The rear axle support force was 62.3 kN, and the total force on all wheels increased to 78.4 kN.

Therefore the front support was 78.4 - 62.3 = 16.1 kN. The location of the center of mass forward of the rear axle, WBR (see Figure 3.3) was determined by summing moments about the point of contact of the rear wheel and the ground. The new center of mass was now located 54.9 cm forward of the rear axle and 2.11 m behind the front axle (compared to 61.7 cm and 2.04 m respectively, a 6.8 cm shift backwards). The center of mass was lowered to approximately 91.7 cm above the ground, a 0.2 cm shift downwards.

4.3. Tractive Performance

Two major categories of tractive performance were investigated; performance on soil and performance on concrete. For each category, further investigation of performance with radial and bias ply tires was performed. In each of these cases, energy and power distribution and dissipation patterns were studied at points of interest in the system.

4.3.1. Performance on Soil

The tractive prediction equation developed by Wismer and Luth (1974) was adapted for use with radial tires by using the drawbar pull to weight ratio data presented by Brixius and Wismer (1978). Curves of net drawbar pull to weight ratio plotted against wheel slippage were presented for 18.4-38 bias ply and 18.4R38 radial tires on wet silty

clay loam soil. The tractive prediction equation for bias ply tires on cohesive frictional soils was given as

$$\frac{P}{W} = 0.75\ (1 - e^{-0.3C_nS}) - \left(\frac{1.2}{C_n} + 0.04\right) \quad \ldots\ (3.2)$$

When adjustments in the constants of Equation 3.2 were made for radial tires, Equation 3.2 became:

$$\frac{P}{W} = 0.75\ (1 - e^{-0.39\ C_nS}) - \left(\frac{1.2}{C_n} + 0.04\right) \quad \ldots\ (4.8)$$

The wheel numeric, C_n is a dimensionless term composed of the soil cone index, cross section width, unloaded diameter and dynamic wheel load. Cone Index is measured using a soil cone penetrometer as described in ASAE Standard: ASAE S 313.1 (ASAE 1982b). Bloome et al., (1982) reported a soil cone index of approximately 1.03 MPa for dry untilled soil prior to tillage.

4.3.2. Performance on Concrete

The tractive performance model developed by Zoz and Brixius (1979) for agricultural drive tires on concrete was used. The prediction equation for pull ratio on soil was

$$\frac{P}{W} = 1.02\ (1 - e^{-\left(\frac{kbdS}{W}\right)}) \quad \ldots\ (3.4)$$

where:

$k = 400$ kPa

Summers (1983) used data from Nebraska Tractor Test 1247 to calculate a new coefficient (R) in Equation 3.4 for radial tires. A value of 594 kPa for k yielded the relationship:

$$\frac{P}{W} = 1.02 \left(1 - e^{\frac{-594bdS}{W}}\right) \qquad \ldots (4.10)$$

This equation was used to validate the tractor simulation model by simulating drawbar tests conducted at Nebraska Testing Laboratory.

4.4. Model-Element Functions and Function Parameters

The bond graph modeling of this study was based on the assembly of model components into a multiport system model of the whole. Eight basic modeling elements have been used comprising the energy dissipation elements (R-field), energy conservative (storage) elements (C, I-field) and the general junction structure elements 0, 1, and TF elements. No GY (gyrator) elements need to be used. Please see Appendix A, Figure 4.4 and Rosenberg and Karnopp (1983) for further information.

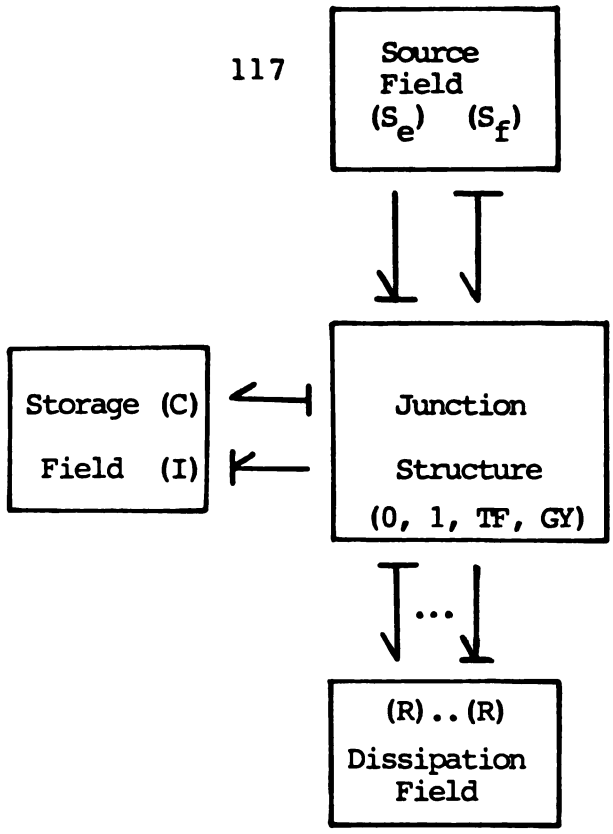

Figure 4.4. The Structure of Multiport Systems Partition of a Bond Graph with Complete Integral Causality (Rosenberg and Karnopp, 1983)

On all bond graphs shown in this study the element labels identify the type of element by the first one or two letters on the label. All elements whose labels begin with the letter C are compliance elements, all labels beginning with the letters TF are transformer elements, all labels beginning with the letter I are inertia elements and all labels beginning with letter R are dissipation elements. Integral causality was used on all elements (See Appendix A). Integral causality was preferred because the digital

computer can integrate numerically with better results than it can differentiate.

The elemental equations for the model are listed in Appendix A. The parameters shown are those used during the validation of the two wheel drive tractor performance. The parameter values were varied (as described in chapter 5) between each of the performance analysis comparisons that were conducted. Table 4.4 shows the general relationships used for the various element types (integral causality):

Table 4.4. General Relationships for C, I, R, SE and SF elements.

Dynamic Aspect	Element Type	Function	State Variable
Linear Acceleration	I	$F.1 = \frac{1}{M} * P$	P
Angular Acceleration	I	$F.2 = \frac{1}{I1} * H$	H
Linear Compliance	C	$E.1 = \frac{1}{C1} * Q1$	Q1
Torsional Compliance	C	$E.2 = \frac{1}{C2} * Q2$	Q2
Energy Dissipation	R	$F.3 = \frac{1}{K} * E3$	-
		or $E.3 = K * F3$	-
Source of Effort	SE	$E.4 = f(t)$	-
Source of Flow	SF	$F.4 = f(t)$	-

F.1 = linear velocity (flow) (m.s)

M = mass (kg)

P = linear momentum (kg.m/s)

F.2 = angular velocity (flow) (rad/s)

I.1 = mass moment of inertia ($kg.m^2$)

H = angular momentum ($kg\ m^2/s$)

E.1 = linear spring force (effort) (N)

C1 = linear spring constant (m/N)

Q1 = linear spring displacement (m)

E.2 = torsional spring torque (effort) (N.m)

C2 = torsional spring constant (rad/N.m)

Q2 = angular spring displacement (rad)

E.3 = dissipation (potential) effort (N)

F.3 = dissipation flow (m/s or rad/s)

K = dissipation coefficient

E.4 = input effort (N, Nm)

F.4 = input velocity (m/s, rad/s)

All the transformer elements used had constant coefficients. The subroutine's user-defined functions for the computation of drive tire thrust forces and chassis motion rolling resistances at the wheels are listed in Appendix A. The parameters used in the subroutine functions during validation of the simulation are listed (subroutine 19 and 20) below:

Subroutine 20: Thrust Force Computation for Elements FCN20LR and FUN20RR (see Figure 3.23)

Parameter	Symbol	Value
Constant	K1	0.75
Tire Width	B	0.556 m
Tire Diameter	D	1.85 m
Cone Index	CI	1.03 GPa
Constant	K2	-0.3
Tire Dynamic Load	W	Variable input
Slip	S	Variable input

Subroutine 19: Rolling Resistance Computation for Elements FCN19LR, FCN19LF, FCN19RR and FCN19RF

Parameter	Symbol	Value	
		Rear	Front
Constant	K3	1.2	1.2
Constant	K4	0.04	0.04
Tire Width	B	0.556 m	0.254 m
Tire Diameter	D	1.85 m	0.894 m
Cone Index	CI	1.03 GPa	1.03 GPa
Tire Dynamic Load	W	Variable input	

Subroutine 18: Subroutine 18 was used to generate the vertical ground velocities (elements FCN18R and FCN18F) at the tires with the input being the horizontal chassis displacement, at the respective tire. The horizontal chassis displacements at both rear and both front tires were assumed equal. The functions in blocks FCN18R and FCN18F could be chosen to be similar or not. Two different

functions of the form shown were used in this study: Equation 4.11 and 4.12 below.

$$Y_1(x) = Y_{max} (1 - e^{-(K1)x}) \quad \ldots \quad (4.12)$$

$$Y_2(x) = Y_{max} * \sin ((K2)x) \quad \ldots \quad (4.13)$$

where:

Y_{max} = height of bump (m)

K1, K2 = constants determining time constant and frequency respectively

All other variables are as previously defined.

Equation 4.11 represents an exponential climb onto a bump while Equation 4.12 represents a sinusoidal bump. The bump sizes used in the simulation varied between 10 and 30 cm in height and 20 cm to 1 m in length.

The complete two wheel drive bond graph model had a total of seven inertia elements, four compliance elements and one displacement signal, the forward motion chassis displacement. The inertia elements represented the pitch, heave, roll, the two drive-tires rotary motion, the forward motion of the chassis and the engine rotary motion. The compliance elements belonged to the spring elements of the four tires. The overall system was twelve degrees of freedom model with the following state variables:

1. P.PM : heave momentum
2. P.HP: roll momentum

3. P.HQ: pitch momentum
4. P.PM1: forward motion (of chassis) momentum
5. P.WRRT: right rear tire angular momentum
6. P.WLRT: left rear tire angular momentum
7. P.EI: engine momentum
8. Q.38: left-front tire (spring) displacement
9. Q.34: right-rear tire (spring) displacement
10. Q.26: right-front tire (spring) displacement
11. Q.26: right-front tire (spring) displacement
12 X: forward motion chassis displacement

These variables were used to determine the initial state of the model as at the selected time. They were also the state variables of the state-space formulation which resulted in twelve first order differential equations governing the dynamics of the twelfth order system. These equations were generated internally by ENPORT and solved in the integrator to produce data for time-response analysis of the system dynamics and the other post-processor operations (see Section 3.3.3).

4.4.1. Drive Train Elements

Utilizing the data listed in Section 4.1.4, computations were carried out to generate the magnitude of the parameters of the drive-line bond graph model elements. The data of Tables 4.1 through 4.3 was used with gear reduction ratios and efficiencies selected being those of

gear 8. This was the gear used in the lugging ability tests of the IH 1086 used in the model verification of chapter 5.

An average input engine torque of 471 Nm was obtained in the speed range between 1196 rpm (125.2 rad/s) and 2153 rpm (225.4 rad/s). The rated engine speed at maximum power was recorded in Nebraska Tractor Test 1247 as 2400 rpm (251.3 rad/s). At this speed the engine input power was recorded as 97.99 kW. A zero power loss was assumed for the clutch when fully engaged. With 0.970 transmission and differential efficiencies (gear 8, Table 4.3) 2.94 kW and 2.85 kW of transmission power were lost in the transmission and clutch respectively. Considering 0.253 and 0.0453 speed reduction ratios (see Table 4.2) for the transmission and differential (including the final drives) respectively, the power losses in the transmission and differential occurred at maximum speeds of 251.3 rad/s and 63.6 rad/s respectively. At these speeds and the corresponding power dissipations, torque looses of 11.7 Nm and 44.81 Nm occurred in the transmission and the differential respectively. At the same speed reduction ratios torque increments occurred rising from 471 Nm to 1815.4 Nm (overall) across the transmission. Accounting for the loss in the differential a torque of 1770.6 Nm at a maximum power of 92.2 kW was available at the differential. This torque was equally transmitted to each of the (left and right) drive axles. At the same time the speed was reduced in half from 63.6 rad/s to 31.8 rad/s for each axle. For a net speed reduction

across the differential of 0.0453 a reduction-ratio of 0.0918 was associated with the final drive of each drive axle. The torques available to the wheels were 19500 Nm at theoretical wheel angular velocities of 2.89 rad/s. With loaded rolling radii of 0.899 m for the drive wheels, the theoretical wheel peripheral velocities obtained were 2.60 m/s at an available tire peripheral force of 21167 N (corresponding to 19029 Nm drive-axle torque) for each wheel. The 2.60 m/s theoretical velocity compared well with the recorded ones of 2.56 m/s for radial and 2.44 m/s for bias ply tires.

In Nebraska Tractor Test 1247, at the maximum available power of the Drawbar Performance Test, tire slippage values of 7.22% and 4.40% were reported for the bias ply and radial ply tires respectively. Utilizing these values and the definition of slip shown on Equation 4.14.

$$S = \frac{V_t - V_a}{V_t} * 100 = \frac{V_s}{V_t} * 100 \quad \ldots \quad (4.14)$$

where:

S = slip (%)

V_t = theoretical (peripheral) velocity

V_a = actual velocity

V_S = slip velocity

and the theoretical velocities computed above, slip velocity values of 0.188 m/s and 0.114 m/s were obtained for the bias

and radial ply tires respectively. These were the slippage velocities at the recorded (Drawbar Performance Tests: NTTL-Test 1247) drawbar forces of 35810 N and 34377 N for the bias and radial ply tires. Assuming a motion resistance value that was 20 percent of the dynamic load on the drive tire (Zoz and Brixius, 1979), the drive tires were required to be capable of developing an additional 13948 N. Summing the drawbar force and the motion resistance force, each drive tire needed to be capable of developing 24775 N if bias ply and 24059 N if radial ply. Assuming a linear relationship between the drawbar force and the wheel slip and using the slippage velocities (0.188 m/s and 0.114 m/s) obtained at test drawbar forces (35810 N and34377 N) slippage velocities of 0.260 m/s and 0.160 m/s were obtained for the bias and radial ply drive tires respectively. These values were used on the LIMITER function bond graph slippage elements RSR and RSL of Figure 3.6 and subsequent ones. Since forces higher than 35810 N and 34377 N were to be applied at the drawbar during the lugging ability tests the model was made capable of handling higher forces by doubling the maximum thrust force each tire was capable of developing. In doing so, the slope of the thrust force-slip velocity curve was kept the same.

The relationship between thrust force P and slip velocity V_s shown on Figure 3.15 was used to select the slippage and the corresponding thrust force for the operating conditions. The quantitative relationship

described in the previous paragraph is an estimation and it was used directly on the simplified model. The expanded model incorporated the Wismer-Luth model. The Wismer-Luth model used the slippage obtained from the relationship of Figure 3.15 and the wheel dynamic load was input directly to elements FCN20RR and FCN20LR for the computation of thrust force P (see equation 3.2). In other words the relationship of Figure 3.15 which was used as a slippage value generator for the Wismer-Luth model did not simultaneously incorporate the effect T (See Figure 3.15) of the dynamic load in which case an accurate value of P would be obtained. The Wismer-Luth model was therefore used to bring the effect T into the relationship between slippage velocity V_s and thrust force P. Thus for given operating conditions Figure 3.15 supplies a V_s value and the corresponding thrust force P. For the simplified model this P drives the tractor forward. For the expanded model Figure 3.15 supplies a V_s value which is used in the Wismer-Luth model to generate a thrust force P (the output of functions FCN20RR and FCN20LR). At the same time thrust force P value as it appears on Figure 3.15 is that of a particular curve P_i with the effect T nonexistent and for the expanded model this P is dormant (it is not used to drive the tractor). Meanwhile a signal (VLRS1 or VRRS1 - see Figure 3.16) keeps track of the forward velocity of the tractor and controls the variability of slippage velocity V_s accordingly.

The dissipating RTRS and RDIF elements of the transmission and differential were modeled as gain type (linear) functions with coefficients of 0.466 Nm.s/rad and 0.705 Nm.s/rad and passing through the origin. These coefficients were obtained from the maximum power loss torque-angular velocity relationships for the transmission and the differential.

5. MODEL VALIDATION, RESULTS AND OBSERVATIONS

5.1. Lugging Test Validation

The bond graph model was validated by simulating the lugging ability data from Nebraska Tractor Test 1247. Simulated data are steady state forward velocity, wheel slippage, engine speed and drawbar pull using the slope of the drawbar pull - forward velocity curve as the input coefficient for the drawbar element function. The drawbar force was input as a unit of forward velocity (unit pull) establishing a linear (GAIN-function) drawbar load. The GAIN function, based on zero pull or zero velicity was assumed to have a y-intercept of zero. The vertical drawbar component was estimated at 10 percent (see Section 3.3.2) of the horizontal component. The validity of the model was determined by the residual mean square and standard error of estimate.

An unbiased estimate of the time variance about a regression is given by the residual mean square (Steel and Torrie, 1980). The residual mean square, S^2_{yx} has n-2 degrees of freedom and is determined by:

$$S^2_{yx} = \frac{\Sigma (y - \hat{y})^2}{n - 2} \qquad \ldots \quad (5.1)$$

where:

$\hat{y}$ = predicted value

y = observed value

n = number of observations.

The standard error of estimate or the standard deviation of Y for fixed X is the square root of the residual mean square. The root mean square error, RMS, is obtained from:

$$RMS = \frac{S_{yx}}{\bar{y}} * 100 \qquad \ldots \quad (5.2)$$

Where:

$\bar{y}$ = mean of the observed values

Tenant et al. (1979) used the root mean square error to compare engine performance models.

The validation process was done in two parts, one with the simplified model shown in Figure 3.7 and the other with the expanded model of Figure 3.16. Engine performance data for the IH 1086 tractor along with the physical data for the tractor with single drive wheels were used as input data for the bond graph model.

5.1.1. Simplified Model

Results of the simulated performance during the lugging ability test for the IH 1086 with bias ply tires using the simplified model (Figure 3.7) are shown on Table 5.1. Also

included in the table are the correlation results of the statistical analysis. The standard error of estimate and the root mean square error for each measured parameter are listed at the bottom of Table 5.1.

The correlations of the simulated and actual data in Table 5.1 are shown in Figures 5.1, 5.2, 5.3 and 5.4 for the forward velocity, wheel slippage, engine speed and drawbar pull respectively. A perfect correlation of the simulated and the actual data would plot as a line of unity slope and a zero intercept. The plot of the simulated forward velocity versus the actual data (Figure 5.1) has a slope of 0.908 and an intercept of -0.338 m/s. The correlation coefficient (R) is 0.972. The standard error of estimate was 0.611 m/s with a root mean square error of 52.2 percent. From Figure 5.1 it can be clearly seen that in the full range of forward velocities measured, the forward velocity was underpredicted.

Figure 5.2 shows the simulated wheel slippage data correlated with the actual wheel slippage data. The range of wheel slippage for normal tractor operation is 5 to 15 percent. The slope of the correlation is 2.386 with an intercept of -6.648 percent. The correlation coefficient is 0.980. The standard error of estimate is 10.64 percent with a root mean square error of 59.9 percent. From Figure 5.2, wheel slippage will be underpredicted in the range of wheel slip values below about 3.3 percent and overpredicted in the range of slippage values greater than 3.3 percent.

Table 5.1: Simulated, Actual and Correlation Data for the IH1086 Tractor with Bias Ply Tires Using the Simplified Model.

Unit Pull (kN.s/m)	Parameter Measured	Actual Data	Simulated Data	% Difference
16.148	FV* (m/s)	2.27	1.85	18.5
	WS (%)	7.22	11.10	-53.7
	ES (rad/s)	251.3	201.5	19.8
	Pull (kN)	36.655	29.875	18.5
21.187	FV (m/s)	2.01	1.43	28.9
	WS (%)	8.85	14.10	-59.3
	ES (rad/s)	226.2	198.3	12.3
	Pull (kN)	42.586	29.920	29.7
26.070	FV (m/s)	1.76	1.17	33.5
	WS (%)	9.99	16.50	-65.2
	ES (rad/s)	201.2	173.1	13.9
	Pull (kN)	45.88	30.180	34.2
31.626	FV (m/s)	1.52	0.969	36.3
	WS (%)	11.24	19.47	-73.2
	ES (rad/s)	176.3	116.5	33.9
	Pull (kN)	48.071	30.630	36.3
37.122	FV (m/s)	1.30	0.828	36.3
	WS (%)	11.52	22.08	-91.6
	ES (rad/s)	150.6	103.0	31.6
	Pull (kN)	48.258	30.750	36.3
39.794	FV (m/s)	1.10	0.774	29.6
	WS (%)	9.56	23.29	-143.6
	ES (rad/s)	125.5	97.7	22.5
	Pull (kN)	43.773	30.796	29.6

Statistical Results

	Standard Error of Estimate	Root Mean Square Error (RMS - %)
Forward Velocity	0.611 m/s	52.2
Wheel Slip	10.64 %	59.9
Engine Speed	51.6 rad/s	34.8
Pull	17.551 kN	57.8

* FV = Forward Velocity (m/s)
WS = Wheel Slip (%)
ES = Engine Speed (rad/s)
Pull = Drawbar Pull (kN)

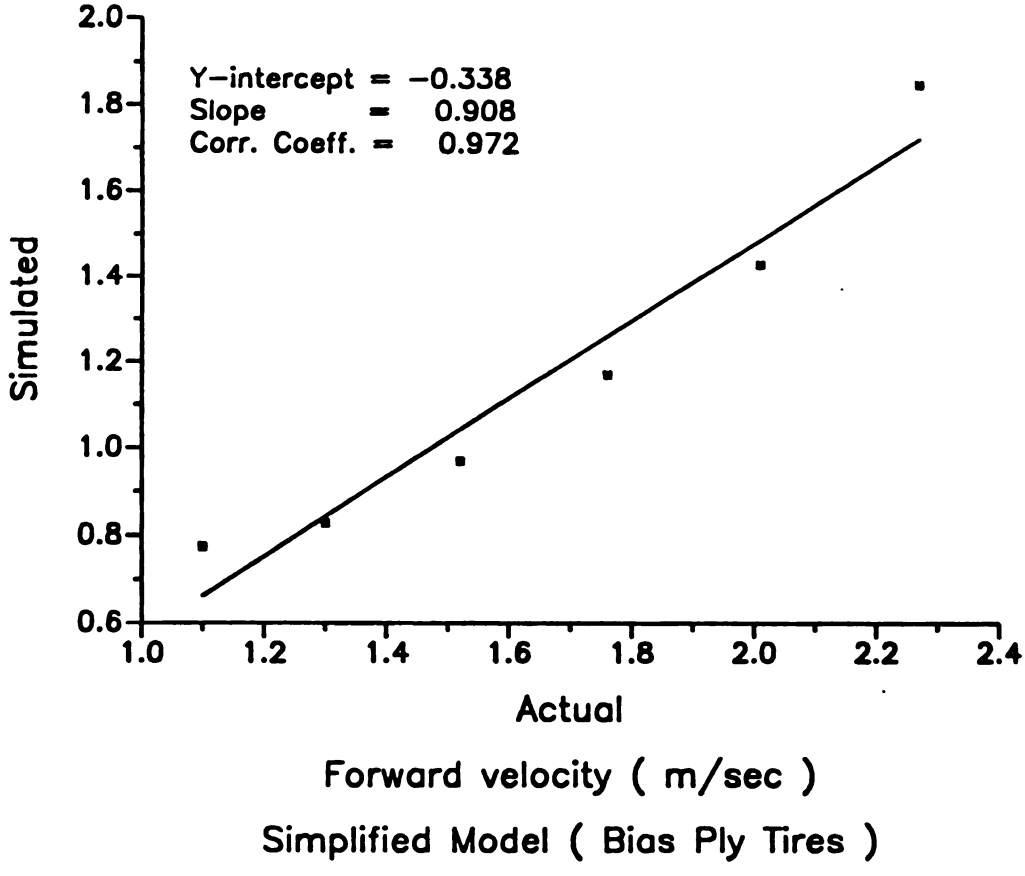

Figure 5.1: Relation of Simulated Forward Velocity with Actual Data from Nebraska Tractor Test 1247 for the IH1086 Tractor with Bias Ply Tires and Using the Simplified Bond Graph Model

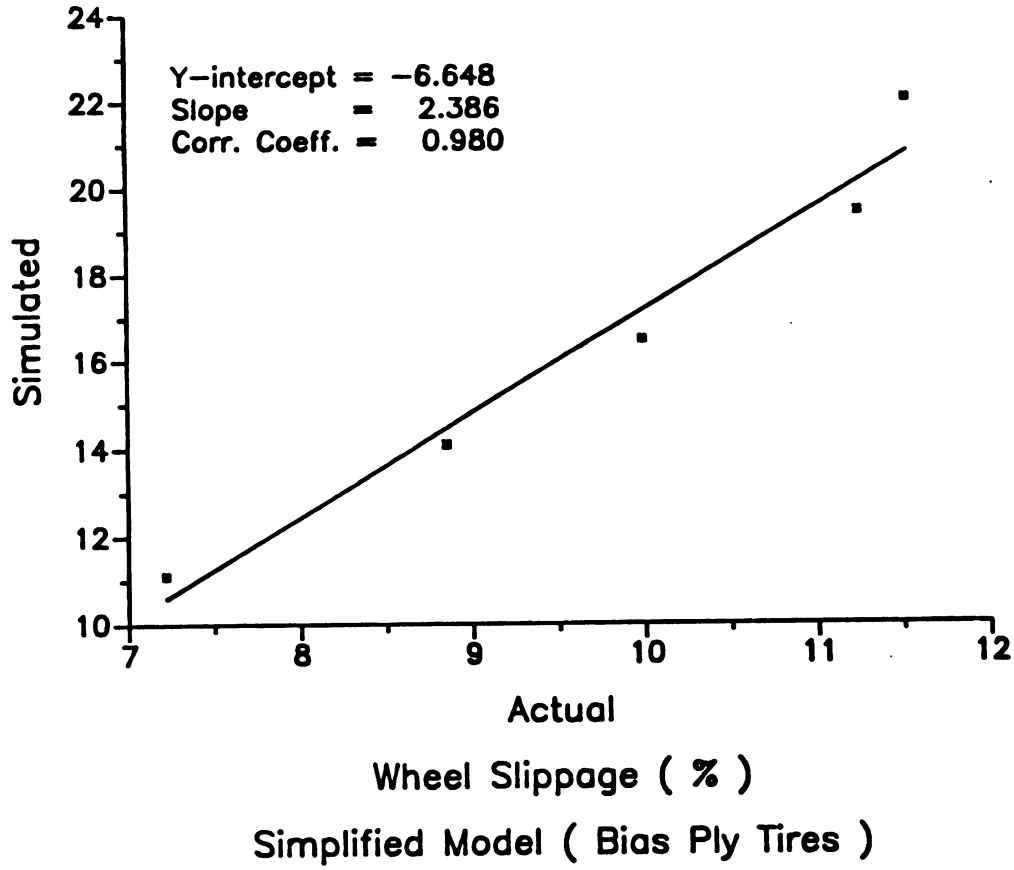

Figure 5.2: Relation of Simulated Wheel Slippage with Actual Data from Nebraska Tractor Test 1247 for the IH1086 Tractor with Bias Ply Tires and Using the Simplified Bond Graph Model

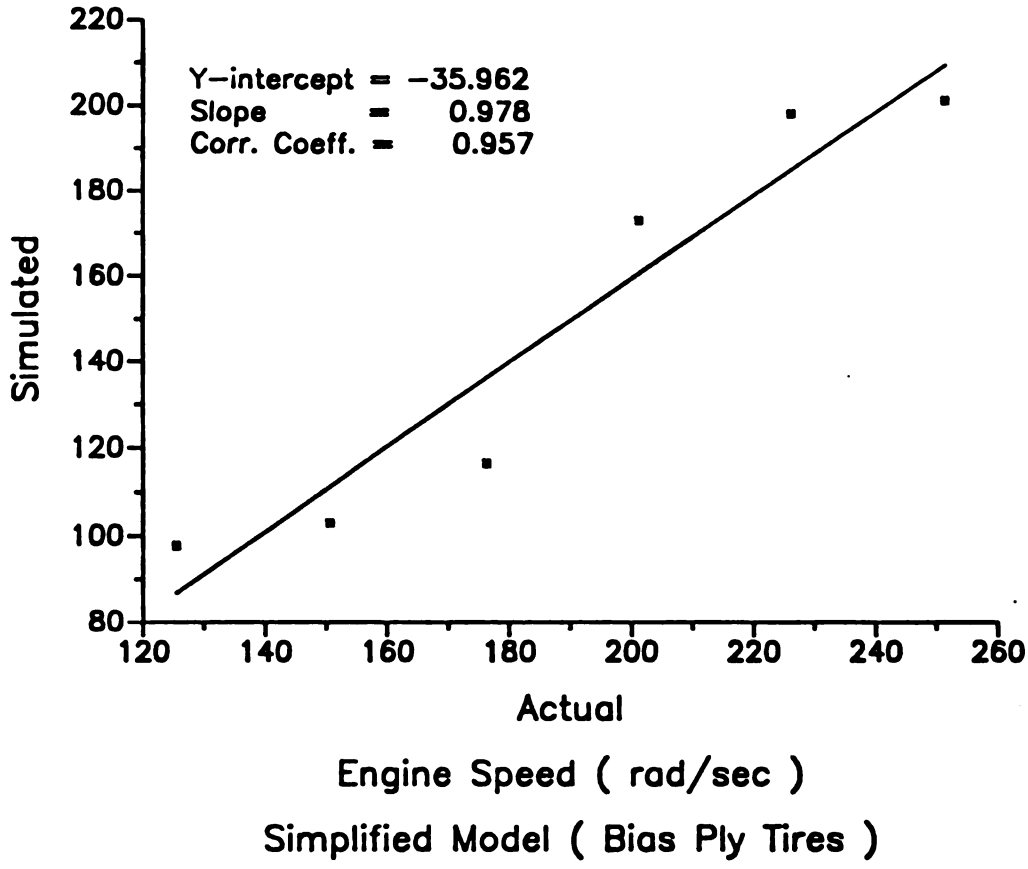

Figure 5.3: Relation of Simulated Engine Speed with Actual Data from Nebraska Tractor Test 1247 for the IH1086 Tractor with Bias Ply Tires and Using the Simplified Bond Graph Model

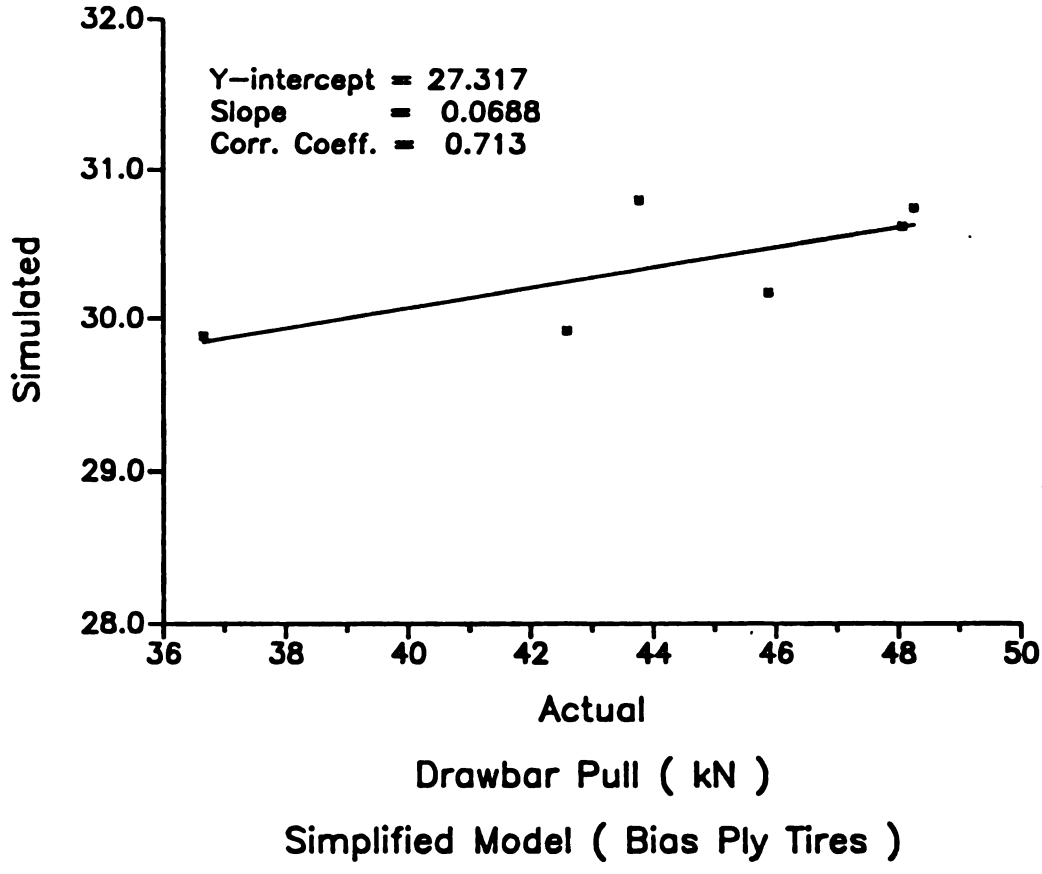

Figure 5.4: Relation of Simulated Drawbar Pull with Actual Data from Nebraska Tractor Test 1247 for the IH1086 Tractor with Bias Ply Tires and Using the Simplified Bond Graph Model

Figure 5.3 shows the simulated engine speed data correlated with the actual engine speed data. The slope of the correlation is 0.978. The intercept is -35.96 rad/s and the correlation coefficient is 0.957. The standard error of estimate is 51.6 rad/s with a root mean square error of 34.8 percent. Figure 5.3 shows that the engine speed will be underpredicted over the entire range of the actual engine speed data from the lugging test.

Figure 5.4 has the simulated steady state drawbar pull data correlated with the actual drawbar pull data. The slope of the correlation is 0.069 with an intercept of 27.297 kN. The standard error of estimate is 17.551 kN with a 57.8 percent root mean square error. The correlation coefficient had a value of 0.717. For the entire range of drawbar loads used in the lugging test, the simplified model would overpredict loads in the range below about 28.600 kN and underpredict those in the range about the same value.

The simplified bond graph model has very poor prediction qualities as the presented analysis of results shows. The model consistently underpredicted drawbar load, overpredicted wheel slippage, underpredicted forward velocity, and underpredicted the engine speed. The underpredicted drawbar load and the over-predicted slippage supply little reaction load to the engine, thus lowering the effective input torque and underpredicting engine speed. At constant engine input torque the velocity is lowered for the low power demand of the drawbar and the wheels.

The correlation coefficients have consistently acceptable values for all parameters measured. This means that for all it is worth in the ability to predict, the model was consistent in performance though its prediction qualities were poor. The model was unable to predict accurately because it neglected the variations in dynamic load on the tire.

5.1.2 Expanded Model

The weakness of the simple model was addressed by incorporating the Wismer-Luth mathematical model into the bond graph model. This model (Wismer and Luth, 1974) had the necessary quantitative quality with parameters that could be varied to analyze additional aspects of the traction process like tire tread configuration. The incorporation of this mathematical model is described in Section 3.4.3. It is referred to as the expanded model.

5.1.2.1 Bias Ply Tires

Results of the simulated performance during the lugging ability test for the IH 1086 with bias ply tires using the expanded model (Figure 3.16) are shown in Table 5.2. The correlation analysis results are also included in Table 5.2 and shown in Figures 5.5, 5.6, 5.7 and 5.8 for forward velocity, wheel slippage, engine speed and drawbar pull.

Table 5.2: Simulated, Actual and Correlation Data for the IH1086 Tractor with Bias Ply Tires Using the Expanded Model.

Unit Pull (kN.s/m)	Parameter Measured	Actual Data	Simulated Data	% Difference
16.148	FV (m/s)	2.27	2.29	0.88
	WS (%)	7.22	9.05	-25.3
	ES (rad/s)	251.3	244.1	2.87
	Pull (kN)	36.655	37.017	-0.38
21.187	FV (m/s)	2.01	1.86	7.46
	WS (%)	8.85	10.96	-23.8
	ES (rad/s)	226.2	203.3	10.10
	Pull (kN)	42.586	39.593	7.03
26.069	FV (m/s)	1.76	1.58	10.23
	WS (%)	9.99	12.70	-27.1
	ES (rad/s)	201.2	175.7	12.67
	Pull (kN)	45.883	41.280	10.03
31.626	FV (m/s)	1.52	1.34	11.84
	WS (%)	11.24	14.71	30.8
	ES (rad/s)	176.3	152.9	13.27
	Pull (kN)	48.258	42.583	11.42
37.122	FV (m/s)	1.30	1.17	10.00
	WS (%)	11.52	16.60	-44.1
	ES (rad/s)	150.6	135.9	9.80
	Pull (kN)	48.258	43.450	9.96
39.794	FV (m/s)	1.10	1.09	0.91
	WS (%)	9.56	17.50	-83.0
	ES (rad/s)	125.5	129.2	-2.95
	Pull (kN)	43.773	43.766	0.016

Statistical Results

	Standard Error of Estimate	Root Mean Square Error (RMS - %)
Forward Velocity	0.162 m/s	10.39
Wheel Slip	5.38 %	39.60
Engine Speed	29.06 rad/s	16.75
Pull	4.569 kN	11.07

The plot of the simulated forward velocity versus the actual data (Figure 5.5) has a slope of 1.020 and an intercept of -0.138 m/s. The correlation coefficient is 0.981. The standard error of estimate is 0.162 m/s with a root mean square error of 10.39 percent. The actual forward velocity is slightly and almost equally underpredicted over the range of forward velocities between zero and 2.5 m/s. This includes the range of velocities used in the lugging ability test.

The slope, intercept and correlation coefficient (R square) of the other plots are also shown in the respective Figures. Figure 5.6 shows the wheel slippage was underpredicted below and overpredicted above the value of about 3 percent slip. The corresponding standard error of estimate was 5.38 percent with a root mean square error of 39.60 percent. Figure 5.6 shows the plot of the data point for the last set of correlation data on Table 5.2 to be uniquely in larger prediction error than the others. This is because the actual data for this one point (unit load 39.74 kN.s/m) was obtained in the governor controlled range. Leaving this data point out of the analysis changed the correlation data by only 5 percent. Figure 5.7 shows the engine speed was overpredicted below and underpredicted above a speed of about 30 rad/s. The standard error of stimate was 29.06 rad/s with a root mean square error of 16.75 percent. The drawbar pull was overpredicted below and

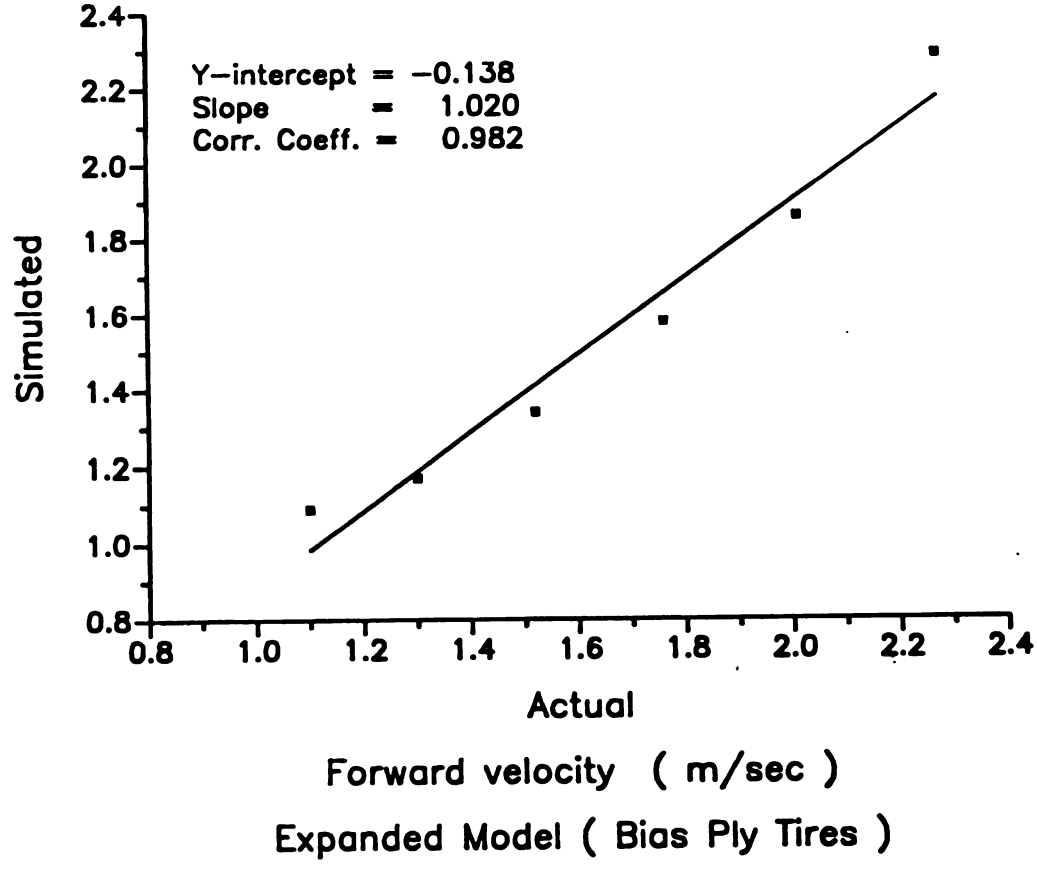

Figure 5.5: Relation of Simulated Forward Velocity with Actual Data from Nebraska Tractor Test 1247 for the IH1086 Tractor with Bias Ply Tires and Using the Expanded Bond Graph Model

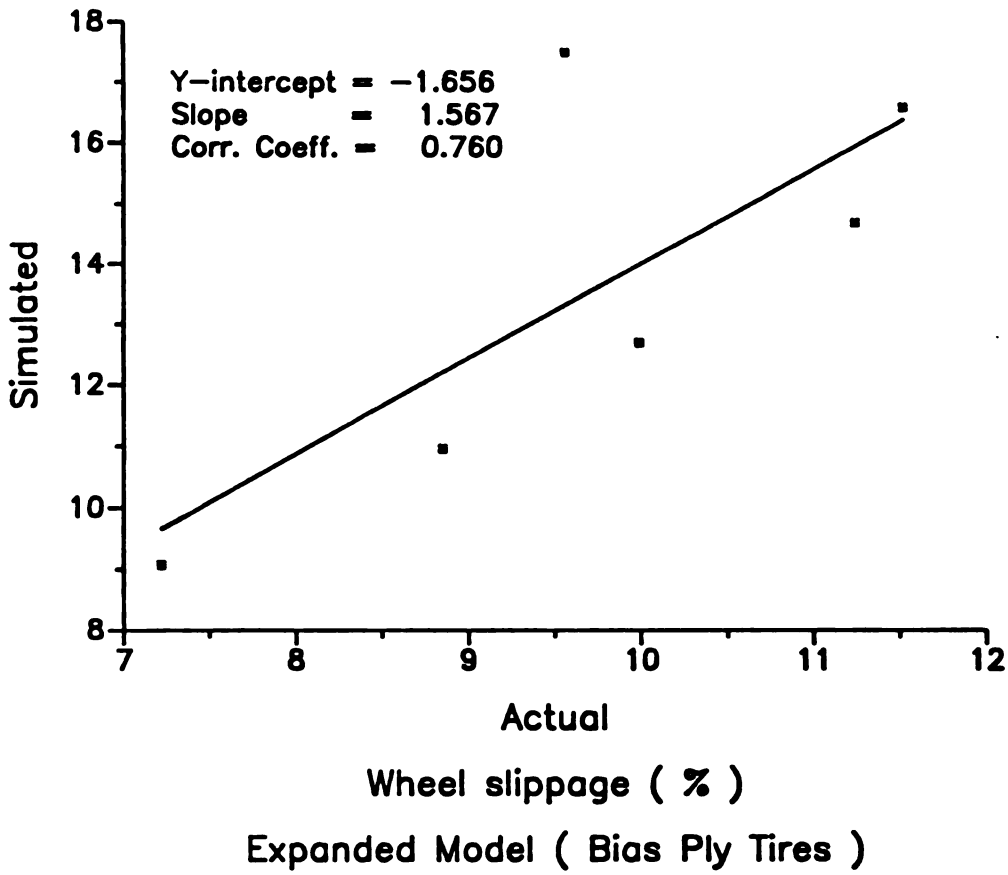

Figure 5.6: Relation of Simulated Wheel Slippage with Actual Data from Nebraska Tractor Test 1247 for the IH1086 Tractor with Bias Ply Tires and Using the Expanded Bond Graph Model

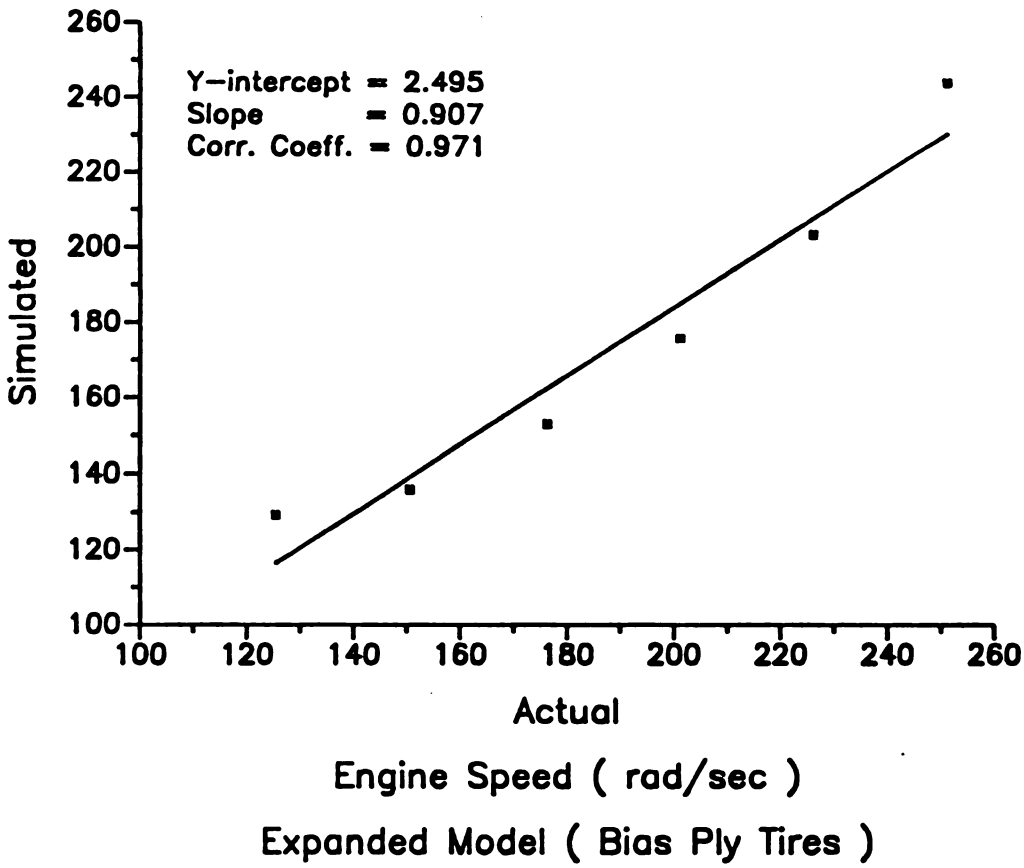

Figure 5.7: Relation of Simulated Engine Speed with Actual Data from Nebraska Tractor Test 1247 for the IH1086 Tractor with Bias Ply Tires and Using the Expanded Bond Graph Model

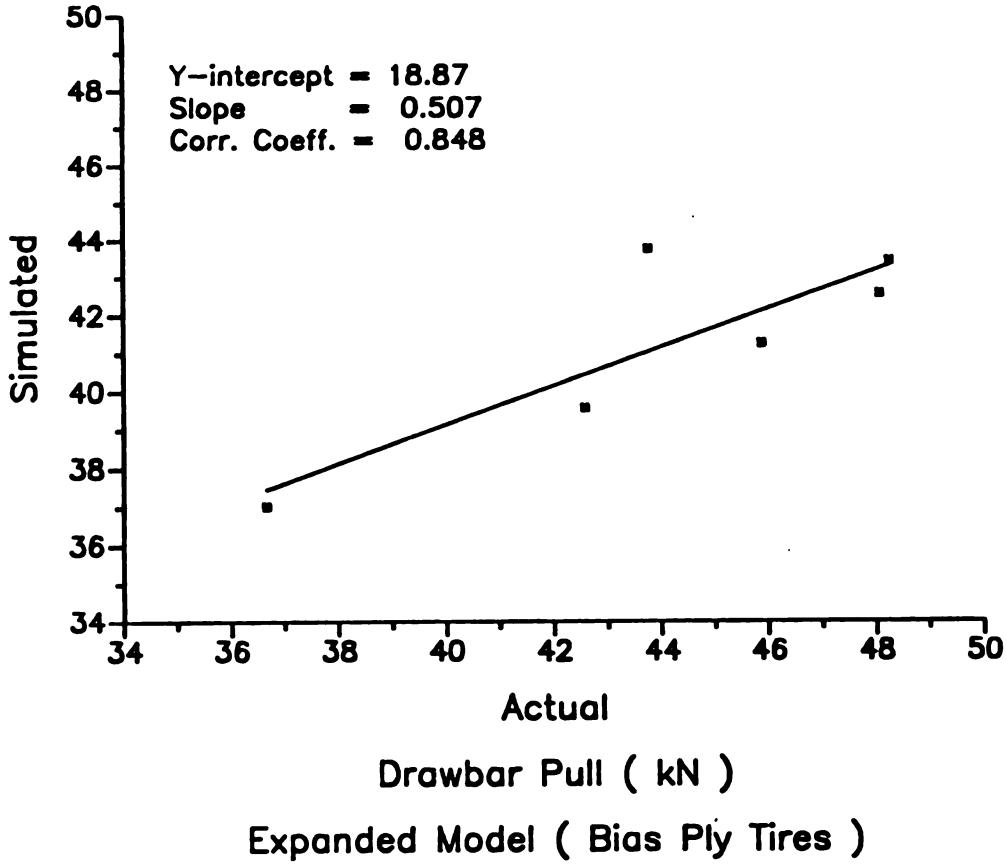

Figure 5.8: Relation of Simulated Drawbar Pull with Actual Data from Nebraska Tractor Test 1247 for the IH1086 Tractor with Bias Ply Tires and Using the Expanded Bond Graph Model

underpredicted above a pull of about 38.500 kN. The corresponding standard error of estimate was 4.569 kN with a root mean square error of 11.07 percent.

The expanded model with bias ply tires predicted the actual tractor performance with highly improved accuracy. The prediction error for wheel slippage was still the dominant one even with the expanded model.

5.1.2.2. Radial Ply Tires

Results of the simulated performance during the lugging ability test for the IH 1086 tractor with radial ply tires and using the expanded model are shown in Table 5.3. Figures 5.9, 5.10, 5.11 and 5.12 show the correlation results for forward velocity, wheel slippage, engine speed and drawbar pull. The slope, intercept and correlation coefficients of the plots are shown in the figures.

The simulation results of the various measured parameters were further improved in accuracy relative to those of the bias ply tire test with both the simplified and expanded models. The slopes are 0.922, 1.442, 0.862 and 0.789 for the plots of simulated versus actual data for the forward velocity, wheel slip, engine speed and drawbar pull.

Table 5.3: Simulated, Actual and Correlation Data for the IH1086 Tractor with Radial Ply Tires Using the Expanded Model.

Unit Pull (kN.s/m)	Parameter Measured	Actual Data	Simulated Data	% Difference
14.429	FV (m/s)	2.45	2.46	-0.41
	WS (%)	4.40	5.52	-25.51
	ES (rad/s)	251.5	252.4	-0.35
	Pull (kN)	35.352	35.521	-0.478
18.722	FV (m/s)	2.18	2.04	6.42
	WS (%)	5.40	6.64	-22.9
	ES (rad/s)	225.4	211.7	6.08
	Pull (kN)	40.815	38.214	-6.37
22.605	FV (m/s)	1.94	1.84	5.15
	WS (%)	6.05	7.33	-21.21
	ES (rad/s)	201.5	192.5	4.47
	Pull (kN)	43.854	41.623	5.09
27.289	FV (m/s)	1.68	1.60	4.76
	WS (%)	6.53	8.39	-28.48
	ES (rad/s)	176.2	168.9	4.14
	Pull (kN)	45.847	43.572	4.96
31.944	FV (m/s)	1.45	1.41	2.75
	WS (%)	6.85	9.45	-37.96
	ES (rad/s)	151.1	150.6	0.33
	Pull (kN)	46.319	44.959	2.94
34.294	FV (m/s)	1.21	1.32	-9.09
	WS (%)	5.72	10.04	-75.52
	ES (rad/s)	125.2	142.0	-13.42
	Pull (kN)	41.496	45.224	-8.96

Statistical Results

	Standard Error of Estimate	Root Mean Square Error (RMS - %)
Forward Velocity	0.112 m/s	6.28
Wheel Slip	8.33 %	36.55
Engine Speed	12.30 rad/s	6.60
Pull	2.859 kN	6.89

The corresponding standard errors of estimate are 0.112 m/s, 8.33%, 12.30 rad/s, 2.859 kN with root mean square errors of 6.28, 36.55, 6.60 and 6.89 percent for forward velocity, wheel slippage, engine speed and drawbar pull respectively.

The forward velocity is overpredicted below and underpredicted above an actual forward velocity of about 1.4 m/s. The wheel slip is underpredicted below an actual wheel slip of about 1.3 percent and overpredicted in the range of actual slip values above 1.3 percent. Slip was overpredicted in the entire range of actual slip data used in the lugging ability test. In fact in all three sets of prediction setups (with the two models and tire types) slip carried the largest prediction error and it was overpredicted within the entire ranges of actual test data from Nebraska Tractor Test 1247. With the radial tires and using the expanded model engine speed is overpredicted below and underpredicted above the actual engine speed of 173 rad/s. Drawbar pull is overpredicted below and underpredicted above an actual pull of about 39.000 kN.

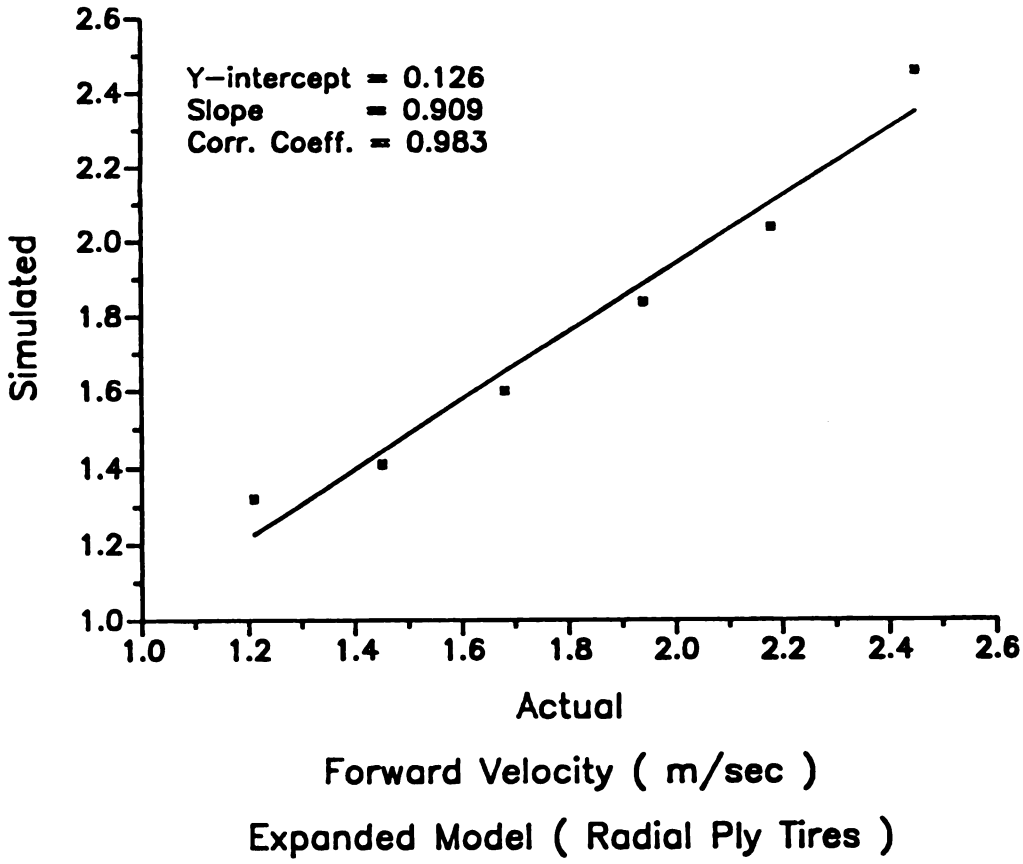

Figure 5.9: Relation of Simulated Forward Velocity with Actual Data from Nebraska Tractor Test 1247 for the IH1086 Tractor with Radial Tires and Using the Expanded Bond Graph Model

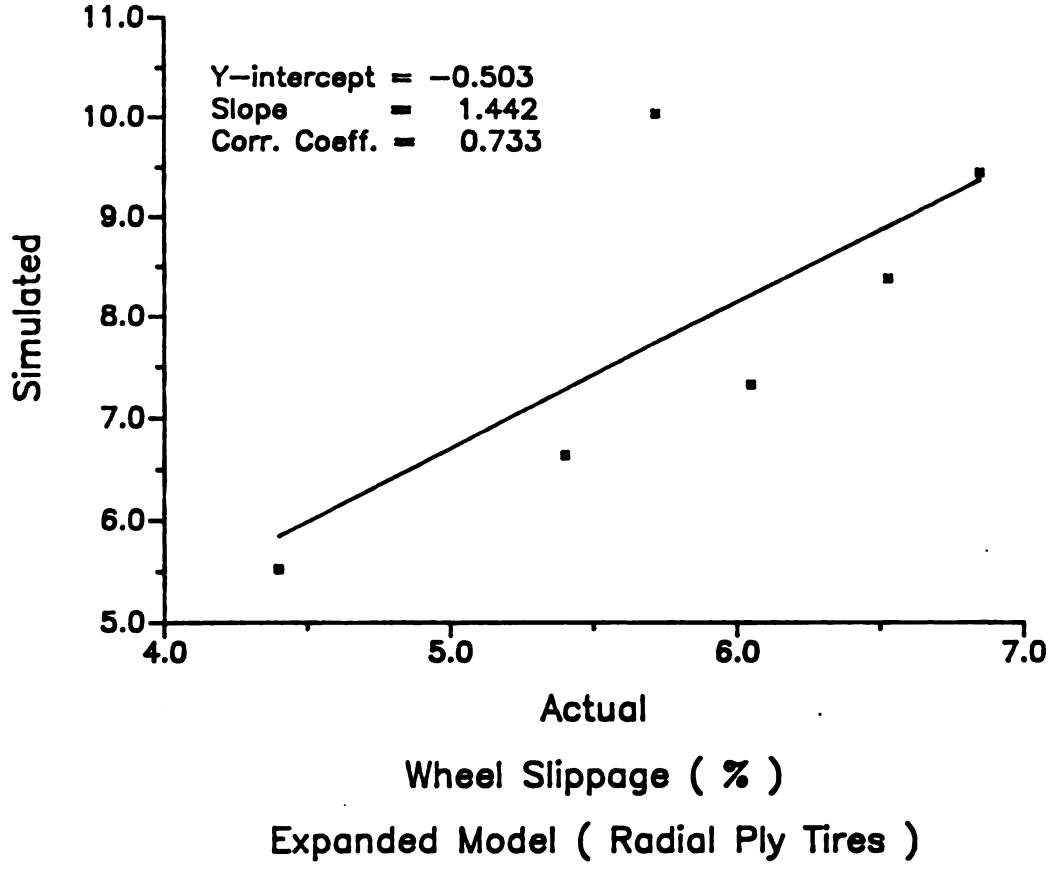

Figure 5.10: Relation of Simulated Wheel Slippage with Actual Data from Nebraska Tractor Test 1247 for the IH1086 Tractor with Radial Ply Tires and Using the Expanded Bond Graph Model

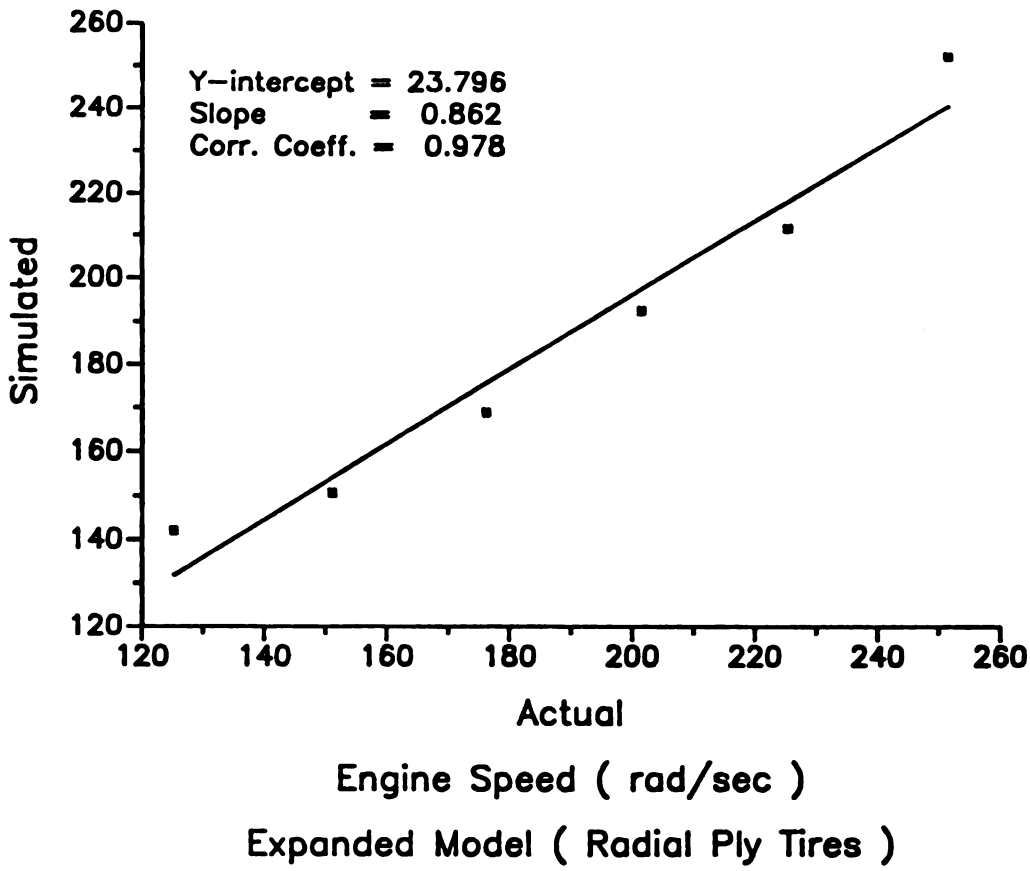

Figure 5.11: Relation of Simulated Engine Speed with Actual Data from Nebraska Tractor Test 1247 for the IH1086 Tractor with Radial Ply Tires and Using the Expanded Bond Graph Model

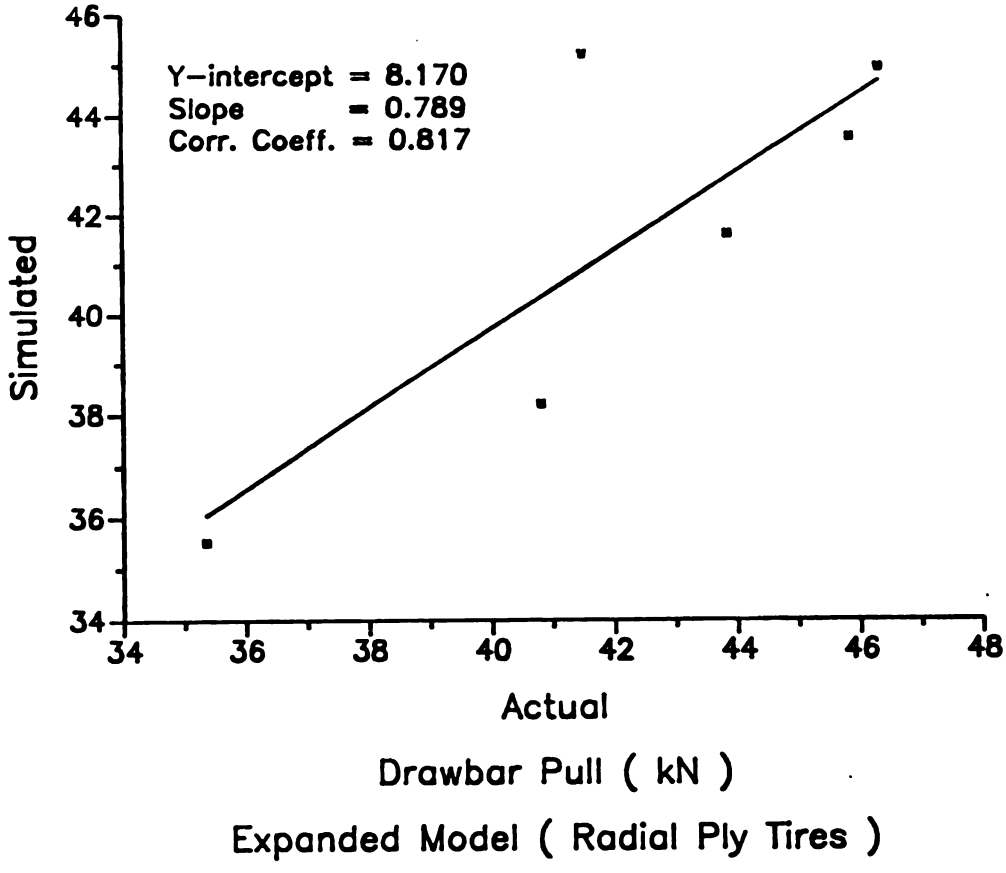

Figure 5.12: Relation of Simulated Drawbar Pull with Actual Data from Nebraska Tractor Test 1247 for the IH1086 Tractor with Radial Ply Tires and Using the Expanded Bond Graph Model

5.2 Model Response

The bond graph model was run for the two wheel drive tractor with single radial ply drive wheels on concrete to demonstrate model response to a LIMITER-function (see Appendix A) drawbar loading. The slope was set at the unit drawbar load of the first lugging ability validation test on Table 5.3 (14.429 kN.s/m). The limiting drawbar force was set at the recorded lugging test value of 35.352 kN. This setup was different from the one used in the model validation test (GAIN-function) in that the limiting steady state (time-response assymptote) drawbar load was selected as opposed to letting the system dynamics "naturally" settle around it.

A comparison of Figures 5.13 and 5.14 with Figures 5.15 and 5.16 shows that the steady state engine speeds and forward velocities attained are approximately equal (257.8 rad/s and 259.5 rad/s, and 2.52 m/s and 2.54 m/s respectively). The main difference with the LIMITER function is the system took about 14 seconds to reach steady state while it took about 8.5 seconds with the GAIN function. All other measured parameters also attained similar steady state values with the longer response time being the only difference.

A second test on the model response was made with a drawbar load of the BACKLASH (see Appendix A) function type. With the tractor operating initially at wide open throttle and with no drawbar load (on concrete), a GAIN-function load

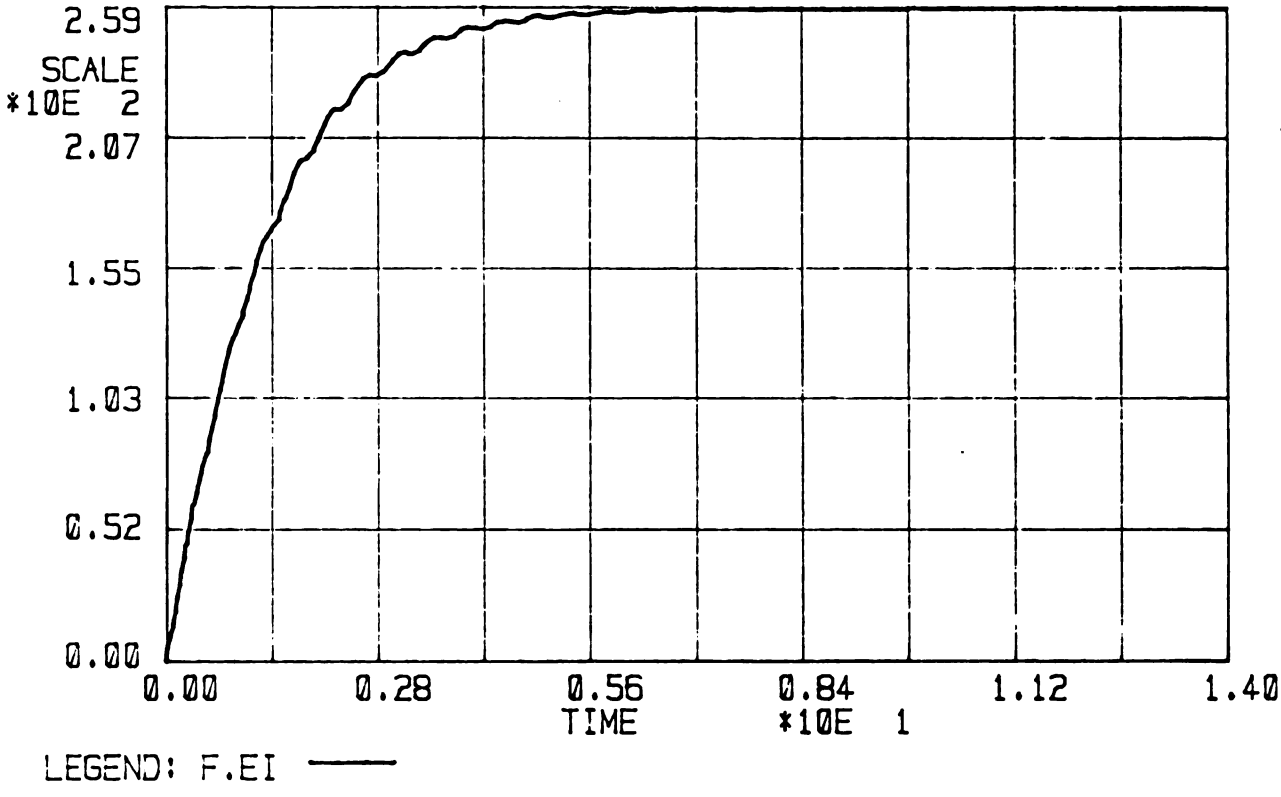

Figure 5.13: Time Response of Engine Speed Due to a Gain-Function Drawbar Load

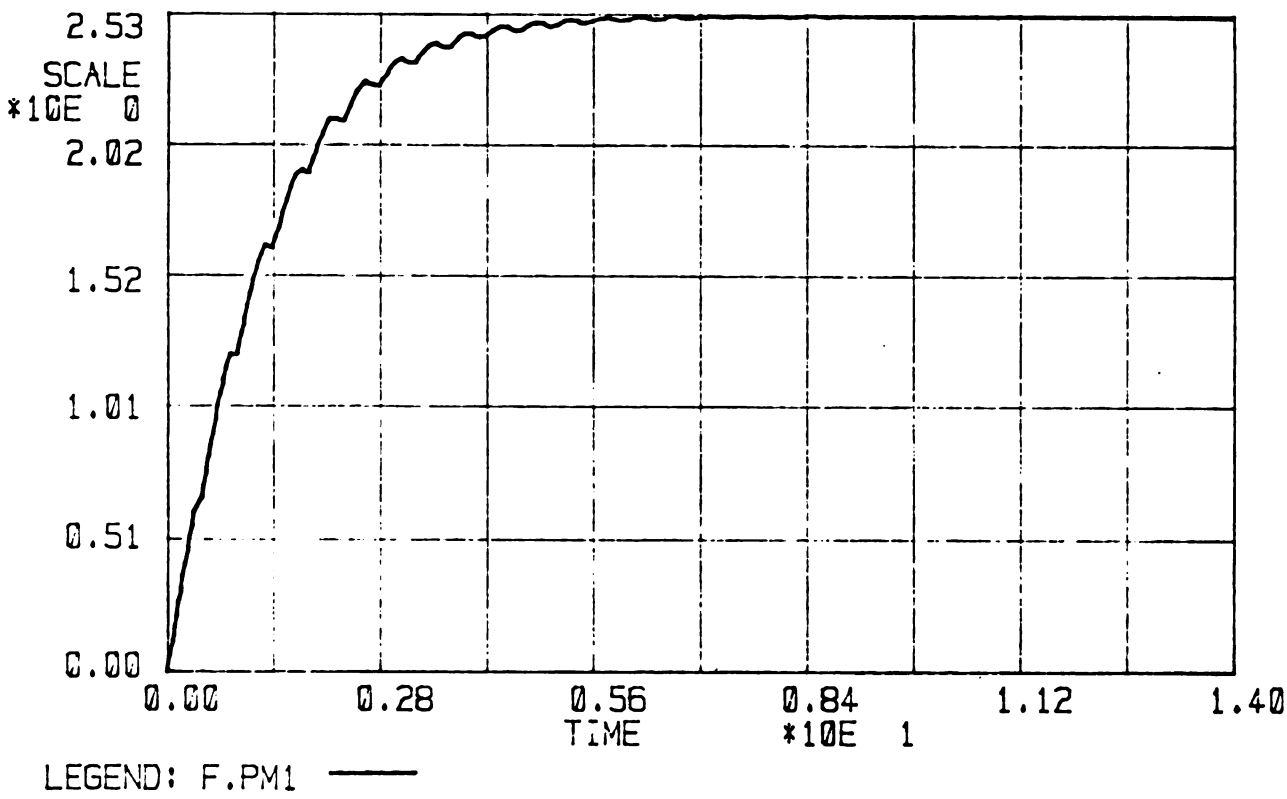

Figure 5.14: Time Response of Forward Velocity Due to a Gain-Function Drawbar Load

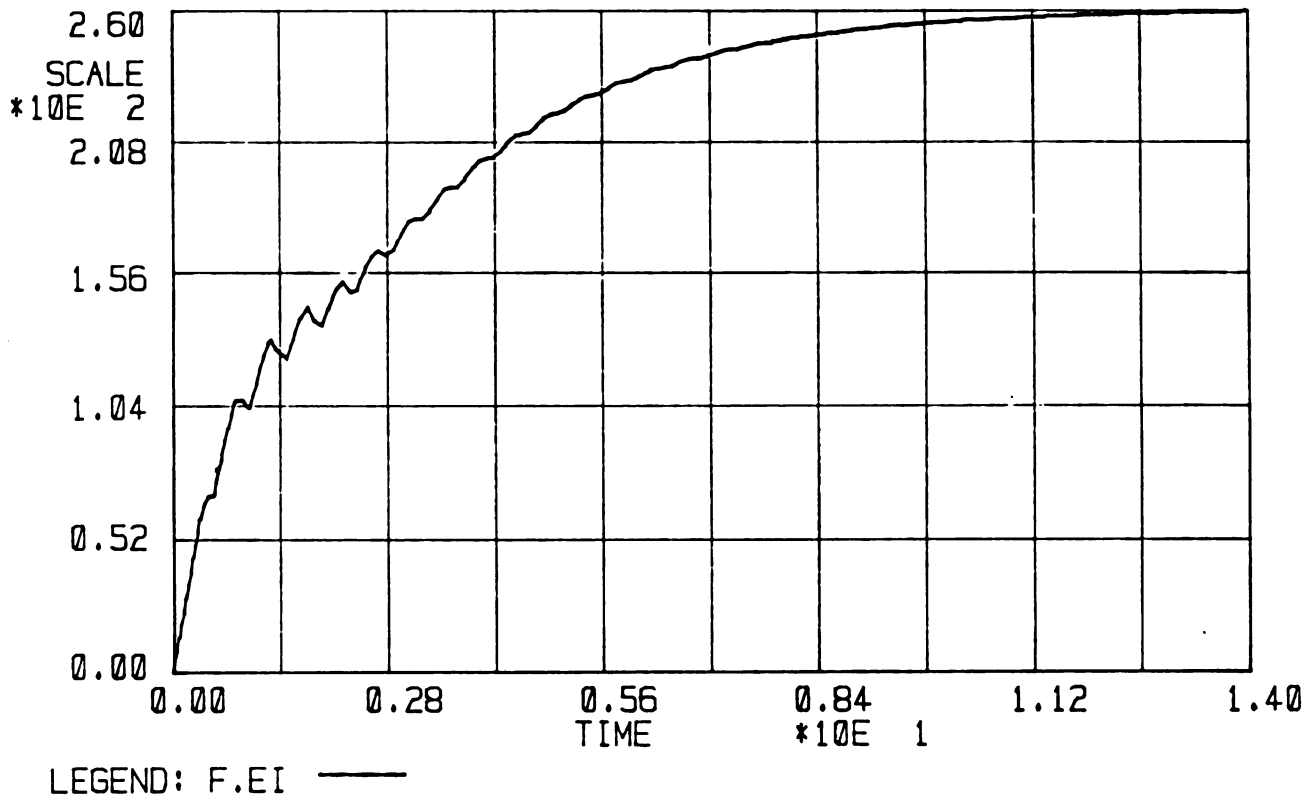

Figure 5.15: Time Response of Engine Speed Due to a LIMITER-Function Drawbar Load

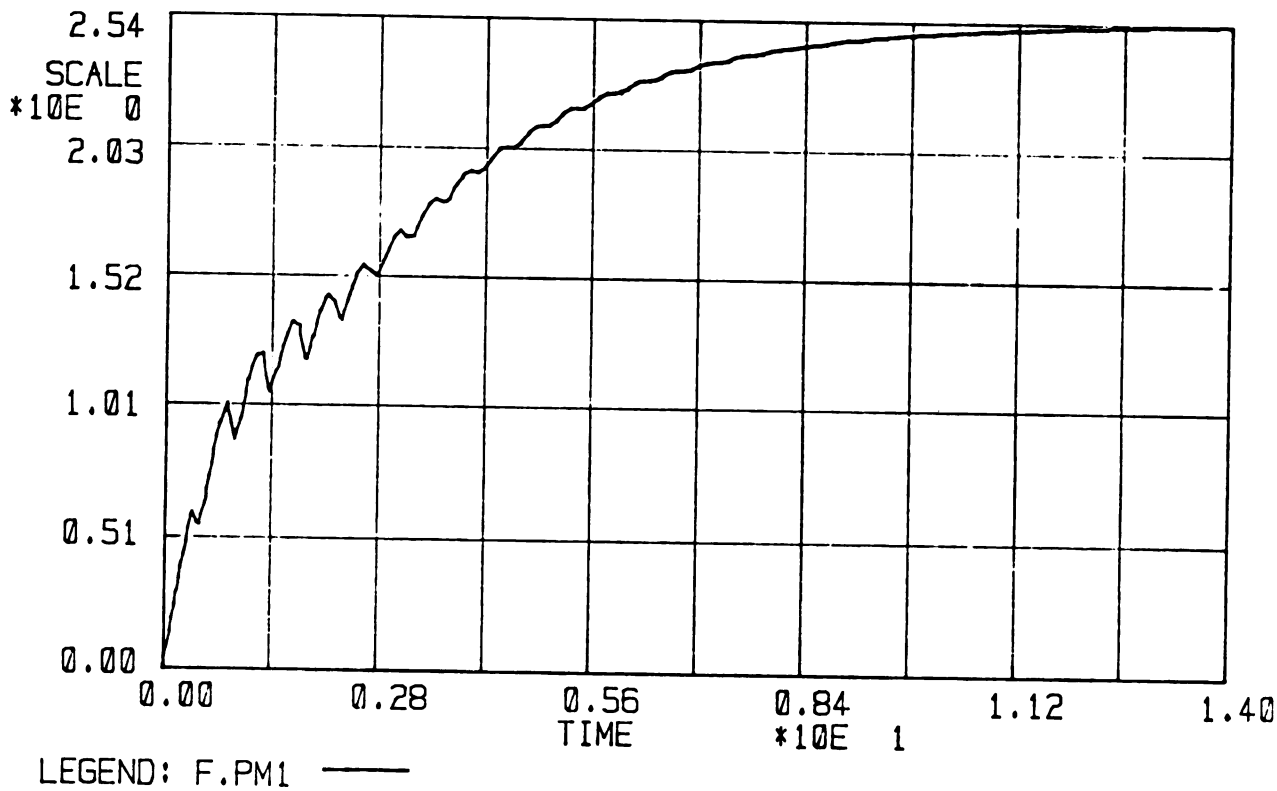

Figure 5.16: Time Response of Forward Velocity Due to a LIMITER-Function Drawbar Load

was applied after 1.2 seconds of simulation time. The drawbar unit load was given the same slope value (14.429 kN.s/m) as with the LIMITER function setup. The load as earlier was a function of forward velocity.

Figures 5.17 and 5.18 show the time response of engine speed and forward velocity under the BACKLASH-function load conditions. The steady state values (for engine speed and forward velocity) are higher than before and different because the system dynamics settle into steady state from a different set of initial conditions upon the application of the load and the steady state drawbar load attained is smaller. From the response results reported above, with the LIMITER drawbar load, it follows that, had the rise part of the BACKLASH function been truncated and kept constant at the steady state drawbar load, the system would attain the same steady state values as before.

Figure 5.17 and 5.18 compared to Figures 5.13 and 5.14 show a smoother response for the engine speed and forward velocity to the delayed velocity-dependent drawbar load. Figures 5.19 and 5.20 (see Appendix B) show the plots of transient to steady state slip under the drive tire for GAIN and BACKLASH-function drawbar loads respectively. The slip variation with the BACKLASH load is less drastic than with the GAIN-function load for the first two seconds of simulation. The steady state slip value is lower for the BACKLASH function - 3.97 percent compared to 5.41 percent for the GAIN function load. This is attributable to the

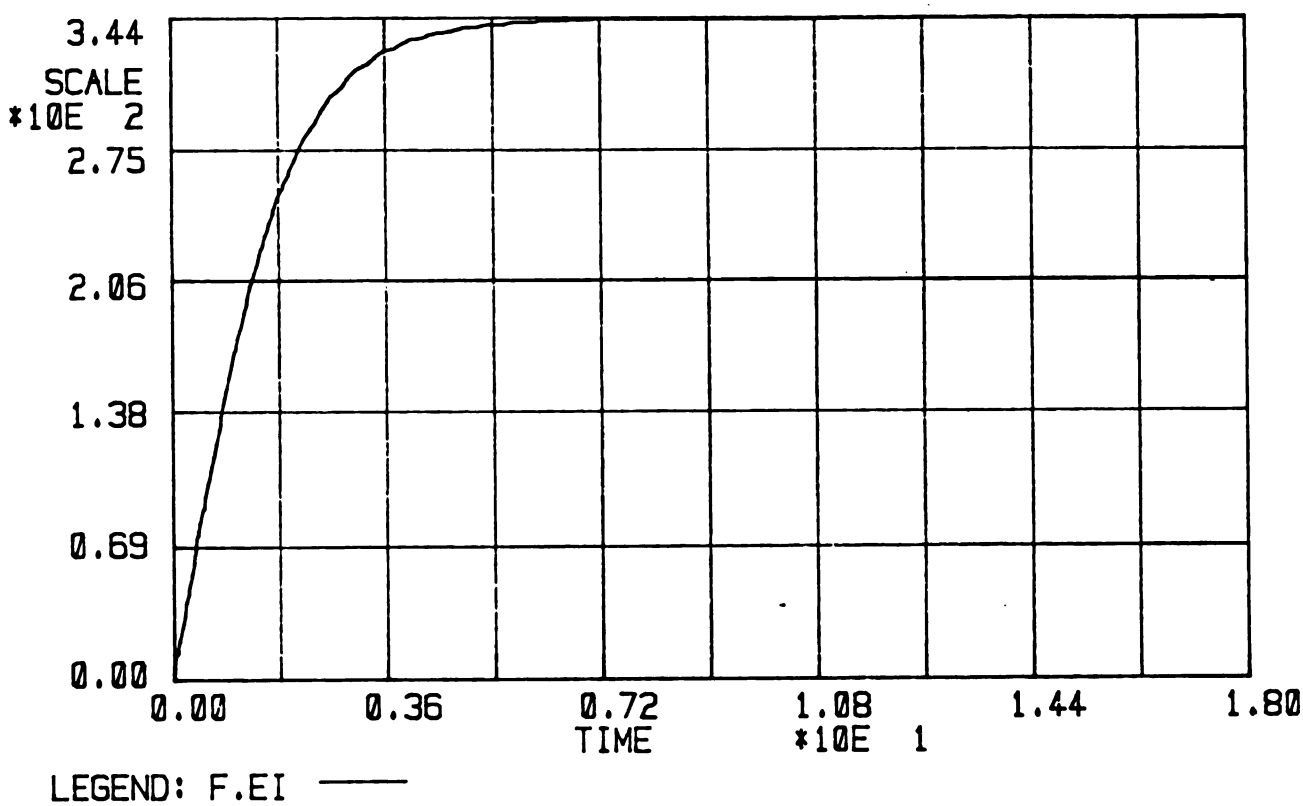

Figure 5.17: Time Response of Engine Speed Due to a BACKLASH-Function Drawbar Load

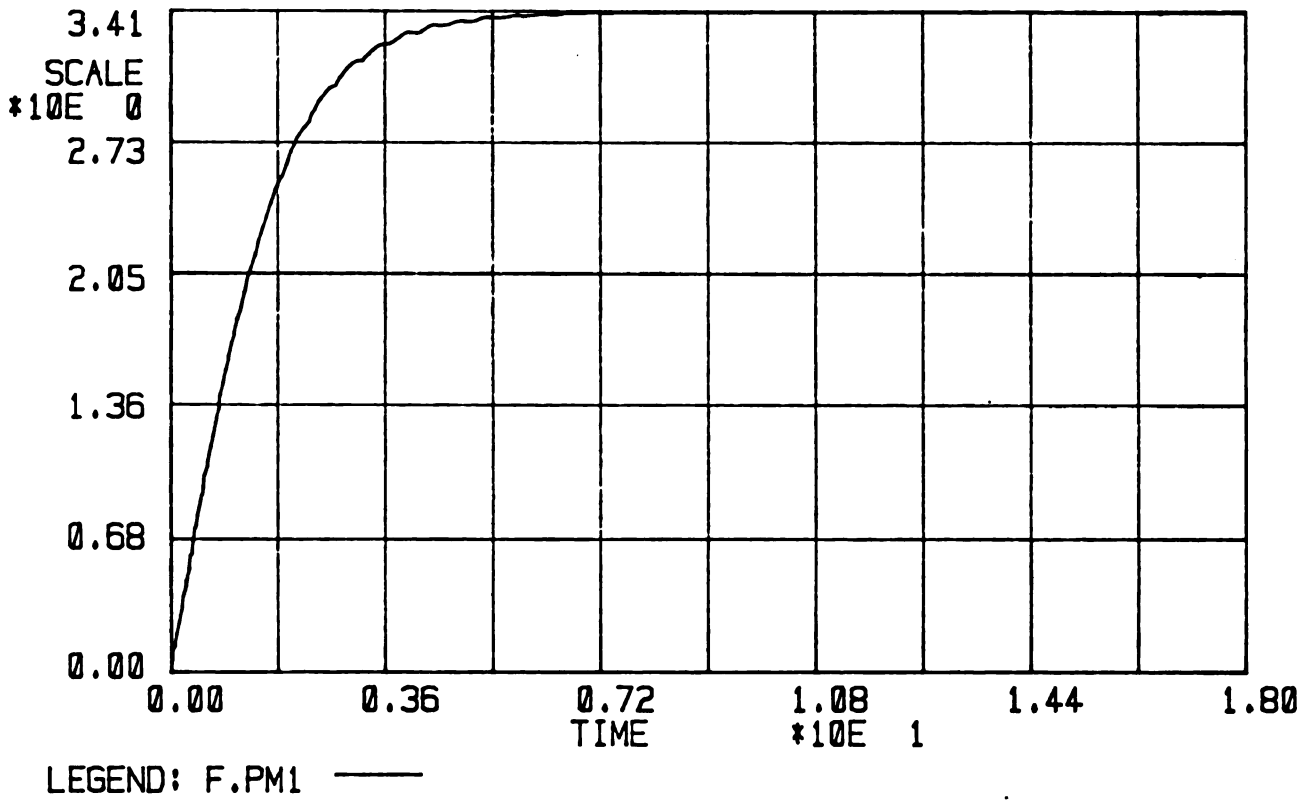

Figure 5.18: Time Response of Forward Velocity Due to a BACKLASH-Function Drawbar Load

lower steady state drawbar load attained with the BACKLASH-function setup.

Figure 5.19 and Figure 5.20 (see Appendix B) show the pitch motion displacement of the tractor with respect to time, for the GAIN-function and BACKLASH-function drawbar loads respectively. With the GAIN-function load a steady state drawbar load of 36.311 kN was attained while a drawbar load of 30.878 kN was attained with the backlash setup. These Figures show steady state pitch displacements of positive 3.8×10^{-3} (0.217 degrees) and 2.3×10^{-3} (0.132 degrees) radians for the BACKLASH and the GAIN-function loads respectively. It is observable from Figures 5.19 and 5.20 that the more drastic GAIN-function drawbar load (Figure 5.19) causes the tractor to pitch slightly forwards (hence the negative values of pitch displacement) while the BACKLASH-function load (Figure 5.20) only pitches the tractor backwards. The more drastic steady state load of the GAIN-function gives the tractor a smaller (positive) pitch displacement angle as it has a larger (negative) pitch moment about the transverse axis through the center of gravity. The GAIN-function load is large enough to apply a moment of a magnitude capable of overcoming the tendency for the tractor chassis to pitch backwards upon the initial acceleration.

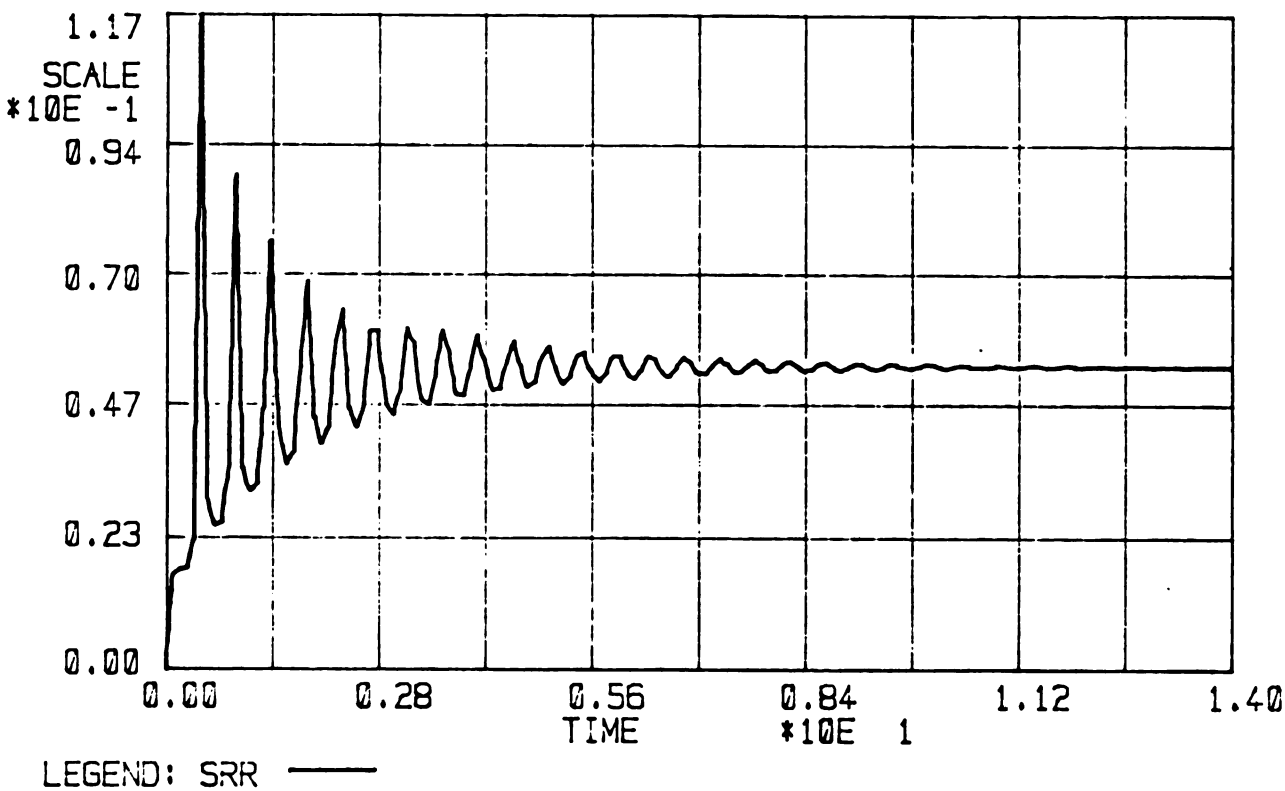

Figure 5.19: Transient Time-Variation of Tire Slippage for a Tractor Exposed to Gain-Function Drawbar Load.

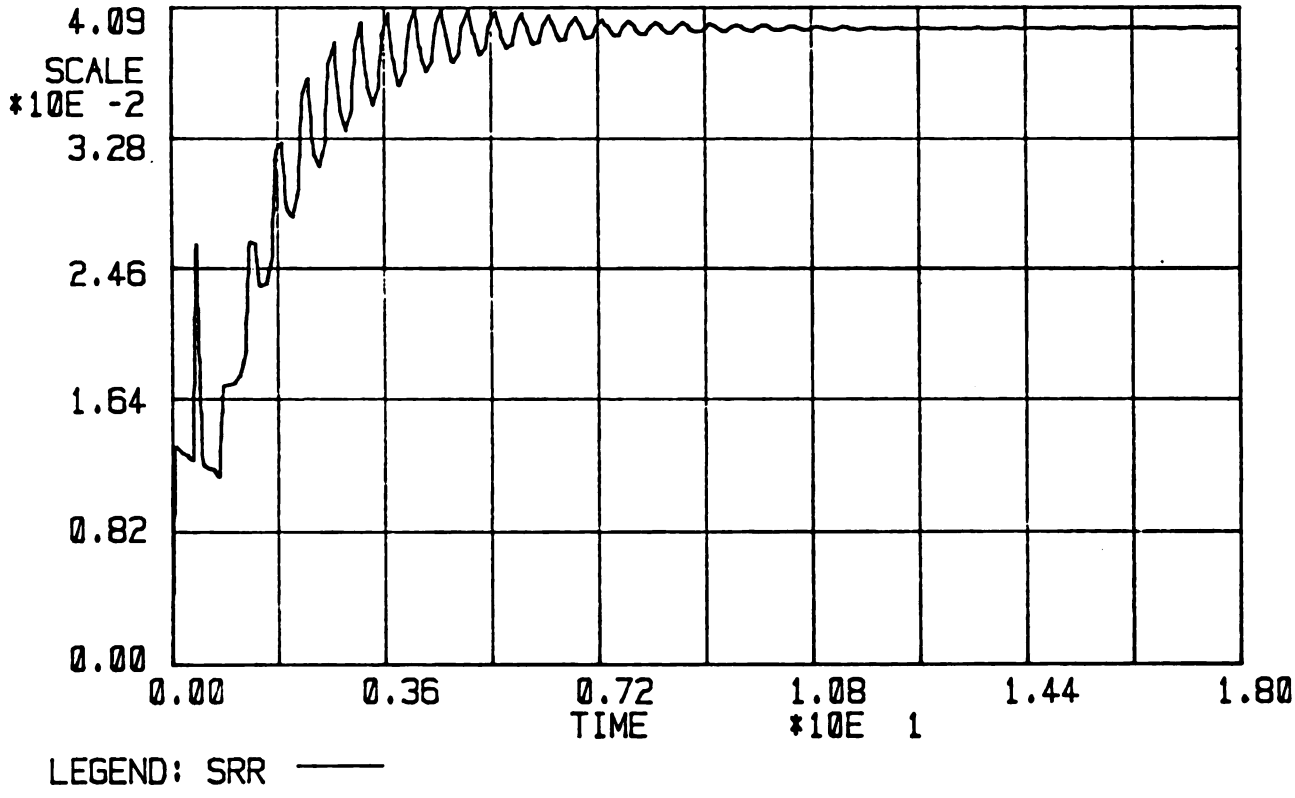

Figure 5.20: Transient Time-Variation of Tire Slippage for a Tractor Exposed to BACKLASH-Function Drawbar Load.

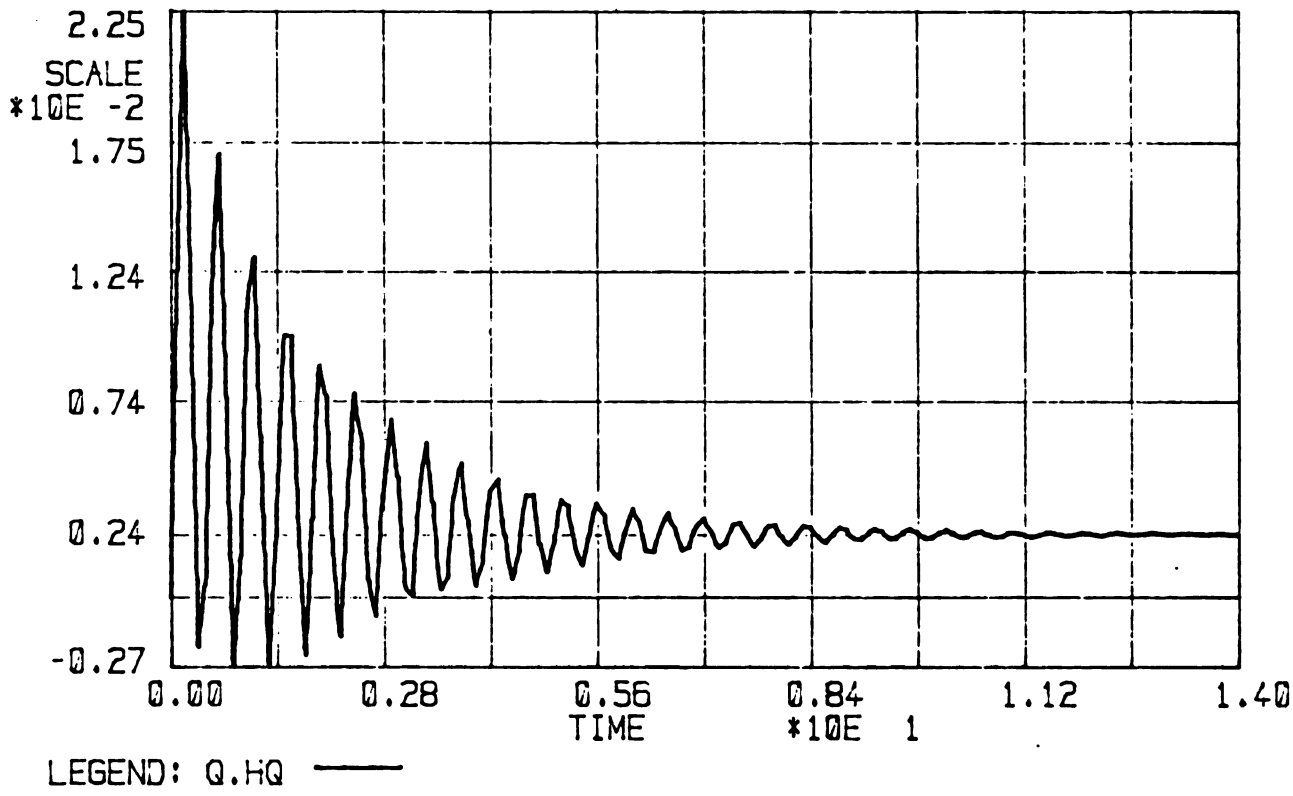

Figure 5.21: Pitch-Motion Transient Displacement of a Tractor Exposed to Gain-Function Drawbar Load.

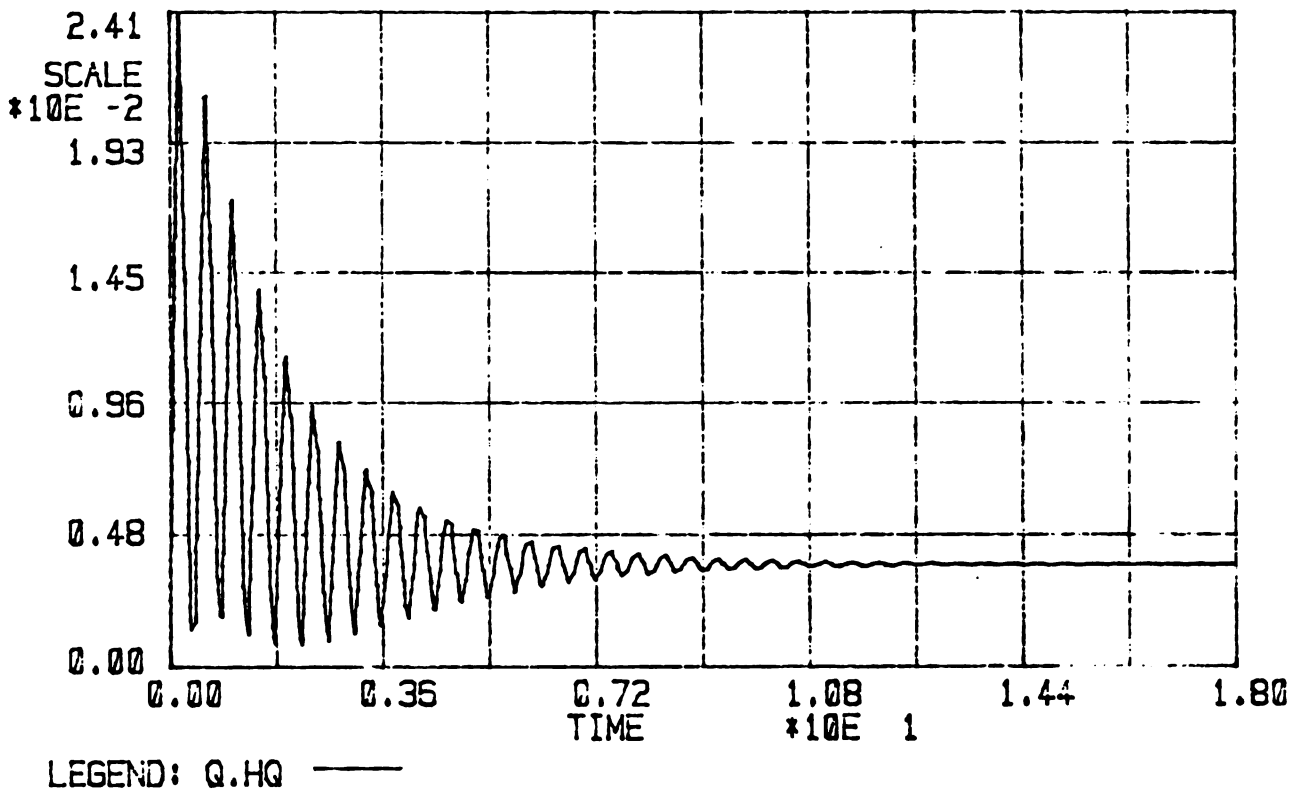

Figure 5.22: Pitch-Motion Transient Displacement of a Tractor Exposed to BACKLASH-Function Drawbar Load.

5.3. Model Demonstration

The model was demonstrated by simulating the performance of the tractor while moldboard plowing a dry untilled soil. A comparison was made between the simulated performance of the tractor with radial and bias ply drive-tires, single and dual drive radial ply tires and the performance with ballasted and non ballasted (single-radial ply) drive tires. A non-statistical quantitative comparison of simulated performance data was conducted.

The implement model supplied by ASAE Data: ASAE D230.3 (ASAE, 1982a) was used to generate the moldboard plow drawbar force. The mold board plow draft model operating on a Decatur clay loam soil is listed as:

$$P = 6 + 0.053\ \dot{x}^2 \qquad \ldots (5.3)$$

Where:

P = unit draft (force) (N/cm^2)

$\dot{x}$ = forward velocity (km/h)

The plow was assumed to be a five bottom plow with moldboards 40.6 cm wide and operating 20 cm deep. The tractor was assumed to operate with on-land hitching so that the drive tires operate on undisturbed soil with a soil Cone Index of 1.03 MPa. The plow hitch was further assumed to be adjusted such that significant vertical force was not applied to the tractor drawbar.

5.3.1. Single Drive Wheels

Table 5.4 lists the simulation data for radial ply and bias ply drive tires while moldboard plowing. The table shows the kind of data that the model generates directly as ENPORT-7 post-processor outputs. The steady state drawbar load generated by the radial ply drive tires setup is larger than that generated by the bias ply setup. The radial tires displayed better tractive efficiency, a case that leads to higher drawbar work at a lower engine speed (hence lower fuel consumption).

Figure 5.23 shows a plot of traction power characteristics relating the single drive-axle (one wheel) input power to the slippage power (of one wheel) and the total drawbar power. The visible waveform of the plots during steady state performance (after about 10 seconds of simulation time) is a result of the relatively large computation interval used in the integration as a means of reducing the total computation time.

The wave form visible during the computation time range (transient time) between zero and about 10 seconds could have been reduced in amplitude with a smaller computation interval. The wave form is in part a result of the transient variation in dynamic load on the drive wheel. When the dynamic load on the tire falls the slippage power (W.LRS) rises causing the drawbar power (W.FDX) to fall. The wave form of the slippage power therefore lags that of the drawbar power by about 180 degrees.

Table 5.4: Simulation Data for the Performance of the Tractor with Radial Ply and Bias Ply Drive Tires While Moldboard Plowing

Parameter	Radial Ply Tires	Bias Ply Tires
Forward Velocity* (m/s)	0.893**	0.874**
Engine Speed* (rad/s)	98.90	109.34
Wheel Slippage* (%)	14.55	20.79
Tractive Efficiency* (%)	76.59	71.19
Distance Covered in 14 seconds (m)	11.91	11.56
Mean Drive Axle Power (kW)	42.82	47.48
Mean Slippage Power (kW)	6.38	9.96
Rear Wheels Mean Motion-Resistance Power (kW)	3.14	3.22
Front Wheels Mean Motion-Resistance Power* (kW)	1.62	1.62
Mean Drawbar Power (kW)	25.27	23.96
Mean Drawbar Force* (kN)	28.266	27.446

* Steady State Value

** Forward Velocity is 2.56 m/s at Zero Slip and Rated Engine Speed of 251.3 rad/s

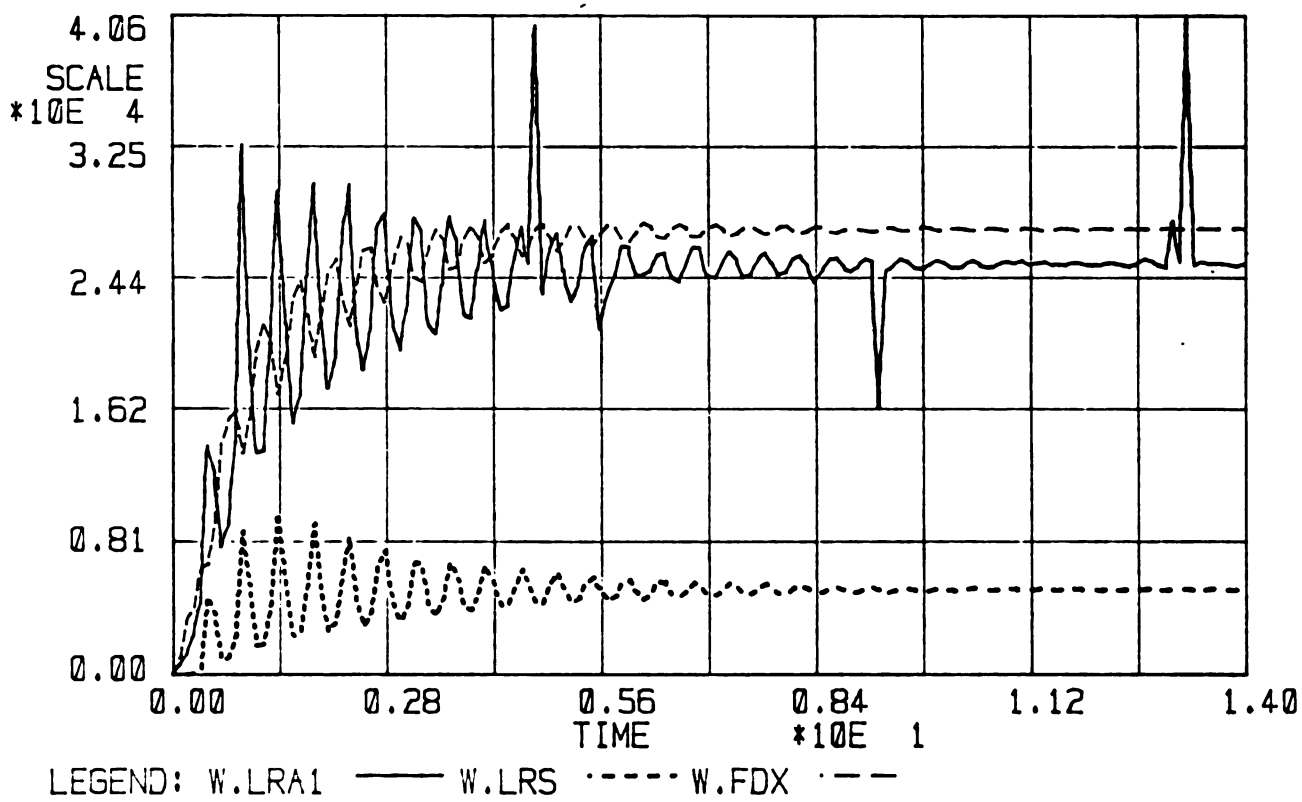

Figure 5.23: Variations of a Single Drive Axle Power, Single Wheel Slippage Power and Drawbar Power During Transient Motion of the Drive-Wheel

Figure 5.24 is a plot of the variation of tractive efficiency (TEF) of the drive wheel with respect to time. It shows the tractive efficiency rising to a constant (steady state) value in approximately 10 seconds of simulation time. Figure 5.25 shows the variation of tractive efficiency with slip (SRR). The plot displays the apparent variation of tractive efficiency during the transient motion before a steady state value of 71.19 percent at a slippage value of 20.7 percent is attained. The plot accommodates the jerkiness of the magnitude of slip and tractive efficiency during transient motion under variable dynamic load on the tire.

5.3.2 Dual Drive Wheel

Table 5.5 has comparative simulation data for the performance of a tractor with single and dual drive tires while moldboard plowing. It is apparent from this data that the dual drive tires have an advantage over the single drive tire as would be expected. The dual drive tires have a larger slippage power loss compared to the single drive tire, but their higher tractive efficiency makes more of the input axle power available at the drawbar. Overall, the forward velocity of the tractor attained is higher with the dual drive tires.

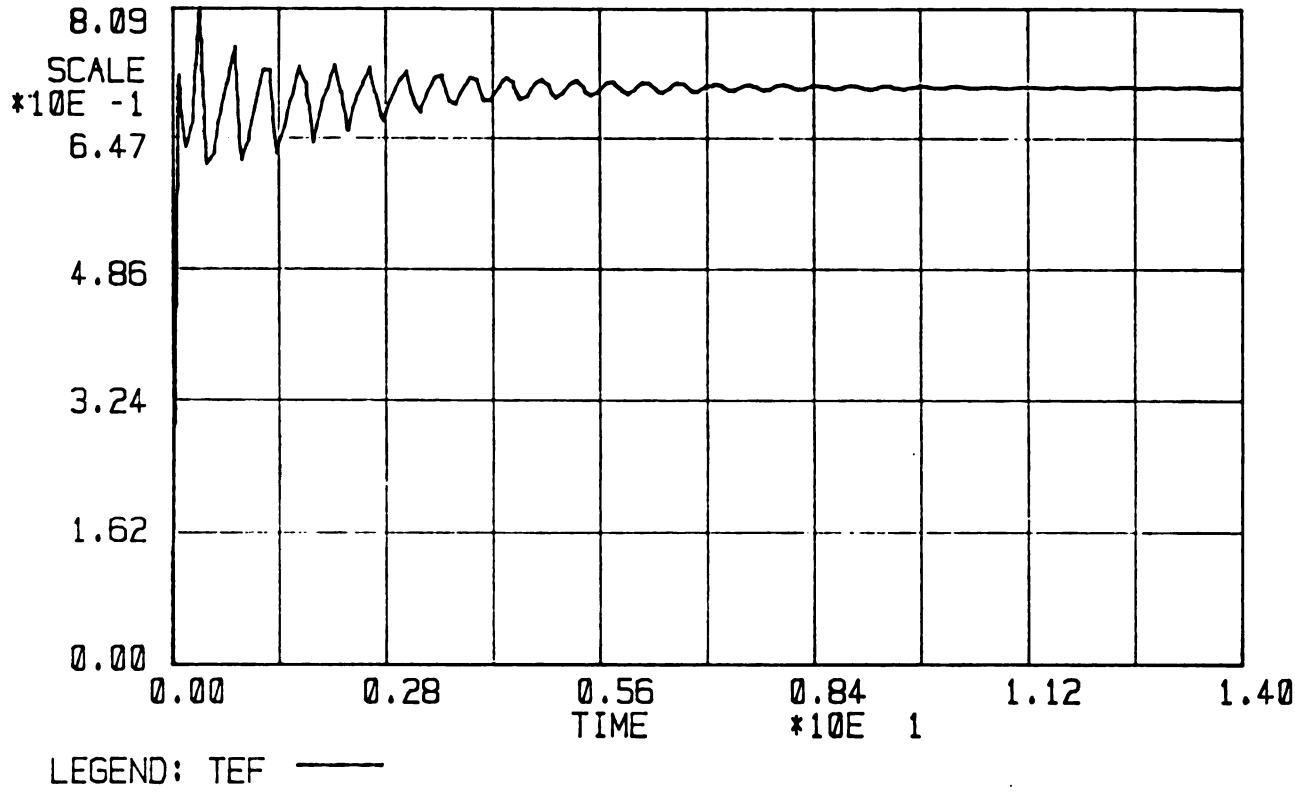

Figure 5.24: Variation of Tractive Efficiency of the Drive Wheel with Time During Transient Motion

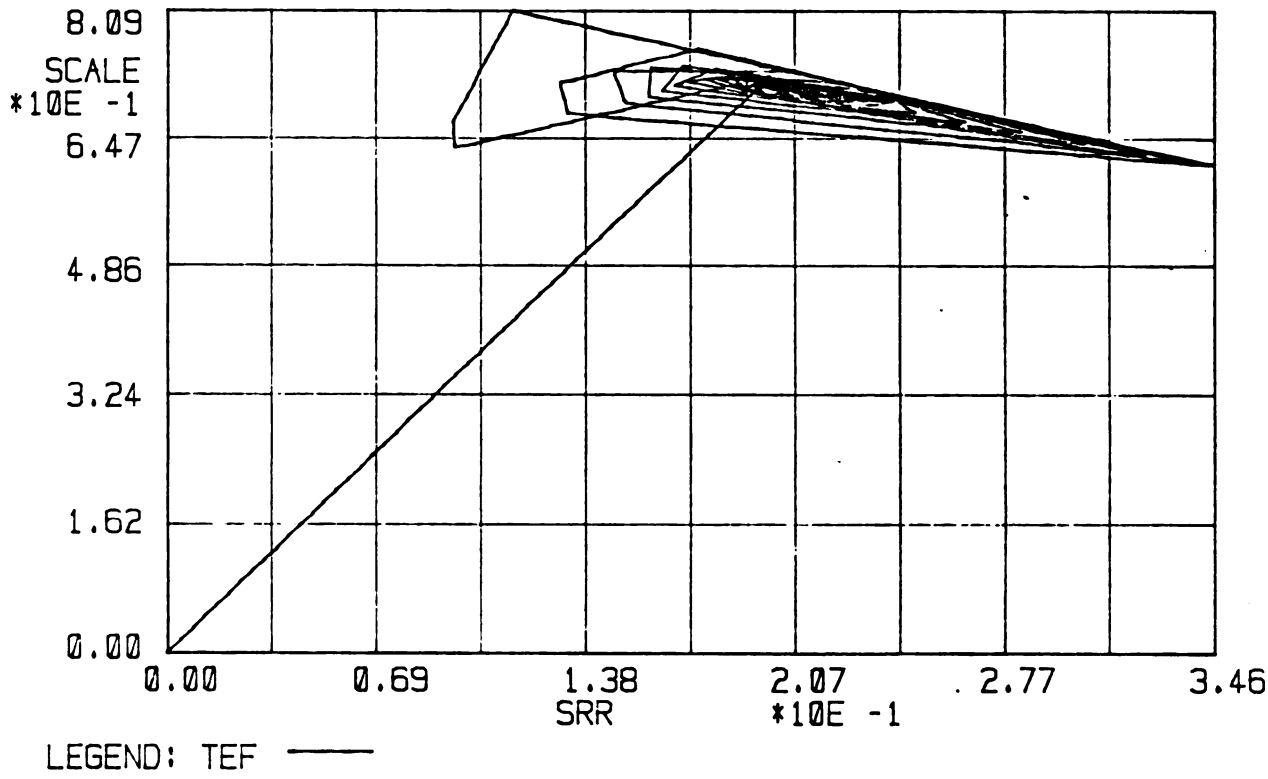

Figure 5.25: Variation of Tractive Efficiency (TEF) with Slip (SRR) of a Bias Ply Drive Tire

Table 5.5: Simulation Data from the Performance of the Tractor with Single and Dual Drive Tires While Moldboard Plowing

Parameter	Single (Radial) Drive Tires	Dual (Radial) Drive Tire
Forward Velocity* (m/s)	0.893**	1.05**
Engine Speed* (rad/s)	98.90	122.8
Tractive Efficiency*	76.59	78.82
Mean Drive Axle Power (kW)	42.82	51.6
Mean Slippage Power (kW)	6.38	7.16
Rear Wheel Mean Motion-Resistance Power (kW)	3.14	3.72
Front Wheel Mean Motion-Resistance Power (kW)	1.62	2.00
Mean Drawbar Power (kW)	25.27	32.68

* Steady State Value

** Forward Velocity is 2.56 m/s at Zero Slip and Rated Engine Speed of 251.3 rad/s.

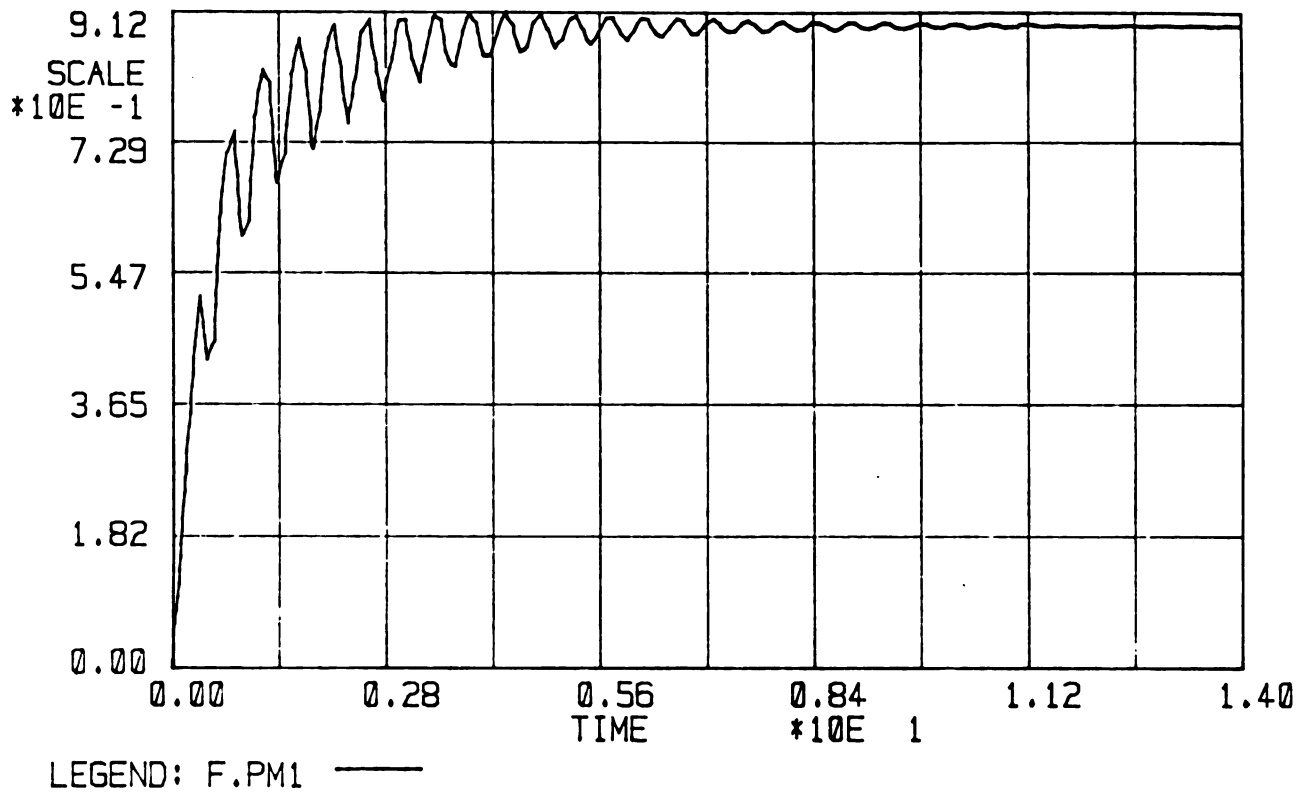

Figure 5.26: Forward Velocity of a Tractor Simulated with Single Drive Radial Tires While Moldboard Plowing

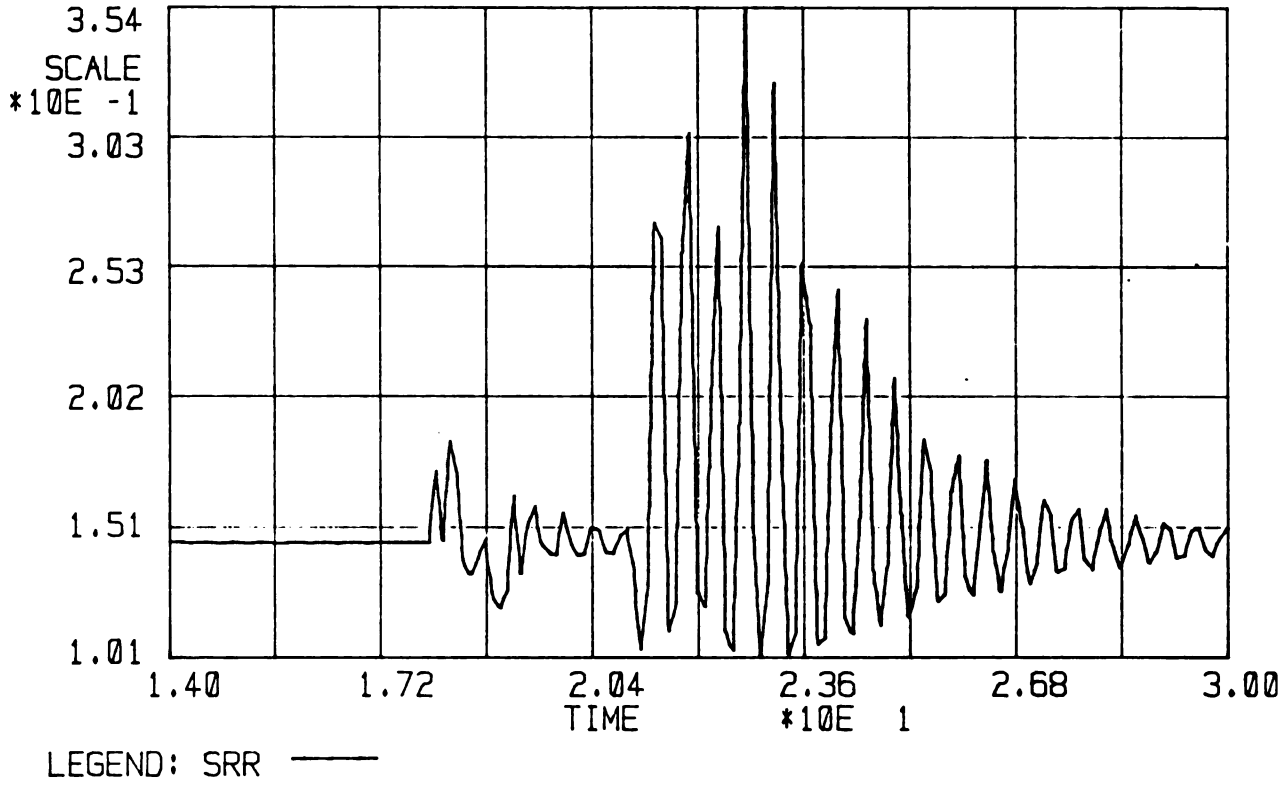

Figure 5.27: Simulated Slip Velocity of The Drive Tire of a Tractor Traversing over a Sinusoidal Bump

Figures 5.26 and 5.27 are the plots of foward velocity of the tractor moldboard plowing, with single and dual drive tires respectively. It can be seen that in operation with dual drive tires it takes the forward velocity longer to reach steady state. It is this difference that must make the slippage power loss higher for the dual drive wheel operation. It is also apparent that the rise time of the forward velocity is generally larger for the operation with dual drive wheels. The dual drive wheels have a lower value of damping coefficient than single drive wheels (see Appendix C for Dual Drive Operation Tractor Physical Data).

5.3.3. Effect of Ballast on Performance

Another one of the many ways in which the bond graph model could be used is for studies on the effects of ballast on the dynamics and energy distribution within the tractor implement system.

Table 5.6 summarizes the simulation data usable in comparing the tractor performance with and without ballast in the drive tires. The physical system input data for a ballasted tractor is listed in Appendix C. Ballasting redistributes the static and dynamic weight on the wheels of a tractor. It in turn changes the moment of inertia of the drive wheels.

The data of Table 5.6 shows that the ballasted tractor outperformed the non ballasted one in all aspects useful to the tractor operator. The additional dynamic load on the

Table 5.6: Simulation Output Data for Radial Ply Single Drive Wheel Tractor Operated with and without Ballast While Moldboard Plowing

Parameter	Ballasted	Non-Ballasted
Forward Velocity* (m/s)	0.892	0.781
Engine Speed* (rad/s)	98.90	90.03
Wheel Slippage* (%)	14.55	16.00
Tractive Efficiency* (%)	76.58	76.40
Distance Covered (14 seconds) (m)	11.60	10.49
Mean Drive Axle Power (kw)	42.96	39.28
Mean Slippage Power (kw)	6.38	6.48
Rear WheelsMean Motion-Resistance Power (kw)	3.14	1.68
Front Wheels Mean Motion-Resistance Power (kw)	1.61	1.08
Mean Drawbar Power (kw)	23.97	19.51

* Steady State Value

drive (rear) tires increased rolling resistance while the increased engine speed might imply higher fuel consumption. The forward velocity, however, increased and the additional distance covered by the tractor operating with ballast (a result of the slightly higher tractive efficiency) would predict that more work would be accomplished per unit time with the ballasted tractor. The simulation results of Table 5.6 also demonstrate the usefulness of the model in studies based on the effects of tractor weight-transfer on performance.

5.3.4. Performance on Varying Terrain

To study the dynamics of the rigid body chassis of the tractor, simulations were conducted for the performance of the tractor as it traveled over a sinusoidal bump. Simulations were conducted for both single drive wheel and dual drive wheel performance of the tractor while moldboard plowing. A sinusoidal bump was selected because it is of a shape commonly encountered in field operations. A bump 1 m long and 20 cm high was used in this study.

Table 5.7 carries data usable for comparison of performance between single and dual drive - two wheel drive tractor. The simulation was carried out with the initial conditions set at the values of state variables at 14 seconds. The simulation was then run through the 30th second of simulation time. This data recorded for forward velocity, engine speed, wheel slippage and tractive

Table 5.7: Simulation Output Data for the Performance of Tractor While Moldboard Plowing over Varying Terrain and Using Single and Dual Drive Wheels

Parameter	Single Drive Wheel	Dual Drive Wheel
Forward Velocity* (m/s)	0.864	1.05
Engine Speed* (rad/s)	98.58	123.05
Wheel Slippage* (%)	15.11	13.05
Tractive Efficiency* (%)	76.37	79.22
Mean Drive Axle Power (kw)	44.54	53.6
Mean Slippage Power (kw)	7.00	7.90
Rear Wheels Mean Motion-Resistance Power (kw)	3.22	3.82
Front Wheel Mean Motion-Resistance Power (kw)	1.63	2.04
Mean Drawbar Power (kw)	23.97	32.790

* Final Value

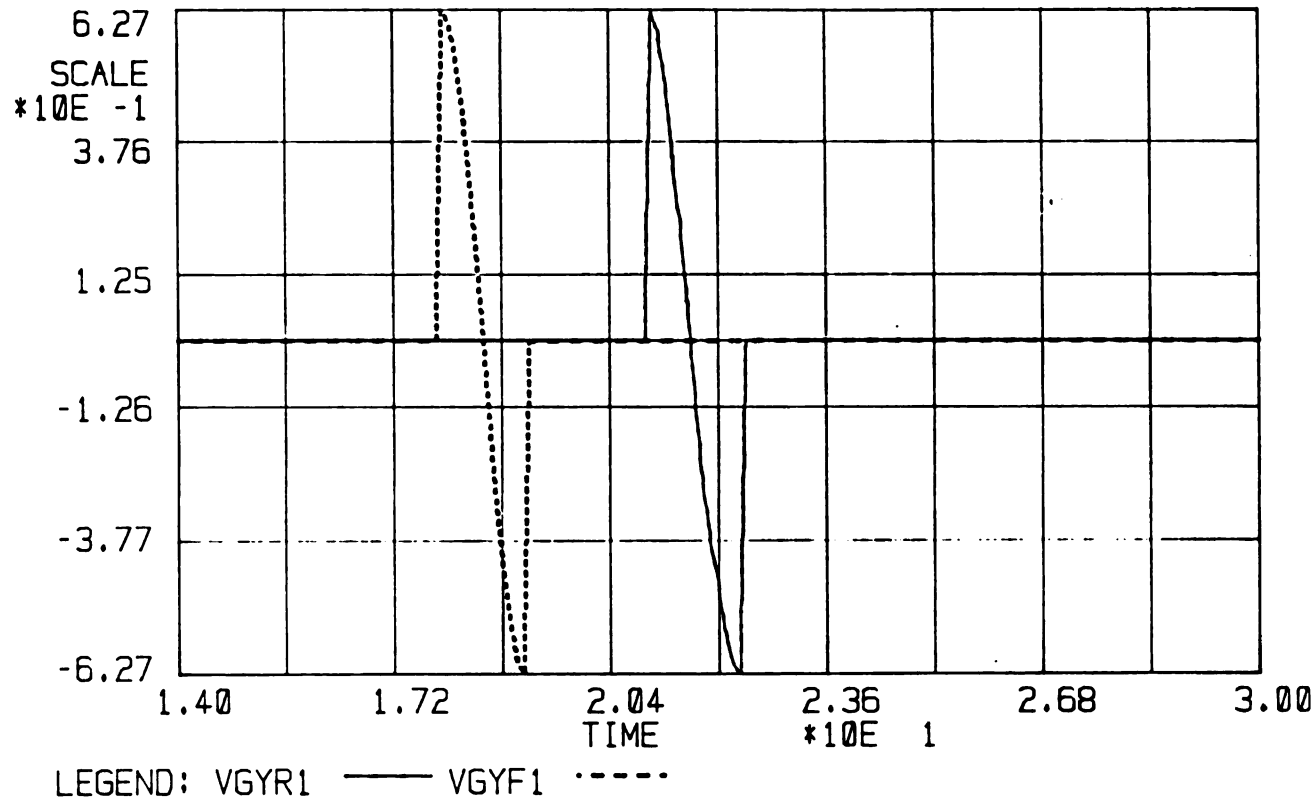

Figure 5.28: The Vertical Ground Velocity at the Front (VGYF1) And Rear Tires (VGYR1) of a Tractor as It Traverses over a Sinusoidal Bump

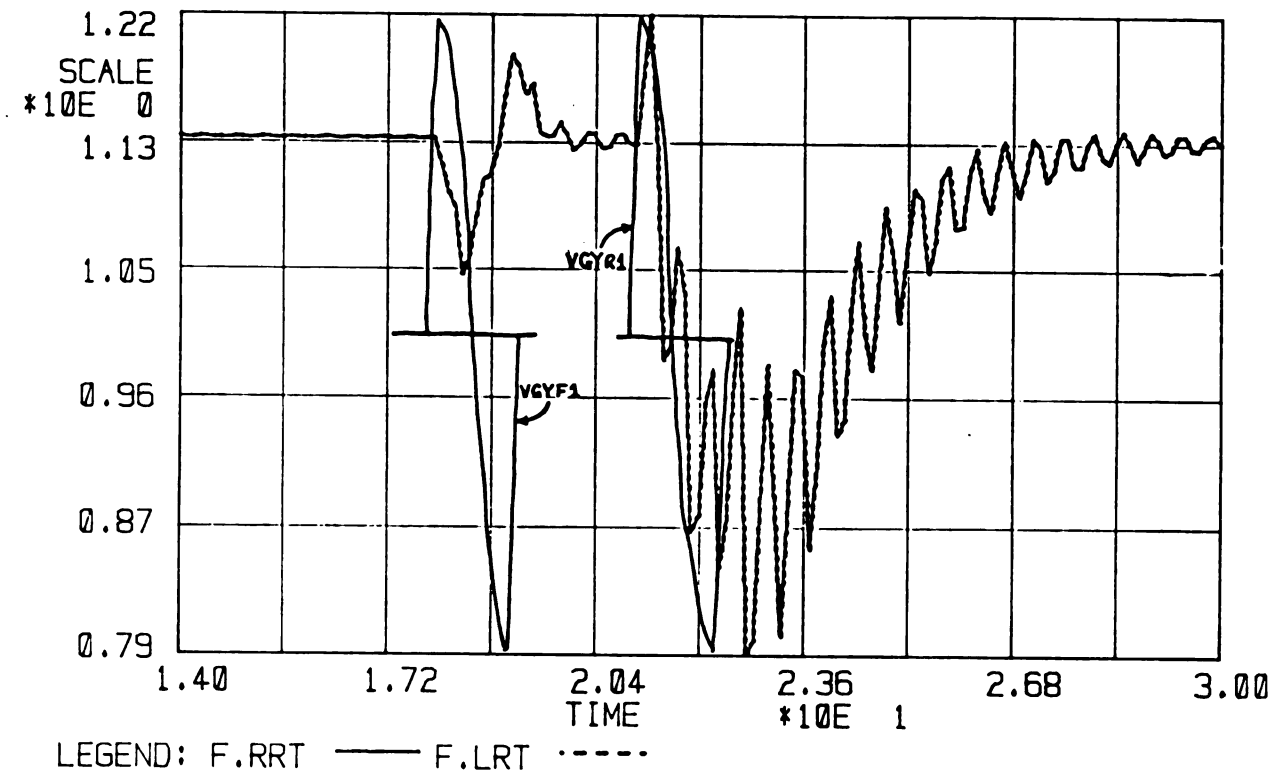

Figure 5.29: A Plot of the Simulated Drive Wheel rotary Velocity as the Tractor Traverses over a Sinusoidal Bump. The Vertical Ground Velocity under the Wheels is Inscribed.

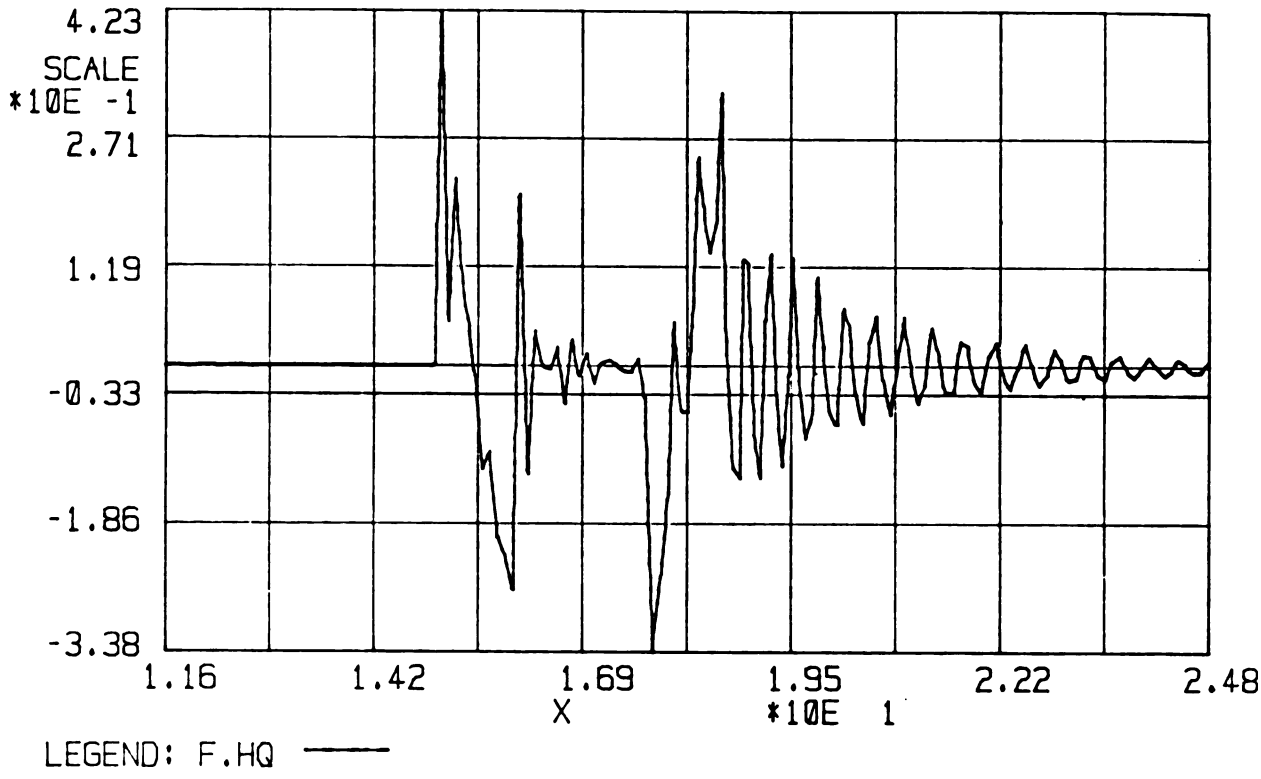

Figure 5.30: Simulated Pitch-Motion Velocity of a Tractor as a Function of Forward Displacement as It Traverses over a Sinusoidal Bump

efficiency is the final value and not the steady state value since the system did not quite reach steady state by the 30th second of the simulation.

The results of Table 5.7 compared with those of Tables 5.5 and 5.6 show approximately the same steady state values for forward velocity, engine speed, wheel slippage and tractive efficiency. The mean power values are however consistently larger (except for drawbar power which stayed essentially the same) as was expected as a consequence of the motion over the bump. The slippage power and motion resistance mean power values show more dramatic increase than the other types of power.

Figure 5.28 shows the vertical ground velocity at the tire-ground interface as the tractor traversed a sinusoidal bump. The velocity at the rear wheel (VGYR1) follows that at the front wheel (VGYF1) by a time equivalent to that required to travel a distance of one wheel base (2.66 m). Figure 5.29 is the simulation plot for the right rear (F.RRT) and left rear (F.LRT) drive wheels rotary velocity. Inscribed into the rotary wheel velocity plot (Figure 5.29) is the vertical ground velocity (VGYR1 and VGYF1) so as to show its relative location and effect. As the front wheel of the tractor goes over the bump (equivalent to VGYF1) the drive wheel rotary velocity falls by about 0.08 rad/s (0.76 rev/min) for a period of about 5 hundredths of a second. This can be attributed to the decreased slippage of the drive tire as the front end of the tractor travels over the

bump and the associated weight transfer. A look at Figure 5.30 (simulated plot of pitch-motion velocity) supports this observation. Figure 5.29 also shows the fall in rotary drive wheel velocity as the drive wheel itself goes over the sinusoidal bump. As it traverses over the bump the drop causes a vibration of the drive tire spring element. The general behavior as the drop takes place is a general decrease followed by a increase of the rotary (wheel) velocity as slippage velocity Fig 5.27 settles back to its steady state value.

Figure 5.30 shows that as the tractor's front wheel climbs over the bump, the chassis pitches backward (positive pitch motion) and then forward (negative pitch motion) as the tractor front wheel travels over the bump and then the chassis settles back to about its initial velocity. As the rear tire reaches the bump the tractor pitches forwards then backwards followed by a vibration back to the original pitch velocity.

Figure 5.31 is a plot of the simulated front (Q.26) and rear tire (Q.30) spring element displacements as the tractor travelled over the sinusoidal bump. It is observed from Figure 5.31 that the front tire spring element undergoes additional vibratory displacement (from a steady state displacement of about 4 cm) as the (front) wheel climbs onto and off the bump and again as the rear wheel does the same. The maximum displacement of both the front and the rear tire spring element takes place as the rear tire climbs off the

bump. It is at this time, too, that the maximum reduction in drive wheel rotary velocity was observed (Figure 5.29).

The tire spring deflections are positive when the net force (between the wheel axle and the ground) on the spring is compressive. This is the case on Figure 5.31 over the time range considered. It means that during the traverse of the sinusoidal bump the tires did not leave the ground. Had this happened the deflections would have acquired negative values. In practice, when tires leave the ground slippage can be considered to have a maximum value and wheel-axle torque and thrust force of a drive wheel to tend towards zero values. In it's present form the model would not reflect these changes. A flag for signaling the changes that occur when tires leave the ground (equivalent to negative tire deflection), hence incorporating the above drastic changes in vehicle dynamics could be added making the model more realistic.

Figure 5.32 is a plot of the bounce (heave) velocity of the tractor body (with respect to horizontal displacement) at the center of gravity. For bounce motion, velocity is positive downwards therefore negative velocity represents a bounce upwards.

Figure 5.33 is a plot of tractive efficiency of the drive wheel as the tractor traverses the bump. A comparison of Figures 5.32 and 5.33 shows that every time the tractor bounces upwards, the tractive efficiency decreases. Figure 5.34 is a comparison plot for the simulated drive axle

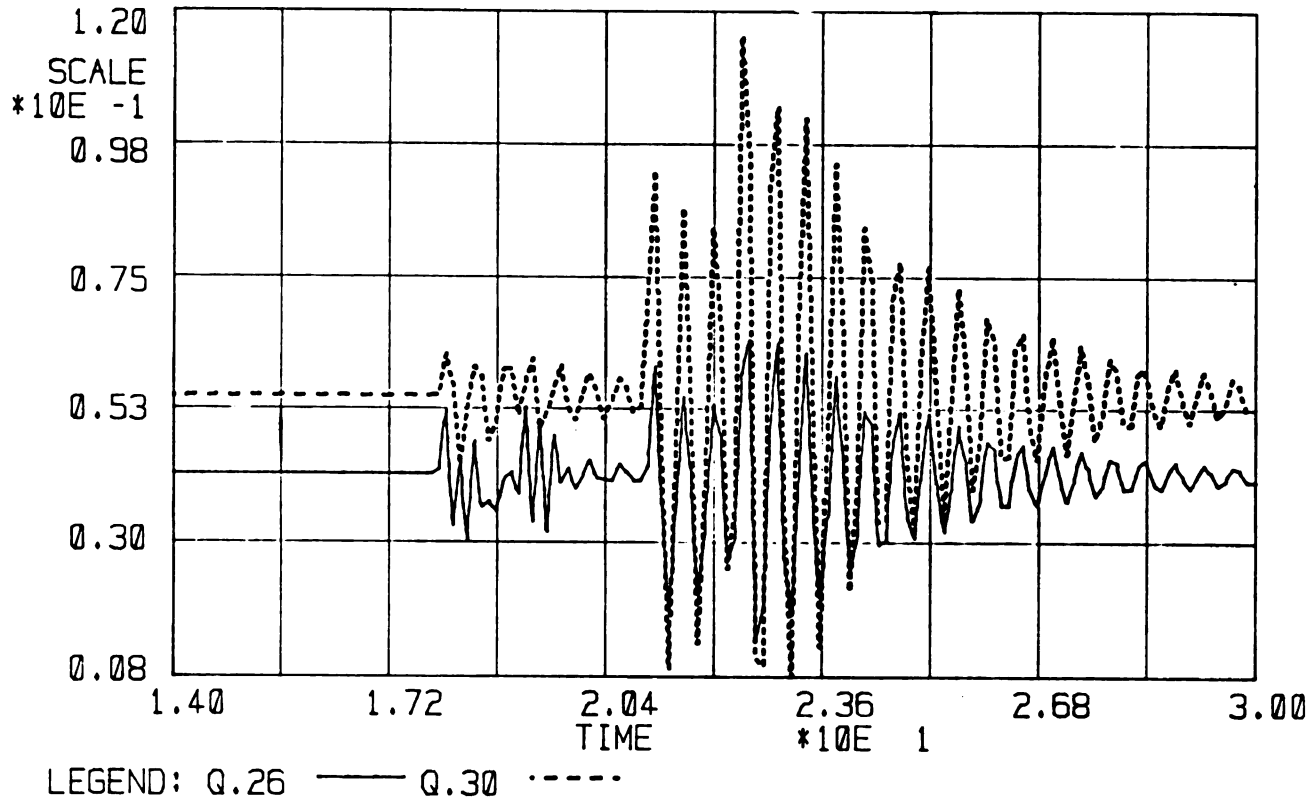

Figure 5.31: Simulated Front Tire (Q.26) and Rear Tire (Q.30) Spring Element Displacement as the Tractor Traverses a Sinusoidal Bump

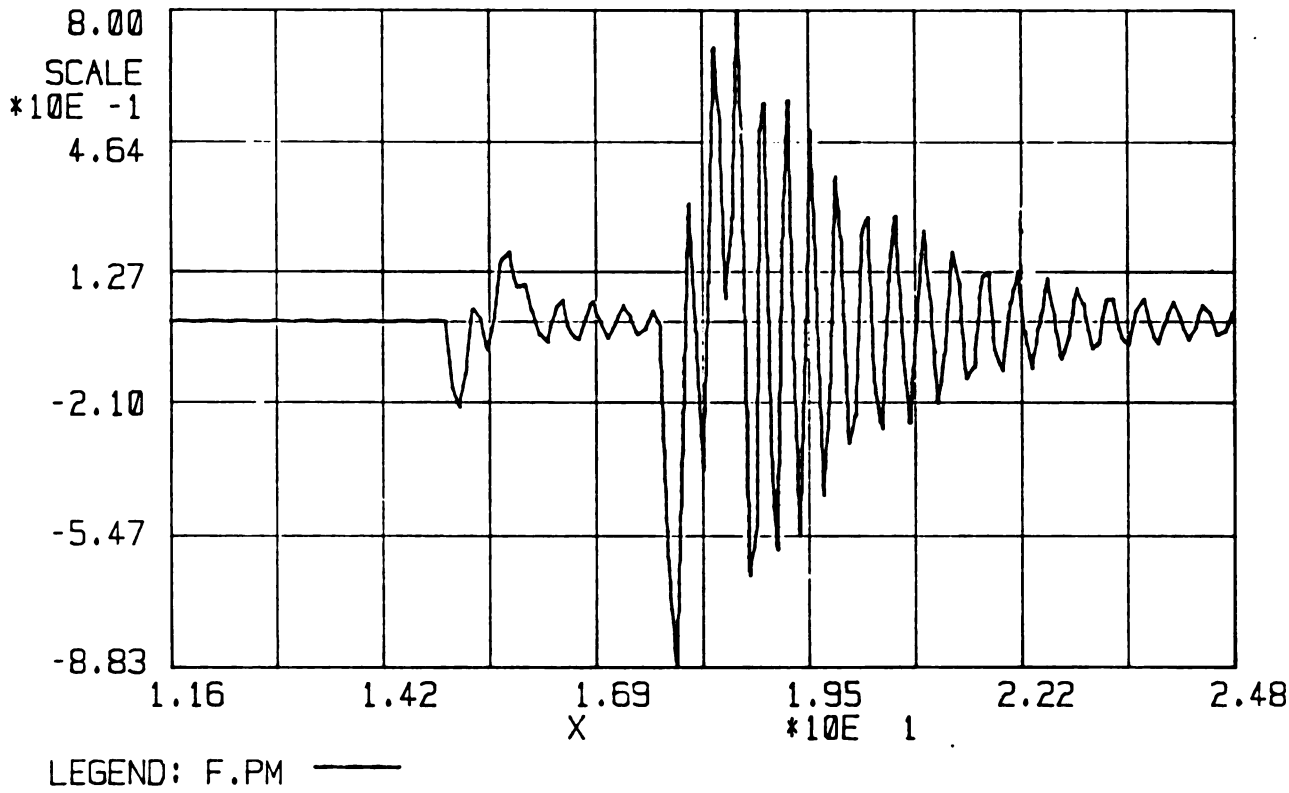

Figure 5.32: Simulation Plot of the Bounce (Heave) - Motion Velocity of the Tractor Body Center of Gravity as the Tractor Traverses a Sinusoidal Bump

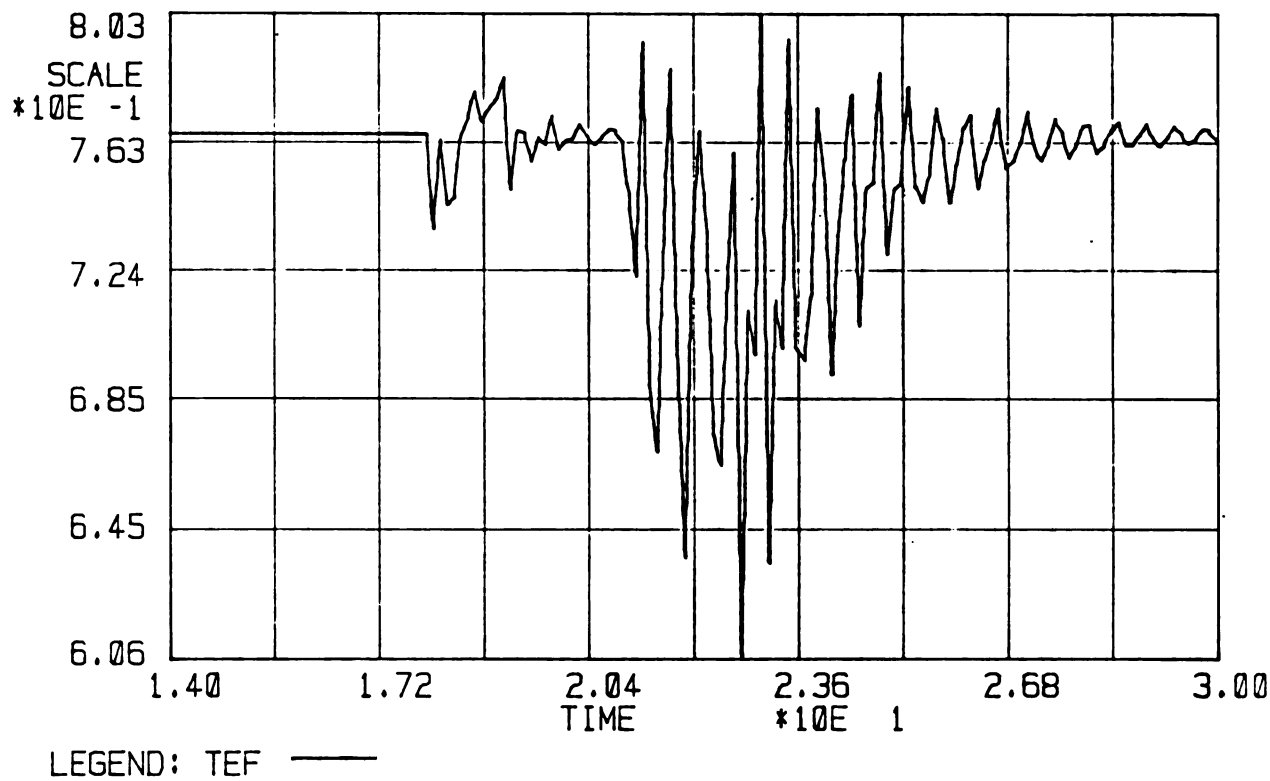

Figure 5.33: Simulated Drive Wheel Tractive Efficiency as the Tractor Traverses a Sinusoidal Bump

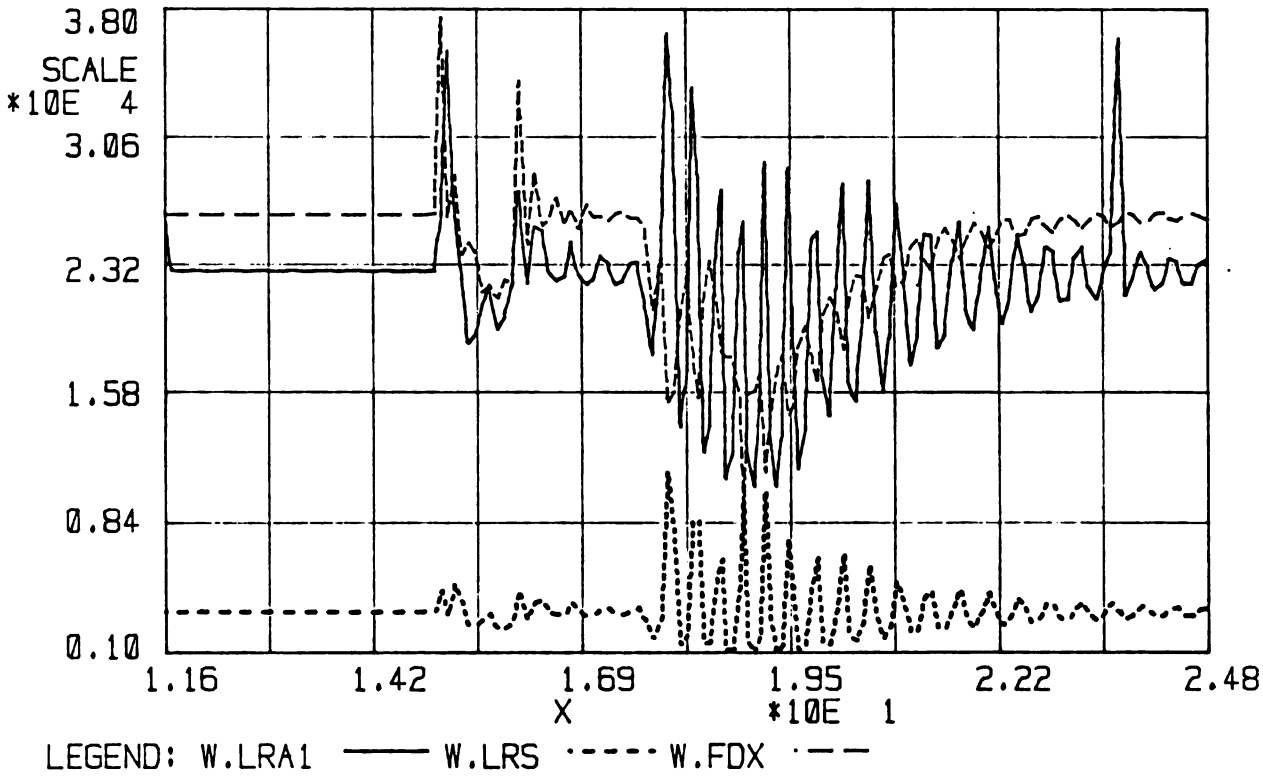

Figure 5.34: A Comparison Plot for the Drive Axle Power (W.LRA1), Slippage Power (W.LRS) and Drawbar Power (W.FDX) as a Tractor Traverses a Sinusoidal Bump

power, wheel slippage power and the drawbar power. For the drive axle power and slippage power, only one drive wheel was considered. To compare total magnitudes of the powers, the drive axle power and slippage power would have to be doubled.

5.4. Power and Energy Distribution

5.4.1. Effect of Varying Drawbar Load

Tests were conducted to study the effect of varying drawbar load on the mean power exchange and mean energy transferred within bonds at points of interest in the tractor-implement system. The variables selected were the drive axle, tire slippage, rolling resistance (front and rear) and drawbar for element power exchange comparison. Slippage, rolling resistance, transmission, differential and clutch elements were compared for energy dissipation. Table 5.8 shows the recorded data for the drawbar loads of 37.02 kN, 41.28 kN and 43.45 kN.

The data of Table 5.8 reveals that as the drawbar load was increased, slippage power exchange and energy dissipated increased consistently. The increasing drawbar load was observed (see Section 5.1) earlier to consistently decrease the engine speed in this constant engine-input-effort performance simulation model. The decreased engine speed can be considered as the explanation for the consistently decreasing power exchange in the drive axle, motion rolling

Table 5.8: Mean Power Exchange and Mean Energy Transferred Within the Specified Bonds as the Drawbar Load on the Tractor was Varied.

		Mean Bond Power		Mean Energy Transferred	
Drawbar Load (kN)	Element Symbol	Amount (kW)	% of Maximum*	Amount (kJ)	% of Maximum*
37.02	FDX	78.92	72.03		
	LRA1	51.42	46.93		
	LRS	4.58	4.18	29.01	2.30
	RRR	1.05	0.955	12.12	0.960
	RLF	0.50	0.457	5.74	0.454
	TR			29.01	2.30
	RRD			28.09	2.23
	CR			0.240	0.019
41.28	FDX	61.49	77.20		
	LRA1	38.14	47.89		
	LRS	4.86	6.11	56.09	6.05
	RRR	0.72	0.90	8.39	0.906
	RLF	0.36	0.45	4.18	0.451
	TR			15.41	1.66
	RRD			0.556	0.060
43.45	FDX	48.11	77.68		
	LRA1	30.15	48.68		
	LRS	5.07	8.18	59.72	8.25
	RRR	0.53	0.85	6.23	0.860
	RLF	0.27	0.44	3.18	0.440
	TR			9.36	1.29
	RRD			9.06	1.25
	CR			0.019	0.026

Element Symbol Definition:

FDX: Drawbar (Output) Element
LRA1: Drive Axle Input Power Element
LRS: Slippage Dissipation Element
RRR: Rear Wheel Rolling Resistance Element
RLF: Front Wheel Rolling Resistance Element
TR : Transmission Dissipation Element
RRD: Differential Dissipation Element
CR : Clutch Dissipation Element

*The maximum power and energy observed were at the engine input bond (SENG)

resistance and energy dissipation in the transmission and the differential.

Table 5.9 is a listing of the power exchange that occurs within all the nodes of the two wheel drive tractor when the tractor is exposed to a medium size drawbar load and is traversing uniformly horizontal terrain. A look at Table 5.9 reveals that the largest amount of power exchange takes place within the power train and at the points of interaction between the tractor and the ground. These latter points include the rolling resistance to motion and implement drawbar load. All the elements ordered (see Table 5.9) 1 through 26 belong to these categorized points. It is of particular interest to note that the bonds associated with the rigid body dynamics involve minimal power exchanges. The dynamics of roll motion carry essentially zero power exchange. Figure 5.35 is a plot of the simulated roll-motion displacement under the same conditions as described for the data on Table 5.9. On uniform terrain Figure 5.35 shows roll-motion displacement is zero for all practical purposes. Results reported are basically computational noise because under the test conditions described, roll motion displacement should remain zero. A maximum displacement of the order of 10E-13 radians was recorded. In the dynamic analysis of tractor performance under varying drawbar load on uniformly horizontal ground the roll vibration mode can be ignored without loss of analytical accuracy. Table 5.9 demonstrates the power of

Table 5.9. A System Element Power Exchange Listing Showing the Power (Watts) Exchanged within all Nodes in the Model and their Percentage of the Maximum (Engine) Power Exchanged as the Tractor Operated under Average Drawbar Load on Uniformly Horizontal Terrain

Processed data list in order:

ORDER	BOND	MEAN POWER	% OF MAX
1	TE	0.1112E+06	100.000
2	EC	0.1067E+06	95.884
3	CT	0.1066E+06	95.865
4	RT	0.1039E+06	93.426
5	RAT1	0.1039E+06	93.426
6	RAT	0.1013E+06	91.064
7	FDXU	0.8030E+05	72.178
8	FDX	0.8029E+05	72.175
9	RRA	0.5065E+05	45.532
10	RRA1	0.5065E+05	45.532
11	LRA	0.5065E+05	45.532
12	LRA1	0.5065E+05	45.532
13	RRT	0.4981E+05	44.774
14	RRT1	0.4981E+05	44.774
15	VRR	0.4981E+05	44.774
16	LRT	0.4981E+05	44.774
17	LRT1	0.4981E+05	44.774
18	VLR	0.4981E+05	44.774
19	URR	0.4714E+05	42.369
20	ULR	0.4714E+05	42.369
21	FLR	0.4264E+05	38.331
22	FRR	0.4264E+05	38.331
23	EI	0.4579E+04	4.116
24	TR	0.2713E+04	2.439
25	DVRR	0.2675E+04	2.404
26	RRS	0.2675E+04	2.404
27	LRS	0.2675E+04	2.404
28	DVLR	0.2675E+04	2.404
29	RRD	0.2628E+04	2.362
30	PM1	0.1580E+04	1.420
31	RLR	0.1200E+04	1.079
32	RRR	0.1200E+04	1.079
33	WRRT	0.8436E+03	0.758
34	WLRT	0.8436E+03	0.758
35	RLF	0.5039E+03	0.453
36	RRF	0.5039E+03	0.453
37	MG	0.2165E+03	0.195
38	27	-0.1147E+03	0.103
39	31	-0.1147E+03	0.103
40	28	0.1147E+03	0.103

Table 5.9. (Continued)

41	32	0.1147E+03	0.103
42	18	0.1064E+03	0.096
43	21	0.1064E+03	0.096
44	29	0.6390E+02	0.057
45	33	0.6390E+02	0.057
46	30	0.5080E+02	0.046
47	34	0.5080E+02	0.046
48	PM	-0.4514E+02	0.041
49	19	0.3062E+02	0.028
50	20	0.3062E+02	0.028
51	23	-0.2478E+02	0.022
52	35	-0.2478E+02	0.022
53	24	0.2477E+02	0.022
54	36	0.2477E+02	0.022
55	CR	0.2141E+02	0.019
56	26	0.1777E+02	0.016
57	38	0.1777E+02	0.016
58	FDY	0.1335E+02	0.012
59	FDYW	0.1242E+02	0.011
60	2	0.8274E+01	0.007
61	9	0.8274E+01	0.007
62	3	0.8274E+01	0.007
63	8	0.8274E+01	0.007
64	25	0.7002E+01	0.006
65	37	0.7002E+01	0.006
66	10	0.5844E+01	0.005
67	17	0.5844E+01	0.005
68	11	0.5843E+01	0.005
69	16	0.5843E+01	0.005
70	FDXQ	-0.3440E+01	0.003
71	22	-0.3440E+01	0.003
72	FDYQ	0.9309E+00	0.001
73	1	0.9309E+00	0.001
74	HQ	-0.4908E+00	0.000
75	14	-0.2314E-08	0.000
76	15	-0.2314E-08	0.000
77	12	-0.2314E-08	0.000
78	13	-0.2314E-08	0.000
79	6	-0.1103E-08	0.000
80	7	-0.1103E-08	0.000
81	5	-0.1103E-08	0.000
82	4	-0.1103E-08	0.000
83	HP	-0.3315E-20	0.000
84	HP	-0.3315E-20	0.000
85	6	-0.1103E-08	0.000
86	7	-0.1103E-08	0.000
87	14	-0.2314E-08	0.000
88	15	-0.2314E-08	0.000
89	12	-0.2314E-08	0.000
90	13	-0.2314E-08	0.000

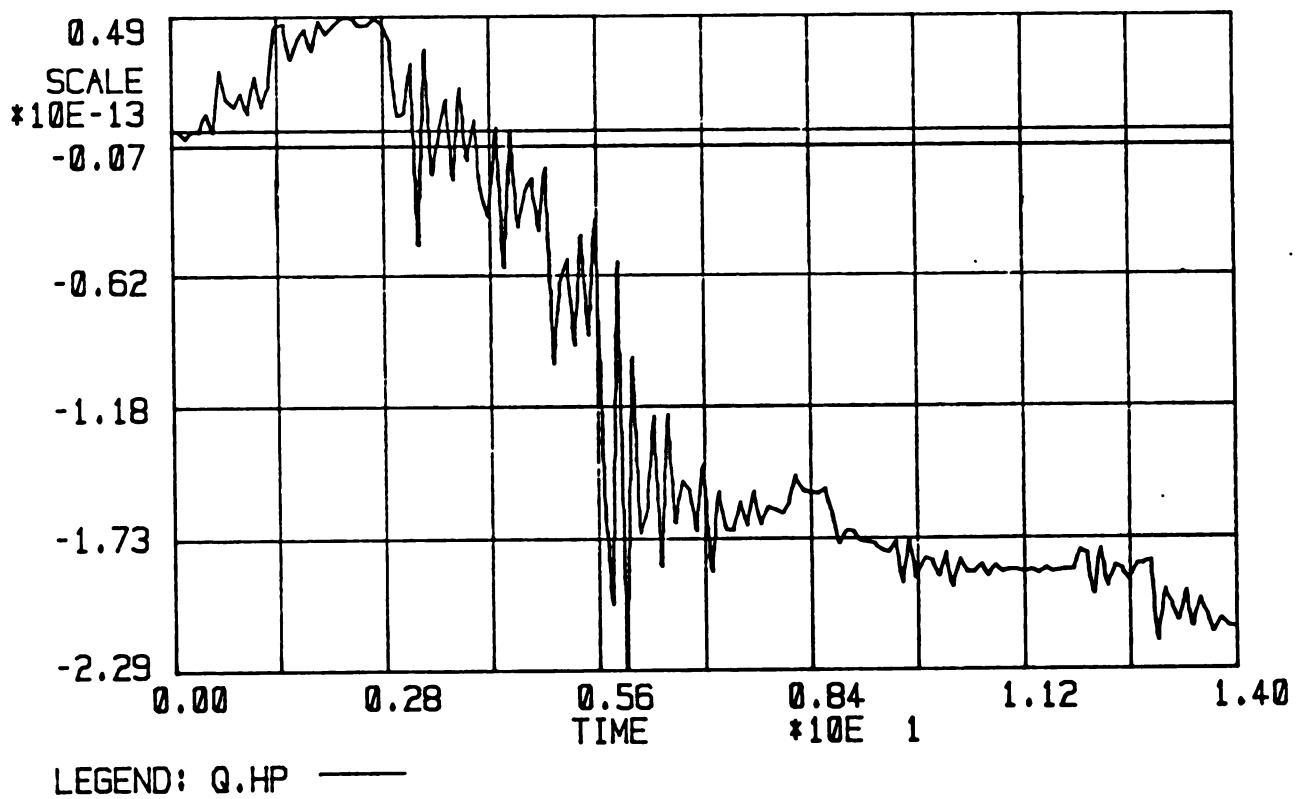

Figure 5.35: Simulation of Roll-Motion Displacement for the Tractor Traversing Uniformly Horizontal Terrain with Medium Drawbar Load

ENPORT-7 (and bond graphs) as tools for studies geared towards establishing the modal decomposition and modal reduction of a dynamic system.

5.4.2. System Graphic Display

With an aim of supplying a visual display of the power exchange and energy distribution in the tractor-implement system another post-processor option utilized in ENPORT-7 is the System Graph Display option. This option display on the computer screen is a pictorial version of the original bond graph model with the bonds or ports color coded and scaled by absolute mean, root mean square or mean value of the selected variable (see Section 3.3.3). The scaling is either an ordered-rank, linear or logarithmic. ENPORT-7 allows not only the whole system display but also the selection of specific elements on the model to be compared in this display.

Figure 5.36 shows an Effort (force or torque) display diagram. Like the key for the display shows, the color code is blue for the lowest division of the scale ranging from - 1.13E-10 to 9.51E+3 N or N.m black for the range from 9.51E+3 to 1.9ØE+4 N or N.m and so on. Within a certain color code the thickness of the bonds varies to reflect variation in the magnitude of the effort within it.

A look at the colors of the bonds in Figure 5.36 reveals for example that the effort leaving the engine is

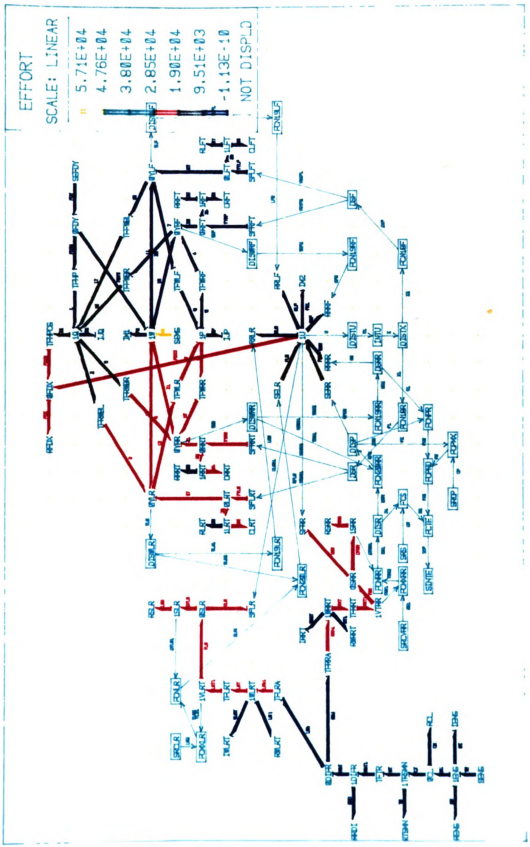

Figure 5.36: A System Graph Display Showing the Color Coded Ranking and Distribution of Effort in a Tractor with Medium Drawbar Load and Traversing Uniformly Horizontal Terrain

within (blue color) range of -1.13E-10 to 9.51E3 N.m. This effort is magnified across the final drive of the drive line (elements TERA and TFLA) into the range 1.90E4 to 2.85E4 N.m range. The effort that goes into accelerating the wheel is within the blue range same as the equivalent effort lost in the dissipation of the tire bearing (elements IRRT and RWRRT, and elements ILRT and RWLRT, respectively) for the right and left rear wheel drive axles. The rigid body chassis sits on ground reaction forces that are larger on the section between the center of gravity and the rear end of the tractor than those on the front end. This is quickly observed from the display by the mostly red coding of the bonds joining the centers of pitch, roll and heave motion (1Q, 1P and 1W) (the center of gravity) to the rear axle force centers, nodes ØYLR and ØYRR, relative to the mostly blue coding of the bonds joining the pitch, roll and heave motion centers to the front axle vertical forces ØYRF and ØYLF).

The thrust forces (of the power bonds at node SELR and SERR) at the rear drive wheels are larger than their motion-resisting forces of the power bonds at node RRLR and RRRR. The individual-wheel, motion resisting forces at the front wheels (node RRLF and RRRF) and the net force driving the tractor forwards all fall in the range that covers the rear wheel individual motion resisting forces. All these forces are in the blue color range.

It can be observed that the largest individual force of the whole system is that (assumed constant) associated with the weight of the tractor, at node SEMG. The damping elements of the front and the rear tires (RLRT and RRRT) have efforts that fall in the same range as those of the front tires (RLFT and RRFT). The spring forces in the rear tires (CRRT and CLRT) are however in a different range from the forces associated with their damping element (RRRT and RLRT).

6. SUMMARY AND CONCLUSION

Bond graph modeling is an alternative to Lagrangian techniques of modeling farm tractor dynamics. Bond graph modeling supplies an ability to formulate a model in a way that allows for the addition or subtraction of degrees of freedom with relative ease.

Bond graph models of the rigid body chassis dynamics, drive train dynamics and the dynamics of the tire-ground and chassis-implement interactions were developed. The generalized coordinates describing the rigid body motion were the forward displacement, vertical, pitch and roll displacements. The torsional drive train was modeled assuming infinite stiffness shafts and axles. The engine angular displacement was used to model the engine without the use of a governor. The velocity attained was governed by the engine-clutch inertia element while constant torque input was assumed (see Section 4.1.2). Model element functions used were relatively simple and based on physical phenomena conceptualized as taking place in the physical system. Computations were made utilizing the gear charts and engine torque-velocity relationships of a specific tractor from which the magnitudes of the parameters for effort-flow relationships were established.

Bond graph models were developed for both two wheel drive and four wheel drive tractors and ENPORT-7 was used to process the graphs. Attempts to process the four wheel drive model were unsuccessful because of the unavoidable derivative causality that resulted. ENPORT-7 is a non-linear system processor and at its present stage of development it is not capable of handling derivative causality. The unavoidable derivative causality of the four wheel drive model made it impossible to look at the dynamics of the front and rear drive axles, (and associated elements) explicitly due to the existence of statically coupled inertia elements. Compliance elements with extremely high stiffness coefficients could have been used to break the static coupling but this would have led to increased model computation time.

The modeling was done in two main stages, one with a simplified bond graph model and the other with a model that had been expanded to make the traction aspect of the model more realistic. The model was validated by simulating a lugging ability test of Nebraska Tractor Tests. Errors of the simulation results were larger for the simplified model. The best validation results obtained were those with the expanded model with radial ply tires. These prediction errors were 6.28% for the forward velocity, 6.60% for engine speed, 6.89% for drawbar load and 36.55% for wheel slippage. The prediction for wheel slippage was consistently large, a condition attributable to assumed linear relationship

between thrust force and slip velocity. For the case of the simplified model the effect T on the relationship of Figure 3.15 due to the varying dynamic load was absent. With the expanded model the relationship of Figure 3.15 was used to establish a slippage velocity for input into the thrust computation function (See Section 4.4.1) and the dynamic load was a direct input of the function computing thrust force.

Most of the computations conducted in the integrator were solved for a period of 14 seconds (simulation time) with 151 stages stored. This meant 9.27×10^{-2} seconds between stages of the output data stored and used for post-processor analysis. The computation interval was about a half of this time. At this interval it took about 6 hours (real time) to obtain a solution from the integrator. This interval was about the maximum one that could be used without overdistorting the response curves. The plots obtained in Chapter 5 show the plots were relatively distorted especially for the tire interface and associated computations. The LIMITER function of the thrust force element was relatively stiff and better results could have been possibly obtained with a smaller computation interval. The computation distorted output graphs but had little or no effect on the accuracy of steady state results obtained.

The weakness of the model is at the tire soil interface. This is a conclusion reached by observing the consistently over-predicted slippage results. An

improvement of the model at this point will lead to a smaller prediction error of engine speed and drawbar pull since the slippage disrupts the continuity of energy flow between the engine and the drawbar point. A raised drawbar load will increase slippage and in turn tend to lower engine speed less than it should.

The demonstration of the simulation model was accomplished by comparing radial ply and bias ply tires, single and dual drive wheels and ballasted and non-ballasted operations. The demonstration derived results that were not only generally correct but also showed the many different ways in which the model could be used in further research studies. The results of the demonstration were not verified due to the lack of actual field data for the scenarios used in the demonstration. The significance of the general differences obtained in the model demonstration comparison studies were not statistically analyzed. This is a situation that could have been more realistic with a randomly selected drawbar load. The trends in the model demonstration data were that the change to radial ply tires from bias ply tires and from single (radial ply) drive tires to (radial) dual drive tires increased forward velocity decreased steady state wheel slippage, decreased engine speed and increased tractive efficiency. The reduced engine speed implied savings in fuel energy and improved power transmission efficiencies. This argument is supported by

the power exchange, energy distribution studies reported in Section 5.4.1.

In addition to the general tractor performance simulation modeling, where engine speed, slippage, forward velocity and drawbar pull are predicted, the capability of bond graph modeling and ENPORT-7 to obtain a power exchange and energy distribution network of the whole tractor-implement system supplies the additional insight stated (at the end of chapter 2) as a major motivation towards the use of bond graphs in this research. It is believed this aspect whose potential is demonstrated in this model will be used by systems and control researchers and tractor designers alike with fulfillment. The system graph displays of Section 5.4.2 go a step into demonstrating this claim. The studies related to variable terrain in Section 5.3.4 will make tractor modeling more realistic eliminating the usual assumption of non-varying terrain, in studies geared towards modeling of the dynamics of the drive train chassis and the implement. The studies of Section 5.3.4 will give insight into the interaction dynamics of drive train components with the added advantage of observing the intercomponent quantity and nature of power exchange.

For the model to be more than just a tool for establishment of trends in data of simulated performance, field work will need to be conducted to come up with means for more rigorous validation processes. The field data required is one that relates power components in a more

physical sense. For example at the tire-soil interface a thrust force-slippage velocity relationship would have been more useful and more directly applied than a thrust force slippage percent relationship.

7. SUGGESTIONS FOR FUTURE WORK

The simulation bond graph model was validated using data from the lugging ability tests reported by Nebraska Tractor Tests. Complete confidence in any model of a physical system is dependent upon experimental verification. However the general trends predicted by even an unverified model can often supply extremely useful insights into the dynamic behavior of the system being modeled. The verification of power and energy flows within the tractor needs carefully-planned experimental measurements. The model developed in this research shows high potential for system power and energy distribution studies but field research data are required. The following suggestions are in order for exploiting the apparent potentials of the model:

a) Conduct field research to specifically develop quantitative drive wheel thrust force - slip velocity (not percentage slippage) relationships taking into account the effects of the dynamic load on the wheel and the tire and soil deformation under dynamic operating conditions. This would quantitatively represent effect T on Figure 3.15 allowing for a direct application of the

relationship of Figure 3.15 to obtain the driving thrust force P.

b) With increased computation time the model in its present form can be used for studies of four wheel drive tractors. The computation time would increase due to the necessary addition of stiff spring elements to break the static coupling between the front and rear drive axles which brought about the derivative causality.

c) Expansion of the model by allowing for large motions of the rigid body will make the model more useful in tractor stability studies.

d) Using the model with a differential that allows for differential (internal) motion will lead to increased insight into the power and energy distributions under more adverse operating conditions than considered in this study.

e) The model presented in this study is open and expandable to accommodate localized component modifications and variations of the physical system while leaving the rest of the model undisturbed. Studies where the ground is modeled as a medium of variable compliance and energy dissipation qualities, for example, would lead to insight into the complex and somewhat unpredictable soil tire interaction behavior.

f) The model presented in this research is an excellent basic model for sensitivity analysis studies geared towards the knowledge of the general tendencies and

effects of changes in the physical system which in some cases would correspond to a mere change in the magnitude of various parameters in the model. The bond graph modeling advantage to be exploited is the unified approach quality where the same basic model elements are usable for example in comparing the performance of mechanical and hydraulic transmissions of a tractor.

g) The bond graph model presented in this research is a tool usable by systems and controls researchers especially in the area of modal decomposition and modal reduction studies. The ability (supplied by ENPORT) to combine bond graphs and block diagrams makes it easy to insert a feedback loop by including an operator and an engine governor in this model as controllers for the input of engine power. This situation would supply a more realistic model usable for optimizing, in an integrated way, the fuel, transmission, traction and drawbar pull efficiencies.

h) With localized dynamics of minor modification this model can be used to study the interaction between the rigid body chassis and a PTO powered implement or implements of dynamic drawbar load including the effects on drive train power demands and energy distribution.

APPENDIX A

Appendix A

Appendix A contains a guideline of bond graph terminology (see Rosenberg and Karnopp, 1972) and a simple example of bond graph modeling of use to the reader unfamiliar with bond graphs. For a more useful guidance on applying bond graphs please see Rosenberg and Karnopp (1983). Appendix A also includes the definitions of GAIN, LIMITER and BACKLASH functions. For more information on the functions or ENPORT please see ROSENCODE (1987). Also included is a listing of user-defined subroutines used in the model.

BOND GRAPH TERMINOLOGY

BASIC DEFINITIONS:

Multiport Elements: The nodes of a bond graph designated by alpha numeric characters like SEK, Ø1, C1, TF1, RK, 1K, IK and SF1 on Figure A.Ø.

Ports: Places of interaction of a node and its environment. Ports are designated by line segments incident on the port element, e.g., Ø1 is a 3 port element, SE1 is a single port element.

Bonds: Connections between pairs of multiport elements, e.g., (bonds) labelled 1 through 7 on Figure A1.

Port Variable: Effort, e(t) and Flow, f(t) are power variables associated with a given port. They are assumed to be scalar functions with an independent variable t.

The half arrows show the direction of power flow. The (short line) strokes on the end opposite the half arrow (the other end of the bond) is the causal stroke that determines the causality of the bond. To understand causality please see Rosenberg and Karnopp, 1983; pp. 85-103.

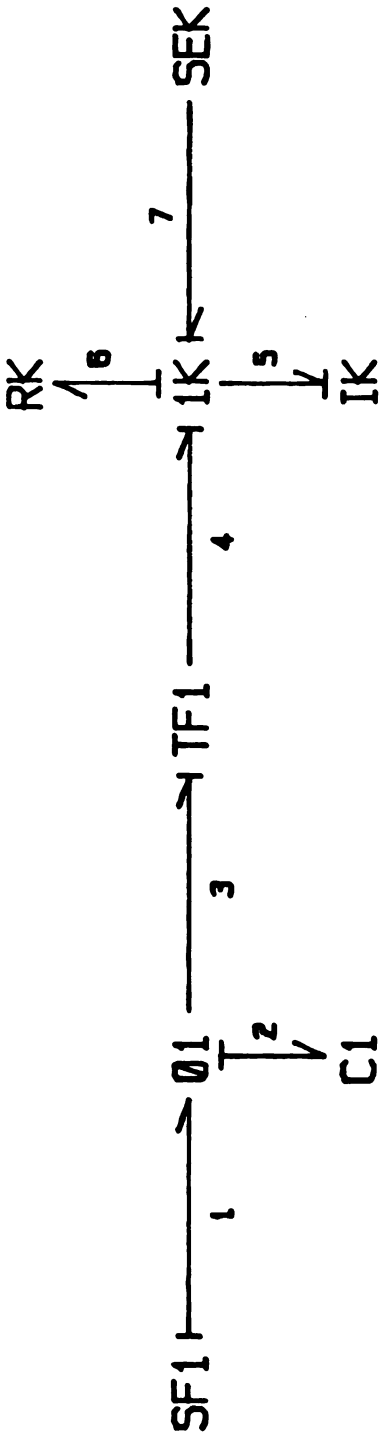

Figure A.Ø : A Bond Graph Showing Power Directions
Causality and Bond Labels

Basic Multiport Elements:

There are nine basic multiport elements, grouped into four categories according to their energy characteristics. These elements and their definitions are summarized in Fig. A.Ø

Sources:

Source of effort, written SE $\underline{e}$, is defined by $e = e(t)$.

Source of flow, written SF $\underline{f}$, is defined by $f = f(t)$.

Storages:

Capacitance, written $\frac{e}{f}$ C, is defined by

$$e = \Phi(q) \quad \text{and} \quad q(t) = q(t_0) + \int_{t_0}^{t} f(\lambda)\, d\lambda$$

That is, the effort is a static function of the displacement and the displacement is the time integral of the flow.

Inertance, written $\frac{e}{f}$ I, is defined by

$$f = \Phi(p) \quad \text{and} \quad p(t) = p(t_0) + \int_{t_0}^{t} e(\lambda)\, d\lambda$$

That is, the flow is a static function of the momentum and the momentum is the time integral of the effort.

Dissipation:

Resistance, written $\frac{e}{f}$ R, is defined by

$$\Phi(e, f) = 0$$

That is, a static relation exists between the effort and flow at the port.

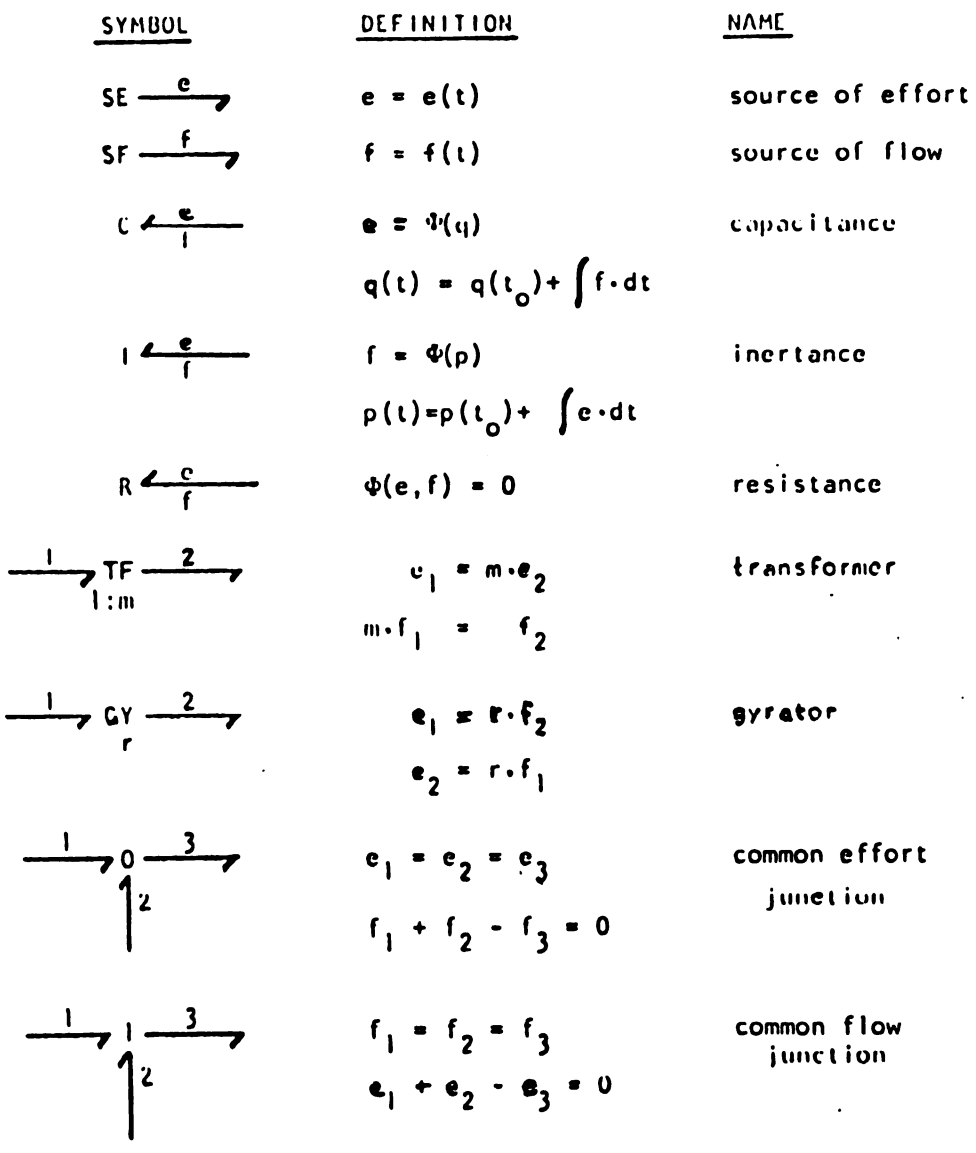

Figure A.2: Definition of the Basic Multiport Elements of a Bond Graph (Rosenberg and Karnopp, 1972)

PHYSICAL INTERPRETATIONS:

The physical interpretations given in this section are very succinctly stated. See Rosenberg and Karnopp, 1983 for extensive descriptions of the physical applications.

Mechanical Translation

To represent mechanical translational phenomena we may make the following variable associations:

1. effort, e, is interpreted as force;
2. flow, f, is interpreted as velocity;
3. momentum, p, is interpreted as impulse-momentum;
4. displacement, q, is interpreted as mechanical displacement.

Then the basic bond graph elements have the following interpretations:

1. source of effort, SE, is a force source;
2. source of flow, SF, is a velocity source (or may be thought of as a geometric constraint);
3. resistance, R, represents friction and other mechanical loss mechanisms;
4. capacitance, C, represents potential or elastic energy storage effects (or spring-like behavior);
5. inertance, I, represents kinetic energy storage (or mass effects);
6. transformer, TF, represents linear lever or linkage action (motion restricted to small angles);

7. gyrator, GY, represents gryational coupling or interaction between two ports;
8. 0-junction represents a common force coupling among the several incident ports (or among the ports of the system bonded to the 0-junction); and
9. 1-junction represents a common velocity constraint among the several incident ports (or among the ports of the system bonded to the 1-junction).

The extension of the interpretation to rotational mechanics is a natural one. It is based on the following associations:

1. effort, e, is associated with torque; and
2. flow, f, is associated with angular velocity.

Because the development is so similar to the one for translational mechanics it will not be repeated here.

USER-DEFINED SUBROUTINE FUNCTIONS FOR BOND GRAPH ELEMENTS

FCN20RR, FCN20LR, FCN19RR, FCN19LR, FCN19LF, FCN19RF,

FCN18F, FCN18R (see, Figure 3.2.3).

SUBROUTINE 18

```
      SUBROUTINE SUBR18(X,P,Y)
C
C--- PROGRAMMING:
C
C--- DESCRIPTION:  Outputs:  DYDX,  ground velocity
C                  Inputs:   XG,    ground displacement
C                  Params:   P(1)= DY
C                            P(2)= P1
C                            P(3)= X1
C                            P(4)= X2
C
C--- INPUTS:  X,   vector of input argument values
C             P,   vector of parameter values
C
C--- OUTPUTS: Y,   vector of output argument values
C
C--- DECLARATIONS:
      DOUBLE PRECISION X(20),P(20),Y(20)
      REAL DYDX, XG, DY, P1, X1, X2, XB, XM
      INTRINSIC COS
C
C***SUBR18**************************************************
C
      XG= X(1)
      DY= P(1)
      P1= P(2)
      X1= P(3)
      X2= P(4)
C
      DYDX= 0.
      XM = 0
      IF ((XG.GE.X1).AND.(XG.LE.X2)) THEN
        XM= XG-X1
        XB= X2-X1
        IF (XB.GT.1.E-3) THEN
          IF (XM.LE.XB) THEN
           DYDX= ((DY*P1)/XB)*COS((P1*XM)/XB)
          ENDIF
        ENDIF
      ENDIF
C
      Y(1)= DYDX
      RETURN
      END
```

SUBROUTINE 19

```
      SUBROUTINE SUBR19(X,P,Y)

      PROGRAMMING:  Pascal Kaumbutho

      DESCRIPTION:  Compute the motion resistance
                    Outputs:   RR,  rolling resistance
                    Inputs:    W,   dynamic weight
                    Params:    P(1)= CI
C                              P(2)= B
C                              P(3)= D
C                              P(4)= K3
C                              P(5)= K4
C
C--- INPUTS:  X,   vector of input argument values
C             P,   vector of parameter values
C
C--- OUTPUTS: Y,   vector of output argument values
C
C--- DECLARATIONS:
      DOUBLE PRECISION X(20),P(20),Y(20)
      REAL RR, W, CI, B, D, K3, K4, CN
C
C***SUBR19*************************************************:
C
      W= X(1)
      CI= P(1)
      B=  P(2)
      D=  P(3)
      K3= P(4)
      K4= P(5)
C
      RR= 0.
      IF (W.GT.1.) THEN
        CN= CI*B*D/W
        IF (CN.GT.1.E-10) THEN
          RR= ((K3/CN)+K4)*W
        ENDIF
      ENDIF
C
      Y(1)= RR
      RETURN
      END
```

SUBROUTINE 20

```
      SUBROUTINE SUBR20(X,P,Y)
C
C--- PROGRAMMING:  "
C
C--- DESCRIPTION:  tire thrust force
C                  Outputs:     Y(1)= PF, thrust force
C                  Inputs:      X(1)= W, dynamic weight
C                               X(2)= S, slip
C                  Parameters:  P(1)= K1
C                               P(2)= B, tire width
C                               P(3)= D, tire diameter
C                               P(4)= CI, cone index
C                               P(5)= K2
C
C--- INPUTS:  X,   vector of input argument values
C             P,   vector of parameter values
C
C--- OUTPUTS: Y,   vector of output argument values
C
C--- DECLARATIONS:
      DOUBLE PRECISION X(20),P(20),Y(20)
C***SUBR20**********************************************
C
C--- Unload the input values
      W= X(1)
      S= X(2)
      K1= P(1)
      B= P(2)
      D= P(3)
      CI= P(4)
      K2= P(5)
C
C--- Evaluate the function for thrust
      IF (W.GT.1.) THEN
        CN= CI*B*D/W
        PF= K2*W*(1.-EXP(K1*CN*S))
      ELSE
        PF= 0.
      ENDIF
C
C--- Load the output
      Y(1)= PF
C
      RETURN
      END
```

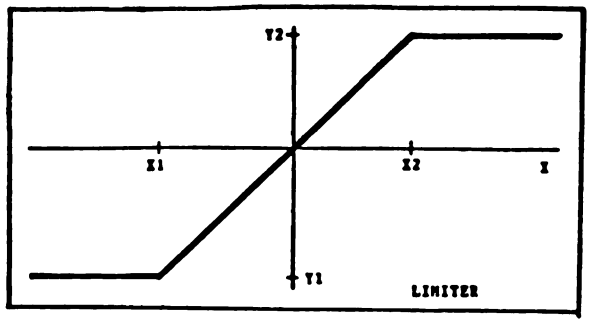

Figure A.1: The LIMITER Function

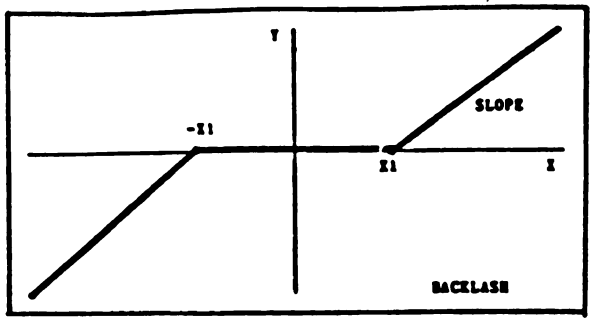

Figure A.2: The BACKLASH function

FUNCTION DEFINITION

GAIN FUNCTION: Y = CON * X

where:

Y = output

X = input

CON = constant

LIMITER FUNCTION: The Limiter Function has the shape shown on Figure A.1. In Fortran it can be defined as follows (see Figure A.1 for variable definition).

```
IF (X.LT. - X1)  THEN
   Y = Y1
ELSEIF (X.LT.X1) THEN
   Y = -Y1 + (Y2 - Y1) * SLOPE
ELSE
   Y = Y2
ENDIF
```

BACKLASH FUNCTION: The BACKLASH function has the shape shown on Figure A.2. In FORTRAN It can be defined as follows (See Figure A.2 for variable definition).

```
IF (X.GT - X1) THEN
   Y = SLOPE * (X - X1)
ELSEIF (X.GT.X1) THEN
   Y = SLOPE * (X - X1)
ELSE
   Y = Ø
ENDIF
```

APPENDIX B

APPENDIX B

Appendix B contains a listing of element equations used in the model during the (two wheel drive tractor), expanded model validation. These equations demonstrate the basis of bond graph modeling by giving the details of parameter magnitudes and relationships as efforts are summed at Common-Flow Junctions and flows are summed at Common Effort junctions according to the power flow and assigned causality. Other details pertaining to power exchange across transformer (TF) elements and distribution to power sources through interconnecting signals are demonstrated by the equations.

The File Title:
TWO WHEEL DRIVE TRACTOR SYSTEM EQUATIONS

The System Equations:

```
F.PM =  1.4070E-04 * P.PM
F.HP =  5.5870E-04 * P.HP
F.HQ =  2.7930E-04 * P.HQ
E.38 =  2.5100E+05 * Q.38
E.34 =  4.8200E+05 * Q.34

E.30 =  4.8200E+05 * Q.30
E.26 =  2.5100E+05 * Q.26
F.PM1 =  1.4070E-04 * P.PM1
F.EI =  4.1150E-01 * P.EI
F.WRRT =  1.3500E-03 * P.WRRT

F.WLRT =  1.3500E-03 * P.WLRT
E.37 =  1.1500E+03 * F.37
E.33 =  2.1700E+03 * F.33
E.29 =  2.1700E+03 * F.29
E.25 =  1.1500E+03 * F.25

E.FDX =  1.4429E+04 * F.FDX
LIMITER FUNCTION:
IF (F.RRS.LT. -3.4700E-01) THEN
  E.RRS = -5.2303E+04
ELSEIF (F.RRS.LT.  3.4700E-01) THEN
  E.RRS = -5.2303E+04 + (F.RRS- -3.4700E-01) *  1.5073E+05
ELSE
  E.RRS =  5.2303E+04
ENDIF
LIMITER FUNCTION:
IF (F.LRS.LT. -3.4700E-01) THEN
  E.LRS = -5.2303E+04
ELSEIF (F.LRS.LT.  3.4700E-01) THEN
  E.LRS = -5.2303E+04 + (F.LRS- -3.4700E-01) *  1.5073E+05
ELSE
  E.LRS =  5.2303E+04
ENDIF
E.RLF =  1.0000E+00 * LFR
E.RRF =  1.0000E+00 * RFR

E.RRR =  1.0000E+00 * RR
E.RLR =  1.0000E+00 * LRR
E.ER =  0.0000E+00
LIMITER FUNCTION:
IF (F.CR.LT. -5.0000E-02) THEN
  E.CR = -7.5400E+02
ELSEIF (F.CR.LT.  5.0000E-02) THEN
  E.CR = -7.5400E+02 + (F.CR- -5.0000E-02) *  1.5080E+04
ELSE
  E.CR =  7.5400E+02
ENDIF
```

```
E.TR =  4.6600E-02 * F.TR

E.RRD =  7.0500E-01 * F.RRD
E.RT1 =  0.0000E+00
E.LR1 =  0.0000E+00
E.MG =  6.9740E+04
F.VYLR =  1.0000E+00 * VGYR1

F.VYRF =  1.0000E+00 * VGYF2
F.VYRR =  1.0000E+00 * VGYR2
F.VYLF =  1.0000E+00 * VGYF1
E.FDY =  4.0000E+03
E.FLR =  1.0000E+00 * GFLR

E.FRR =  1.0000E+00 * GFRR
E.TE =  4.7100E+02
F.ULR =  1.0000E+00 * ULRS1
F.URR =  1.0000E+00 * URRS1
MOD.TFHP =  1.3600E+00

MOD.TFRWBL =  6.2000E-01
MOD.TFFWBR =  2.0400E+00
MOD.TFRWBR =  6.2000E-01
MOD.TFFWBL =  2.0400E+00
MOD.TFWRR =  9.2000E-01

MOD.TFWLF =  1.0600E+00
MOD.TFWLR =  9.2000E-01
MOD.TFWRF =  1.0600E+00
MOD.TFHPCG =  5.1000E-01
MOD.TFRRT =  8.9900E-01

MOD.TFRRA =  1.1013E+01
MOD.TFLRA =  1.1013E+01
MOD.TFLRT =  8.9900E-01
MOD.TFTR =  3.9526E+00
CALL SUBR18(Y,X,P)
Y_list  X_list      Parameters
DYF     X2          2.0000E-01
                    3.1400E+00
                    6.0000E+01
                    6.1000E+01

CALL SUBR18(Y,X,P)
Y_list  X_list      Parameters
DYR     X1          2.0000E-01
                    3.1400E+00
                    6.2660E+01
                    6.3660E+01
RR1 =  1.0000E-03
VRR2    = MAX(VRR1,
          RR1)
LR2 =  1.0000E-03
VLR2    = MAX(VLR1, LR2)

SRR =  1.0000E+00 *DVRR1 / VRR2
SLR =  1.0000E+00 *DVLR1 / VLR2
CALL SUBR20(Y,X,P)
Y_list  X_list      Parameters
GFRR    WRR1        -1.0000E+00
        SRR          5.5600E-01
                     1.8500E+00
                     5.9400E+05
                     1.0200E+00
CALL SUBR20(Y,X,P)
Y_list  X_list      Parameters
GFLR    WLR2        -1.0000E+00
        SLR          5.5600E-01
                     1.8500E+00
                     5.9400E+05
                     1.0200E+00
LFR =  2.0000E-02 * WLF1

RFR =  2.0000E-02 * WRF2
RR =  2.0000E-02 * WRR2
LRR =  2.0000E-02 * WLR1
*D12 = U1
WRR1 = WRR
WRR2 = WRR

WLF1 = WLF
WLR1 = WLR
WLR2 = WLR
X1 = X
X2 = X
U1 = U
VGYR1 = DYR
VGYR2 = DYR

VGYF1 = DYF
VGYF2 = DYF
WRF2 = WRF
F.FDYQ =  1.0000E+00 *MOD.TFHP *F.1
E.1 =  1.0000E+00 *MOD.TFHP *E.FDYQ
F.3 =  1.0000E+00 *MOD.TFRWBL *F.2

E.2 =  1.0000E+00 *MOD.TFRWBL *E.3
F.11 =  1.0000E+00 *MOD.TFFWBR *F.10
E.10 =  1.0000E+00 *MOD.TFFWBR *E.11
E.9 =  1.0000E+00 *MOD.TFRWBR *E.8
F.8 =  1.0000E+00 *MOD.TFRWBR *F.9

F.16 =  1.0000E+00 *MOD.TFFWBL *F.17
E.17 =  1.0000E+00 *MOD.TFFWBL *E.16
F.15 =  1.0000E+00 *MOD.TFWRR *F.14
E.14 =  1.0000E+00 *MOD.TFWRR *E.15
F.7 =  1.0000E+00 *MOD.TFWLF *F.6
```

```
E.6 =  1.0000E+00 *MOD.TFWLF *E.7
E.13 =  1.0000E+00 *MOD.TFWLR *E.12
F.12 =  1.0000E+00 *MOD.TFWLR *F.13
F.4 =  1.0000E+00 *MOD.TFWRF *F.5
E.5 =  1.0000E+00 *MOD.TFWRF *E.4

F.FDXQ =  1.0000E+00 *MOD.TFHPCG *F.22
E.22 =  1.0000E+00 *MOD.TFHPCG *E.FDXQ
F.RRT1 =  1.0000E+00 *MOD.TFRRT *F.RRT
E.RRT =  1.0000E+00 *MOD.TFRRT *E.RRT1
E.RRA1 =  1.0000E+00 *MOD.TFRRA *E.RRA

F.RRA =  1.0000E+00 *MOD.TFRRA *F.RRA1
E.LRA1 =  1.0000E+00 *MOD.TFLRA *E.LRA
F.LRA =  1.0000E+00 *MOD.TFLRA *F.LRA1
F.LRT1 =  1.0000E+00 *MOD.TFLRT *F.LRT
E.LRT =  1.0000E+00 *MOD.TFLRT *E.LRT1

E.RAT1 =  1.0000E+00 *MOD.TFTR *E.RT
F.RT =  1.0000E+00 *MOD.TFTR *F.RAT1
E.PM =  1.0000E+00 * E.MG
      -1.0000E+00 * E.19
      -1.0000E+00 * E.18
      -1.0000E+00 * E.20
      -1.0000E+00 * E.21
      +1.0000E+00 * E.FDYW
E.HP = -1.0000E+00 * E.14
      +1.0000E+00 * E.6
      +1.0000E+00 * E.13
      -1.0000E+00 * E.5
E.HQ =  1.0000E+00 * E.1
      -1.0000E+00 * E.2
      +1.0000E+00 * E.10
      -1.0000E+00 * E.9
      +1.0000E+00 * E.17
      -1.0000E+00 * E.22

F.38 = F.36
F.34 = F.32
F.30 = F.28
F.26 = F.24
E.PM1 = -1.0000E+00 * E.RLF
       -1.0000E+00 * E.RRF
       -1.0000E+00 * E.RRR
       -1.0000E+00 * E.RLR
       +1.0000E+00 * E.FLR
       +1.0000E+00 * E.FRR
       -1.0000E+00 * E.FDXU

E.EI = -1.0000E+00 * E.ER
      +1.0000E+00 * E.TE
      -1.0000E+00 * E.EC
E.WRRT = -1.0000E+00 * E.RT1
       -1.0000E+00 * E.RRT
       +1.0000E+00 * E.RRA1
E.WLRT = -1.0000E+00 * E.LR1
       +1.0000E+00 * E.LRA1
       -1.0000E+00 * E.LRT
F.37 = F.36
F.33 = F.32

F.29 = F.28
F.25 = F.24
F.FDX = F.FDXQ + F.FDXU
F.RRS = F.DVRR
F.LRS = F.DVLR

F.RLF = F.PM1
F.RRF = F.PM1
F.RRR = F.PM1
F.RLR = F.PM1
F.ER = F.EI

F.CR = F.EC - F.CT
F.TR = F.RT
F.RRD = F.RAT
F.RT1 = F.WRRT
F.LR1 = F.WLRT

F.MG = F.PM
E.VYLR = E.28
E.VYRF = E.24
E.VYRR = E.32
E.VYLF = E.36

F.FDY = F.FDYQ + F.FDYW
F.FLR = F.PM1
F.FRR = F.PM1
F.TE = F.EI
E.ULR = E.DVLR

E.URR = E.DVRR
F.1 = F.HQ
E.FDYQ = E.FDY
F.2 = F.HQ
E.3 = E.27

F.10 = F.HQ
E.11 = E.23
E.8 = E.31
F.9 = F.HQ
F.17 = F.HQ

E.16 = E.35
F.14 = F.HP
E.15 = E.31
F.6 = F.HP
E.7 = E.35
```

```
E.12 = E.27
F.13 = F.HP
F.5 = F.HP
E.4 = E.23
F.22 = F.HQ

E.FDXQ = E.FDX
F.RRT = F.WRRT
E.RRT1 = E.VRR
E.RRA = E.RAT
F.RRA1 = F.WRRT

E.LRA = E.RAT
F.LRA1 = F.WLRT
F.LRT = F.WLRT
E.LRT1 = E.VLR
E.RT = E.CT - E.TR

F.RAT1 = F.RAT
E.19 = E.23
E.18 = E.27
E.20 = E.35
E.21 = E.31

E.23 = E.24
E.24 = E.26 + E.25
E.27 = E.28
E.28 = E.30 + E.29
E.31 = E.32

E.32 = E.34 + E.33
E.35 = E.36
E.36 = E.38 + E.37
E.FDYW = E.FDY
E.FDXU = E.FDX

E.VRR = E.DVRR
E.DVRR = E.RRS
E.DVLR = E.LRS
E.VLR = E.DVLR
E.EC = E.CR

E.CT = E.CR
E.RAT = E.RAT1 - E.RRD
F.19 = F.PM
F.18 = F.PM
F.20 = F.PM

F.21 = F.PM
F.23 =   1.0000E+00 * F.11
       -1.0000E+00 * F.4
       -1.0000E+00 * F.19
F.24 = F.VYRF - F.23
F.27 =  -1.0000E+00 * F.3
```

```
      +1.0000E+00 * F.12
      -1.0000E+00 * F.18
F.28 = F.VYLR - F.27

F.31 =  -1.0000E+00 * F.8
      -1.0000E+00 * F.15
      -1.0000E+00 * F.21
F.32 = F.VYRR - F.31
F.35 =   1.0000E+00 * F.16
      +1.0000E+00 * F.7
      -1.0000E+00 * F.20
F.36 = F.VYLF - F.35
F.FDYW = F.PM

F.FDXU = F.PM1
F.VRR = F.RRT1
F.DVRR = F.VRR - F.URR
F.DVLR = F.VLR - F.ULR
F.VLR = F.LRT1

F.EC = F.EI
F.CT = F.RT
F.RAT = F.RRA + F.LRA
VRR1 = F.RRT1
VLR1 = F.LRT1

U = F.PM1
WRF = E.4
DVRR1 = F.DVRR
WRR = E.15
DVLR1 = F.LRS

WLF = E.7
WLR = E.12
URRS1 = F.PM1
ULRS1 = F.PM1
```

End of equations

APPENDIX C

APPENDIX C

Appendix C contains a summary of physical (IH1086) tractor data that have not been mentioned in detail within the text in Chapter 4. Data like that of the weight distribution at the tires with and without ballasting is listed.

IH1086 TRACTOR PHYSICAL DATA*

* (See Figure 3.1 for variable definitions)

VARIABLE	2WD°	2WDD°°
	(m)	(m)
TW3	1.06	1.06
TW2	1.06	1.06
WB	2.66	2.66
WBF	2.04	2.11
WBR	0.62	0.55
TW2	0.92	0.92
TW4	0.92	0.92
HPCH	1.36	1.36
HPCV	0.51	0.51
TWR	2.11	2.11
TWF	1.83	1.83

Static Weight with BALLAST WITHOUT BALLAST

	2WD		2WDD
Front (N)	8066	7988	8050
Rear (N)	26733	20325	31150
Total Mass (kg)	7109	5779	7991

Mass Moments of Inertia for 2WD+ Without Ballast

Pitch	3708 kg.m^2
Roll	1853 kg.m^2

For more data see Nebraska Tractor Test 1247

° Two Wheel Drive Tractor
°° Two Wheel Dual Drive (Tires) Tractor
+ All others given in text or in Nebraska Tractor Test

APPENDIX D

APPENDIX D

Appendix D contains additional empirical and mathematical relationships that were encountered in literature during attempts to obtain a traction model that would characterise the tire-soil interface dynamics most accurately. The models reported here are a continuation of those shown in the text in Section 3.3.

Bekker (1956, 1960) related the pressure sinkage of a flat plate and the coulomb theory of shear stress to develop equations for the prediction of thrust and motion resistance:

$$H_{max} = AC + W \tan \phi \qquad \ldots \quad (D.1)$$

and

$$P = H - MR \qquad \ldots \quad (D.2)$$

where:

H_{max} = maximum value of thrust (H = tractive effort)

A = contact area of traction member

C = cohesion of soil

MR = motion resistance

P = drawbar pull

W = dynamic weight of traction member

ϕ = angle of internal friction of the soil

Maximum thrust could be computed once C and ϕ were known. Bekker based his theories on the fact that soil-shear diagrams either increase monotonously toward a horizontal asymptote (cohesionless soils) or increase to a local maximum and drop towards a horizontal asymptote (cohesive soils) - see Figure D.1.

Bekker (1956) suggested the following equation for the description of shear diagrams of a humped form:

$$\tau = \frac{C + \sigma \tan \phi}{Y_{max}} [e^{(-k_2 + \sqrt{k_2^2 - 1})k_1 \delta} - e^{(-k_2 + \sqrt{k_2^2 - 1})k_1 \delta_2}] \qquad \ldots \quad (D.3)$$

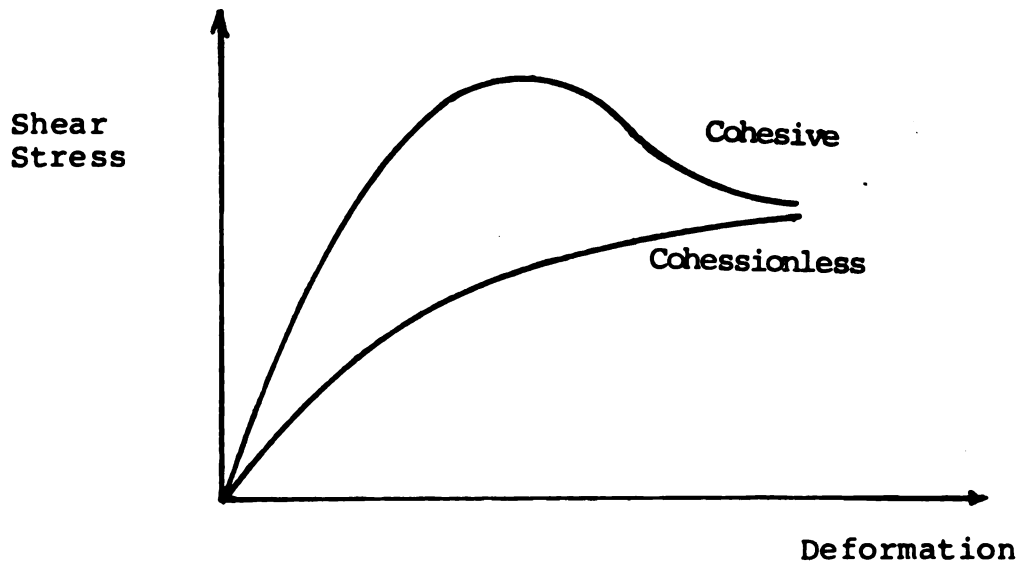

Figure D.1: Shear Deformation Diagram
(Bekker, 1956)

where:

τ = shear stress (kPa)

σ = mean ground pressure (kPa)

k_1, k_2 = soil parameters

Y_{max} = maximum value of the expression in brackets

δ = tire soil shear displacement

δ_2 = SX where S = slip,

X = distance from the point of first contact of the tire with the soil to the point under consideration

Other symbols have been defined previously.

Bekker's theories were further developed by Janosi and Hanamoto (1961). They recommended a simpler equation for

describing asymptotic shear curves by considering that in a majority of cases a numerical value for k_2 was difficult to establish when curves did not drop after reaching a maximum. Their equation was:

$$\tau = (C + \sigma \tan \phi)(1 - e^{-\delta/k}) \quad \ldots \quad (D.4)$$

where:

k = empirical soil parameter

All other variables are as previously defined.

For large deformations Equation 3.5 approached the Mohr-Coulomb equation (Equation D.1). The total tractive effort exhibited by a tire was obtained by integrating the shear stress along the ground contact area assuming constant tire width and uniform normal stress distribution:

$$H = (AC + W \tan \phi) [1 - 1/J (1-e)^{-J}] \quad \ldots (D.5)$$

where:

A = 2bl,

W = σA

J = Sl/k

b = tire contact width

l = tire contact length

All other variables are previously defined.

Bekker (1960) proposed the following equation for total motion resistance of a rubber tire.

$$MR = \frac{[3w/d^{0.5}]^{(2n+2)/(2n+1)}}{(3-n)^{(2n+2)/(2n+1)}} \cdot \frac{}{(n+1)^{1/(2n+1)}(R_c+bR_\phi)} \quad \ldots (D.6)$$

where:

MR = motion resistance

b = tire width

d = wheel diameter

R_c = cohesive modulus of soil deformation

R_ϕ = functional modulus of soil deformation

n = coefficient of wheel sinkage

W = wheel load

Further developing the plate approach Yong et al. (1984) divided motion resistance of a tire into three components.

a) motion resistance due to compaction of bearing subtrate material in the vertical direction,

b) motion resistance due to flexing of the tire and,

c) motion resistance due to bulldozing efforts in the horizontal direction.

Yong et al. (1984) suggested the following relationships for the sinkage (Z_o) and compaction-resistance (R_{cr}) of a rigid wheel:

$$Z_o = \left[\frac{3W}{bkd\ (3-n)}\right]^{2/2n+1} \quad \ldots (D.7)$$

$$R_{cr} = \frac{bk}{n+1}\,[Z_o]^{2n+1/2n+1} \quad \ldots (D.8)$$

Where all variables are as previously defined.

Utilizing passive earth pressure theories Yong et al. (1984) developed the following relationship for motion resistance due to bulldozing (R_b).

$$R_b = \frac{b \sin(\alpha+\phi)}{2 \sin\alpha \cos\phi}[2zck_c + \gamma z^2 k_\gamma] \quad \ldots \quad (D.9)$$

where:

$k_c = (N_c - \tan\phi)\cos^2\phi$

$k_\gamma = (\frac{2N_\gamma}{\tan\phi} + 1)\cos^2\phi$

$\alpha = \cos^{-1}(1 - 2z/d)$

z = sinkage

N_c, N_γ = bearing capacity factors

γ = unit weight of soil

c, ϕ = soil strength parameters (as in Equation D.3)

All other variables are as previously defined.

Motion resistance of a wheel due to flexing is a function of many factors such as: a) the number of plies, b) the thickness of the carcass, c) tread design, d) inflation pressure and e) wheel soil relative stiffness. The following relationship was suggested for motion resistance of a wheel due to flexing (R_f):

$$R_f = W f_t \quad \ldots \quad (D.10)$$

where:

$$f_t = \frac{u}{P_i^a}$$

u, a = empirical constants

P_i = tire inflation pressure

W = tire dynamic load

Janosi and Hanamoto (1961) reported that while motion resistance consists of several components, compaction has a dominating magnitude.

Yong and Webb (1969) utilized governing equations for the viscoplasticity method used in metal processing analysis to analyze soil deformation under a moving wheel. By this approach they were able to compute the rate of plastic work (rate of dissipation of deformation energy) without first determining stresses. Working with a rigid wheel they used the tire soil interface energy relationship in the equation for energy balance similar to Equation 3.1:

$$E_i = D_s + E_f + E_t + P_v \qquad \ldots \quad (D.11)$$

where:

E_i = rate of energy input = Tw

D_s = rate of soil deformation energy = Rv

E_f = rate of interfacial energy = (T/r) (wr - v)

E_t = rate of tire deformation energy = 0 for a rigid wheel

P_v = rate of useful energy = Pv

T = applied (axle) torque

w = rotational wheel velocity

r = rolling radius

v = translational velocity

P = drawbar pull

R = rate of energy loss to soil per unit of travel

$E_l = E_f + D_s$ = rate of energy loss in soil

Interfacial energy (E_f) is a measure of work done by frictional stresses at the wheel-soil interface.

$$E_f = \sum_{\text{Total Area of Contact}} \{ \text{Fractional Stresses} \times \text{Elemental Area} \times \text{Elemental Slip Velocity} \}$$

E_f equals zero in a completely adhesive soil-wheel interface where slip is absent. Frictional stress exists only at the points of contact where there is relative velocity. From Figure D.2:

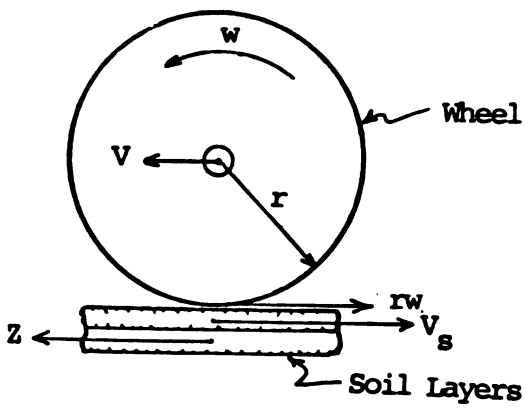

Figure D.2: Tire-Soil Interface Velocity Relationships

$$V_s = rw - V_{soil} \qquad ...(D.12)$$

where:

V_S = slip velocity = 0 for adhesive case

rw = tire peripheral velocity

V_{soil} = forward velocity (V) + instantaneous soil velocity (Z)

w = angular velocity

r = rolling radius

Points of contact where V_S is zero are zones of adhesion. In these zones shear stress changes sign. Z accounts for motion like that of a skidding tire.

Figure D.3 presented a graphical representation of the energy components described above. It was evident from Figure D.3 that after a certain critical slip rate of about 18 percent, interfacial energy dissipation increased rapidly. Below this value, total energy dissipated in the soil could be considered as energy lost to deforming the subsoil. As slip rate increased, interfacial energy loss increased and eventually surpassed energy lost in deformation of the subsoil.

Yong et al. (1980) tested five model tires in a soil bin to investigate the effects of wheel flexibility on the tire-soil performances. A sandy soil and a clay soil were used. Tire flexibility was governed by the various tire inflation pressures used. The results demonstrated that tire flexibility contributes significantly to the

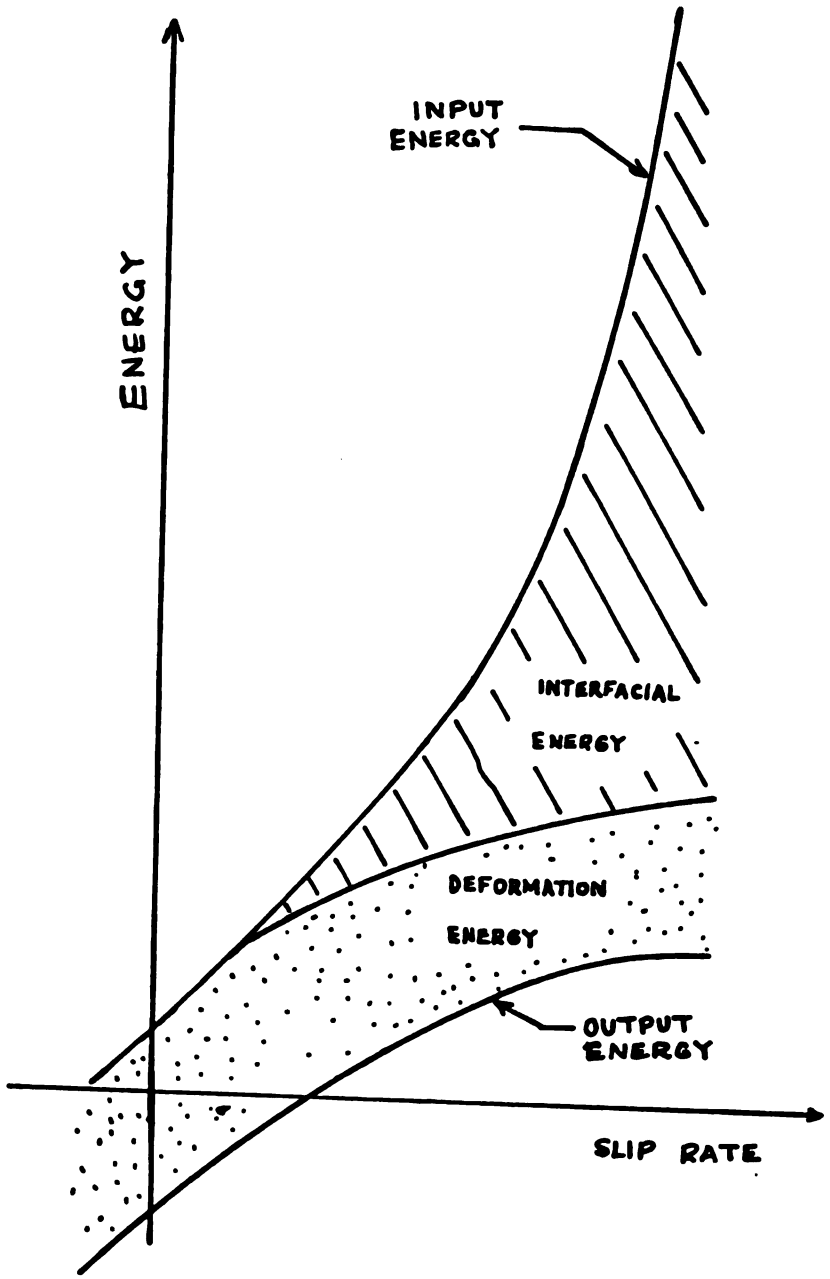

Figure D.3: Energy Balance for a Tire as a Function of Slip (Yong and Webb, 1969)

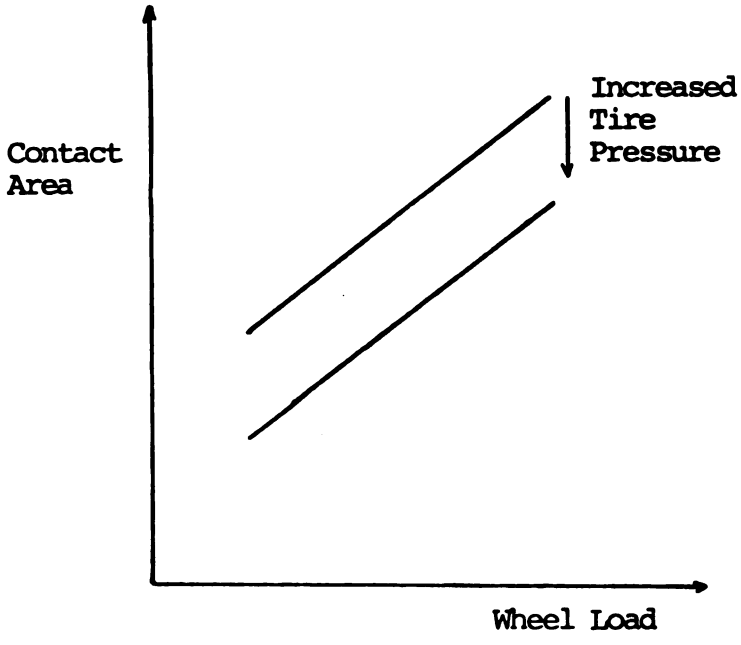

Figure D.4: The Influence of Wheel Load on Tire-Soil Contact Area on a Sandy Clay (Yong et al., 1980)

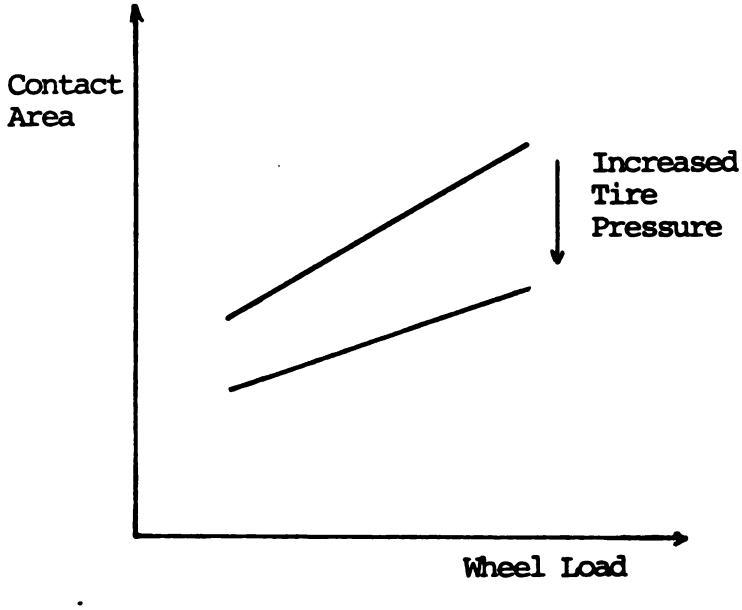

Figure D.5: The Influence of Wheel Load on Measured Tire-Soil Contact Area on a Kaolinite Clay (Yong et al., 1980)

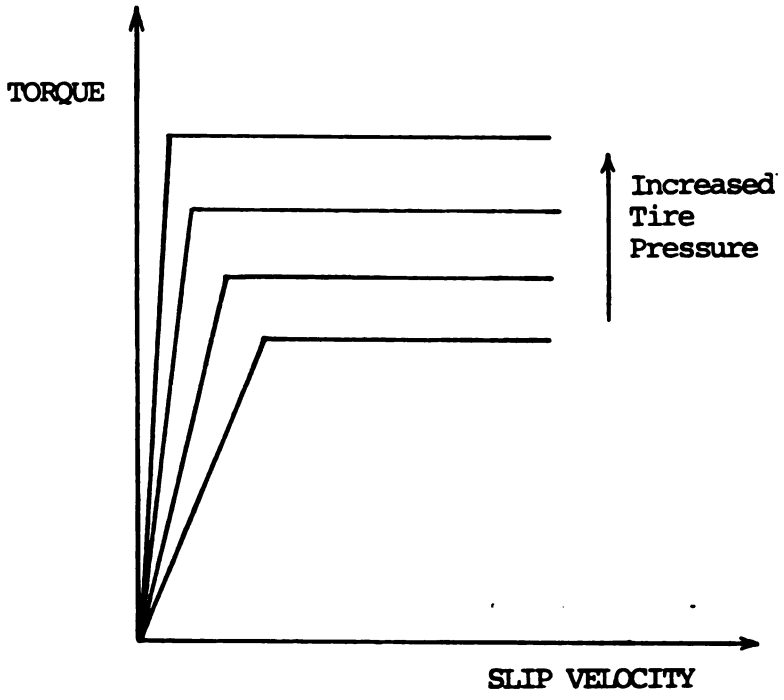

Figure D.6: Relationship between Wheel Torque and Slip Velocity for a Tire Moving on a Sandy Clay (Yong et al., 1980)

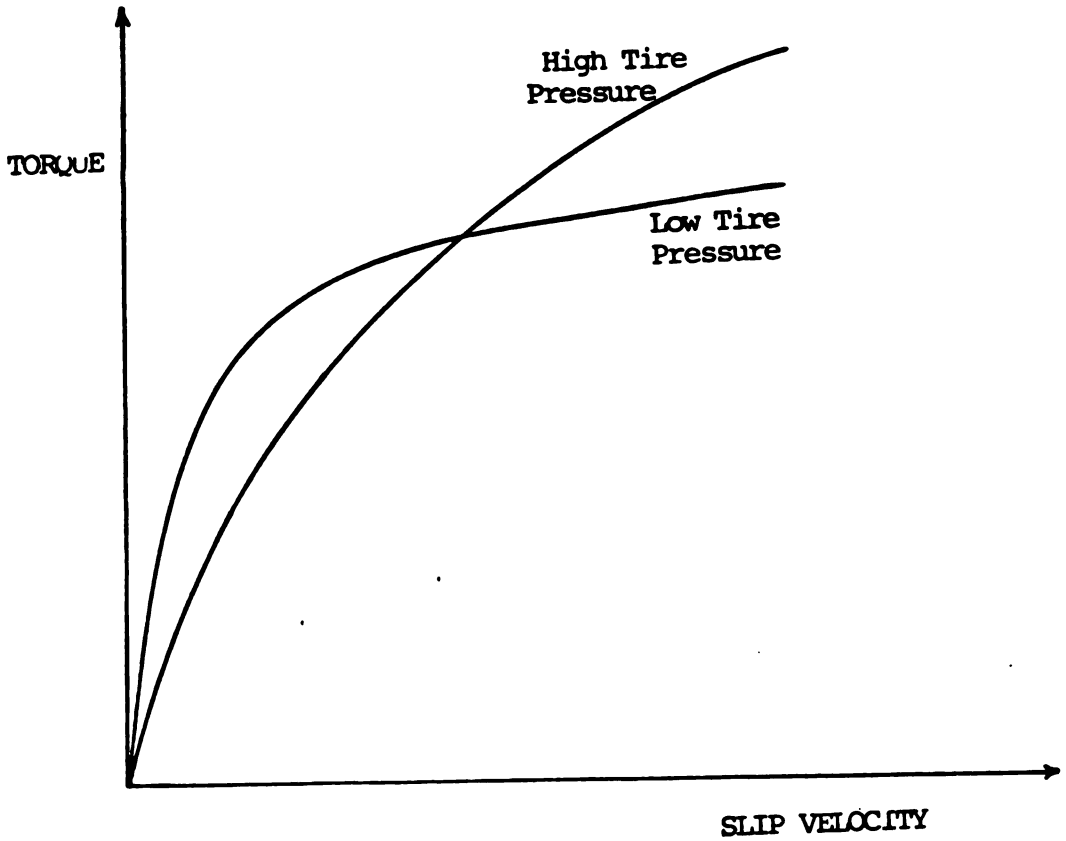

Fig D.7: Relation between Wheel Torque and Slip Velocity for a Tire Moving on Kaolinite Clay Soil (Yong et al., 1980)

development of all energy components in Equation D.11. Yong et al. used a finite element analysis to develop the following model for energy consumed in tire deformation.

$$E_t = \frac{B \sum_{i=1}^{n} P_i \, \delta_i \, V}{\alpha R} \qquad \ldots \quad (D.13)$$

where:

E_t = tire deformation energy lost

B = tire width

P_i = concentrated loading force at node i

δ_i = tire deformation at node i

All other variables are as previously defined.

Yong et al. (1980) presented the general relationships for tire-soil contact area and tangential stress characteristics shown on Figures D.4 through D.6. The major observations were: a) when a supporting soil was stiff, as in the case of a sandy clay, the changes in contact areas due to changes in inflation pressure were more significant (Figure D.4) and b) the torques and the tangential stresses were affected by slip velocity and tire flexibility (Figure D.6). An increase in normal stress also increased average shear stress more dramatically for the stiffer soil.

A comparison of energy balance diagrams for the sandy clay and kaolinite clay soil showed that an increase in inflation pressure led to an increase in useful output energy for sandy clay and reduced the useful output energy for kaolinite clay soil. This could be due to the fact that as the input energy was increased by higher inflation pressures on the sandy clay, combined tire and soil deformation did not change significantly. Although the tire deformation energy was decreased by increased inflation pressure, the soil deformation energy was changed slightly since the sandy clay provides higher resistances at higher confining pressures. This was due to increased normal

pressure at the tire-soil interface. The resultant effect was a net increase in drawbar pull for a higher inflation pressure in exchange for a higher required input energy. With the non-frictional kaolinite clay the useful output energy decreased with increased inflation pressure due mainly to the higher torque required at low inflation pressure (see Figure D.7), together with the lower combined tire and soil deformation energy. Increasing the inflation pressure decreased tire deformation energy and increased the soil deformation energy. This resulted in a higher average normal pressure imposed on the tire-soil interface described in Equation D.11.

BIBLIOGRAPHY

BIBLIOGRAPHY

ASAE 1982a. ASAE D230.3 Agricultural Machinery Management Data. Agricultural Engineers Yearbook. p. 213-220 ASAE St. Joseph MI.

ASAE 1982a. Agricultural Engineers Yearbook. ASAE Standard: ASAE S246.1 Liquid Ballast Table for Drive Tires for Agricultural Machines. pp. 188-189, ASAE St. Joseph MI.

Bailey, A.C., E. C. Burt and J. H. Taylor 1976. Thrust-Dynamic Weight Relationships of Rigid Wheels: II. The Effects of Soil and Wheel Interface. Trans of ASAE 19(1): 37-40.

Barger, E. L., J. B. Liljedahl, W. M. Carleton and E. G. Mckibben 1963. Tractors and Their Power Units. 2nd ed. John Wiley and Sons Inc. New York.

Bekker, M. G. 1969. Introduction to Terrain Vehicle Mechanics, University of Michigan Press, Ann Arbor MI.

Bekker, M. G. 1960. Off-The-Road Locomotion, Research and Development in Terramechanics. University of Michigan Press, Ann Arbor MI.

Binnewies, L., and H. Schwarz 1980. Improvement in Fuel Economy of SI Engines Using Electronic Control of Fuel Injection and Ignition ATZ (Automobiltechnische Zeitschrift) 82 (4): S 169-177.

Bloome, P. D., A. Khalilian, G. P. Riethmuller and D. G. Batchelder. Demonstrating the Effect of Ballast in Tractor/Implement Matching. ASAE Paper No. 82-1054, ASAE St. Joseph MI.

Bos, A. M. and P. C. Breedveld 1985. Update of Bond Graph Bibliography. Dept. of Electrical Engineering, Twente University of Technology. P.O. Box 217, 7500 A. E. Enschede, The Netherlands.

Bowers, C. G. 1986. Tillage Energy Requirements. ASAE Paper No. 86-1524, ASAE St. Joseph MI 49085-9659.

Browning, P. E. 1978. Design of Agricultural Tractor Transmission Elements. ASAE Distinguished Lecture Series. Tractor Design No. 4, ASAE Box 410 St. Joseph MI.

Buchele, W. F. 1962. Mechanics of a Vehicle Operating on a Yielding Soil. Paper Presented at the Society of Automotive Engineers. National Farm Construction and Industrial Machinery Meeting, Milwaukee Wisconsin, September 10-13, 1962.

Burt, E. C., A. C. Bailey, R. M Patterson and J. H. Taylor 1979. Combined Effects of Dynamic Load and Travel Reduction on Tire Performance. Transactions of ASAE 22(1): 40-44.

Burt, E. C., P. W. L. Lyne and J. F. Keen 1982. Ballast and Inflation Pressure Effects on Tractive Efficiency. ASAE Paper No. 82-1567, ASAE St. Joseph, MI.

Burt, E. C. and A. C. Bailey 1975. Thrust-Dynamic Weight Relationship of Rigid Wheels. TRANS of the ASAE 18(5): 811-813, 817.

B F Goodrich 1977. Power Saver Radial HT. Bulletin 5-1677-GT B F Goodrich Company Akron OH 44318.

Chancellor, W. J., and N. C. Thai 1984. Automatic Control of Tractor Transmission Ratio and Engine Speed. Transactions of ASAE 27(3): 642-644.

Chancellor, W. J. 1981. Substituting Information Energy in Agriculture. Transactions of the ASAE 24(4) 802-807, 813.

Clark, R. L. 1984. Tractor Performance in Two and Four Wheel Drive. Transactions of ASAE 8-11.

Clark, R. L. and G. V. Linde 1986. A Rapid Automatic Tractor Ballast System. ASAE Paper No. 85-1550, ASAE St. Joseph MI.

Clark, R. L. 1984. Tractive Modeling and Field Data Requirements to Predict Traction. ASAE Paper No. 84-1005, ASAE St. Joseph MI.

Clark, R. L. 1985. Tractive Modeling with the Modified Wismer Luth Model, ASAE Paper No. 85-1049, ASAE St. Joseph, MI.

Davis, D. C. 1973. Simulation and Model Verification of Agricultural Tractor Overturns. Ph. D. Thesis,

University Microfilm International, Ann Arbor MI 48106.

Dodd, R. B., D. Wolf, T. H. Garner, S. A. Hale and U. R. Pieper 1986. Preliminary Design and Testing of a Variable Geometry Three Point Hitch. ASAE Paper No. 86-1085, ASAE St. Joseph MI 49085.

Domier, K. W. 1971. Traction Characteristics of Two Wheel Drive, Four Wheel Drive and Crawler Tractors. Transactions of ASAE 14(3): 520-522.

Domier, K. W. and S. P. E. Persson 1968. Comparison of Predicted and Measured Drawbar Performance of Tractors on Agricultural Soils. Canadian Agricultural Engineering, Vol. 10. No. 1.

Dommel, H. K. and K. W. Race 1964. Design and Performance Characteristics of Four-Wheel Drive Tractors. Agricultural Engineering 45(8): 424-477, 429.

Finkin, E. 1968. The Consequencies of Spline Friction in Multiple Disc Brake and Clutch Packs. ASAE Transactions. Journal of Lubrication Technology 90(1)-65-71.

Franklin, G. F. and J. D. Powell 1981. Digital Control of Dynamic Systems. Addison Wesley Publishing Co. Reading Massachussetts.

Freitag, D. R. 1965. Dimensional Analysis of Performance of Pneumatic Tires on Soft Soils. Technical Report No. 3-688. U.S. Army Engineer Waterways Experiment Station, Vicks, Mississippi.

Gassman, M. P. 1978. Bond Graphs Applied to a Load Sensing Cylinder. Transactions of the ASAE 21(2), 267-270.

Gill, W. R. and G. E. Vanden Berg 1968. Soil Dynamics in Tillage and Traction USDA Agricultural Handbook No. 316. U.S. Government Printing Office, Washington D. C. 20402.

Goering, G. E. 1965. The Mechanics of Unspring Wheel Tractors Ph.D. Thesis. Iowa State University Library Ames IA.

Goering, G. E. and W. F. Buchele 1967. Computer Simulation of an Unspring Vehicle Part I, II Transactions of ASAE 10: 272-280.

Goyal, M. R. 1978. Simulation of a Turbocharged Diesel Engine to Predict the Transient Response ASAE Paper

No. 78-DPG-11. American Society of Mechanical Engineering NY.

Grecenko, A. 1968. Predicting the Performance of Wheel Tractors in Combination with Implements. Journal of Agricultural Engineering Research 13(1): 49-63.

Greenlee, J. G., J. D. Summers and K. P. Self. Effect of Velocity on Tractive Performance of Tractor Tires ASAE Paper No. 85-1539, ASAE St. Joseph MI.

Grogan, J., D. A. Morris, S. W. Searsy, H. T. Wideman and B. A. Stout 1983. Microcomputer Based Information Feedback System for Improving Tractor Efficiency. ASAE Paper No. 84-1594, ASAE St. Joseph MI 49085.

Hansen, A. C., A. J. Walker, P. W. L. Lyne and P. Meiring 1986. Power Demand Mapping of Tractor Operations. Transactions of the ASAE 29(3): 656-660.

Hausz, F. C. 1985. Traction Characteristics of Radial Tractor Tires. Proceedings Int. Conf. Soil Dyn. Auburn Alabama (4): 723-729.

Hrobat, D. and W. E. Tobler 1985. Bond Graph Modeling and Computer Simulation of Automotive Torque Converters. Journal of the Franklin Institute Vol. 319, No. 1/2 pp. 93-114.

Hudson, T. C., R. G. Diever and E. C. Dubbe 1973. Development of Simplified Equations of Simulation of Tractor Response to Dynamic Trailing Loads. Transactions of the ASAE 16(5): 862-865.

Jahns, G. 1983. A Method of Describing Diesel Engine Performance Maps. ASAE Paper No. NCR 83-103, ASAE St. Joseph, MI 49085

Jahns, G., K. J. Forester and M. A. Hellickson 1987. Mathematical Description of Diesel Engine Performance. ASAE Paper No. 87-1026, ASAE St. Joseph, MI 49085.

Jahns, G. and H. Stenkampf 1983. Tractor-Soil-Implement Computer Model for Tillage Operation. ASAE Paper NCR 83-502, ASAE St. Joseph, MI.

Janosi, Z. and B. Hanamoto 1961. The Analytical Determination of Drawbar Pull as a Function of Slip for Tracked Vehicles in Deformable Soils. Proc. 1st Conf. Terrain Vehicle Systems, Turin, Italy.

Karnopp, D. C. 1976. Bond Graphs for Vehicle Dynamics Vehicle System Dynamics Vol. 5, No. 33: 171-184.

Karnopp, D. C. and R. C. Rosenberg 1970. Application of Bond Graph Techniques to the Study of Vehicle Driveline Dynamics. Transactions ASAE J. Dynamic Syst. Measure. Control, Vol. 92, No. 2, pp. 355-362.

Kim, K. V. and D. L. Hoag 1981. Ride Simulation of Passive, Active and Semi-Active Seat Suspensions for Off-Road Vehicles. ASAE Paper No. 81-1540, ASAE St. Joseph MI.

Kepner, R. A., R. Bainer and E. L. Barger 1978. Principles of Farm Machinery, 3rd ed., AVI Publishing Co. Inc. Westport CT.

Kolozsi, Z. and T. T. McCarthy 1974. The Prediction of Tractor Field Performance. Journal of Agricultural Eng. Research 19: 167-172.

League, R. B. and J. S. Cundiff 1986. Bond Graph Model of a Hydraulic Test Standard ASAE Paper No. 86-1569, ASAE St. Joseph MI.

Leflaive, E. 1966. Mechanics of Wheels on Soft Soils, A Method for Presenting Test Results. Journal of Terramechanics, Vol. 3, No. 4, pp. 13-22.

Liljedahl, J. B., W. M. Carleton, P. K. Turnquist and D. W. Smith 1979. Tractors and Their Power Units, 3rd ed. John Wiley and Sons Inc. New York.

Lyne, P. W. L., E. C. Burt and P. Meiring 1982. Wheel Ballast for Improved Specific Fuel Consumption. ASAE Paper No. 82-1568, ASAE St. Joseph MI.

Lyne, P. W. L., E. C. Burt and P. Meiring 1984. Effect of Tire and Engine Parameters on Efficiency Transactions of ASAE 27(3): 5-7.

Margolis, D. L. 1978. Bond Graph Normal Modes and Vehicular Structures. Vehicle System Dynamics, Vol. 7, pp. 49-63.

Mathews, J. 1967. An Analogue Computer Investigation of the Potential Improvement in Tractor Ride Afforded by a Flexible Front Axle. Journal of Agricultural Engineering Research 12(1): 48-54.

McAulay, K. J., T. Wu, S. K. Chen, G. L. Borman, P. S. Myers and O. A. Uyehara 1965. Development and Evaluation of the Simulation of the Compression - Ignition Engine. SAE Paper No. 650451. SAE Warrendale PA 15096.

McKibben, E. C. 1927a. Kinematics and Dynamics of the Wheel Type Farm Tractor. V. Stability. Agricultural Engineering 8(5): 119-122.

McKibben, E. C. 1927b. Kinematics and Dynamics of the Wheel Type Farm Tractor. VI. Supporting Soil Reactions and Drawbar Pull. Agricultural Engineering 8(6): 155-160.

Meiring, P., A. G. Rennie, A. C. Hansen and P. W. L. Lyne 1987. Tractor Performance Improvements via Power Demand Mapping. ASAE Paper No. 87-1052, ASAE St. Joseph MI.

Meriam, J. L. 1971. Statics 2nd ed. John Wiley and Sons Inc. N. York.

Mueller, J. P. and Treanor R. R. 1985. Performance of a Four Wheel Drive Tractor Equipped with Radial Tires. ASAE Paper No. 85-1048. ASAE St. Joseph MI 49085.

N.T.T.L., 1977. Nebraska Tractor Test 1247 - International Harvester 1086 Diesel, Nebraska Tractor Testing Laboratory, Lincoln, NE 68583.

Osborne, L. E., 1971. A Field Comparison of the Performance of Two and Four Wheel Drive Track Laying Tractors. J. Agricultural Engineering Research 16(1): 46-61.

Pacey, D. A. and M. D. Schrock 1982. Modeling of Tractor Fuel Use. ASAE Paper No. 82-1521, ASAE St. Joseph, MI.

Pershing, R. L. 1966. Transient Motion of Tractors on Side Slopes. Unpublished Ph.D. Thesis, University Microfilms International, 300 N. Zeeb Road. Ann Arbor MI 48016.

Pershing, R. L. and R. R. Yoerger 1969. Simulation of Tractors for Transient Response ASAE Paper No. 68-641, ASAE St. Joseph MI 49085-9659.

Pitts, M. J. and C. E. Goering 1979. Modeling Soil Cone Index Changes Induced by Drive Wheel Traffic. ASAE Paper No. 79-1552. ASAE St. Joseph, MI 49085.

Raney, J. P., J. B. Liljedahl and R. Cohen 1961. The Dynamic Behavior of Farm Tractors. Transactions of the ASAE 4(2): 215-218, 221.

Rocard, Y. 1960. General Dynamics of Vibrations. Fredrick Ungar Publishing Co. New York, NY 10016.

Rosenberg, R. C. 1976. Bond Graphs for Dynamic system Simulation. Agricultural Engineering, Vol. 57, No. 9, pp. 28-29.

Rosenberg, R. C. 1972. Multiport Models in Mechanics Transactions of ASAE Journal of Dynamic Systems Mechanics and Control, Vol. 94: 206-212.

Rosenberg, R. C. 1986. Personal Communication.

Rosenberg, R. C. and D. C. Karnopp 1972. A Definition of Bond Graph Language. Journal of Dynamic Systems, Measurement and Control, Sept. 1972.

Rosenberg, R. C. and D. C. Karnopp 1983. Introduction to Physical System Dynamics. McGraw Hill Book Co. New York.

ROSENCODE Associate Inc. 1987. The ENPORT Reference Manual. ROSENCODE Associates Inc., Lansing MI 48906

Sack, H. W. 1955. Longitudinal Stability of Tractors. Agricultural Engineering 37(5): 328-333.

Shell, R. R., R. Fox and K. Moss 1986. Comparative Evaluation of FWDA to Two-Wheel Drive Tractors. ASAE Paper No. 86-1067, ASAE St. Joseph, MI 49085.

Smith, D. W., J. V. Perumpral and J. B. Liljedahl 1971. A Mathematical Model to Predict the Sideways Overturning Behavior of Farm Tractors. ASAE Paper No. 71-604, ASAE St. Joseph MI.

Smith, D. W. 1974. Variations in the Forward Motion of Farm Tractors. Ph.D. Thesis. University Microfilms International. Ann Arbor, MI.

Smith, D. W. 1977. Computer Simulation of Tractor Ride for Design Evaluation. SAE Paper No 770704, Society of Automotive Engineers Warrendale PA.

Smith, D. W. 1986. The Influence of fore-aft Center of Gravity Location on the Slope Performance of Two Wheel Drive Vehicles. ASAE Paper No. 86-1572.

Smith, D. W. and J. B. Liljedahl 1972. Simulation of Rearward Overturning of Farm Tractors. Transactions of ASAE 15(5): 818-821.

Smith, L. A., G. L. Barker and R. F. Colwick 1981. Instrumentation Used to Monitor Energy Requirements for Agricultural Field Operations. ASAE Paper No. 81-1043, ASAE St. Joseph, MI.

Steel, R. G. D. and J. H. Torrie 1980. Principles and Procedures of Statistics - A Biometric Approach, 2nd ed., McGraw Hill Book Co.

Stroppel, A. 1980. Energie-und Arbeitszeitbedarf fuer Gezogene Geraete der Bodenbearbeitung bei Unterschiedlichen Schleppermotorauslastung. Grundlagen der Landtechnik 30(4): 135-139 (Energy and Time Requirements for Tractor-Drawn Implements under Various Tractor-Implement Loads during Soil Tillage).

Summers, J. D. 1983. Performance Simulation of Two-Wheel Drive and Four-Wheel Drive Tractors. Unpublished Ph.D. Thesis, University Microfilms International, Ann Arbor MI 49085.

Summers, J. D., R. E. Ekstrom and K. V. Bargen 1986. Development of Tractor Performance Simulation Model. Transactions of the ASAE, Vol. 29(3): pp. 661-666.

Takahashi, T., Bekki E. and Takeda T. 1981. Considerations on Dynamic Behavior of Rotary-Tillers Attached to Tractors. Bulletin No. 35: 27-41.

Takahashi, T., H. F. E. Bekki and T. Takeda 1980. Simulation of Forward Motion of Four-Wheel Drive Tractors (Part 1) The Starting Behavior of Rear-Wheel Drive Tractors without Pull-Load. Bulletin NO. 34, Faculty of Agricultural Hirosaki University, Hirosaki 0036 Japan.

Taylor, J. H., E. C. Burt and A. C. Bailey 1976. Radial Tire Performance in Firm and Soft Soil. Transactions of the ASAE 19(6): 1062-1064.

Tembo, S., T. H. Burkhardt, R. H. Wilkinson, M. Hoki and T. Tanone 1986. Performance of the PTO Power Disk Tiller ASAE Paper No. 86-1010 ASAE St. Joseph, MI 49085-9659.

Tennant, J. A., R. A. Giacomazzi, J. D. Powell and H. S. Rao. 1979. Development and Validation of engine Models via Automated Dynamometer Tests. SAE Paper No. 790176.

Tsai, N. T. and S. M. Wang 1974. Delay bond-Graph Models for Geared Torsional Systems. transactions of ASAE Vol. 96: 366-370.

Upadhyaya, S. K., T. X. Ma, Y. M. Zhao and Chancellor 1985. Dynamics of Soil Tool Interaction ASAE Paper, No. 85-1035.

Wang, G. and G. C. Zoerb 1985. A Tractor Gear Selection Indicator ASAE Paper No. 85-1051. ASAE St. Joseph MI.

Whitehouse, N. D., A. Stotter, G. O. Goudie and B. W. Prentice 1962. Method of Predicting Some Aspects of Performance of a Diesel Engine Using a Digital Computer. Proceedings of the Institution of Mechanical Engineers 176(9): 195-217.

Wiedemann, H. T., S. M. Bandy and B. A. Stout 1986. Implement Power Requirements for Reduced Tillage. ASAE Paper No. 86-1588. ASAE St. Joseph, MI 49085.

William, S. D. 1974. Variations in Forward MOtion of Farm Tractors. Unpublished Ph.D. Dissertation, University Microfilms International, 300 N. Zoerb Ann Arbor MI 48106.

Williams, D. E. and N. L. Buck 1985. Low Load Fuel Consumption of Diesel Engines. ASAE Paper No. 85-1057, ASAE St. Joseph MI 49085.

Winterbone, D. E., C. Thiruarooran and P. E. Wellstead 1977. A Wholly Dynamic Model of a Turbocharged Diesel Engine for Transfer Function Evaluation. SAE Paper No. 770124, Society of Automotive Engineers, Warrendale, PA 15096.

Wismer, R. D. and H. J. Luth 1972. Off Road Traction Prediction for Wheeled Vehicles. ASAE Paper No. 72-619, ASAE St. Joseph MI.

Wismer, R. D. and H. J. Luth 1974. Off-Road Traction Prediction for Wheeled Vehicles. Transactions of the ASAE 17(1): 8-10, 14.

Woerman, G. R. and L. L. Bashford 1983. Performance of a Front-Wheel Assist Tractor. ASAE Paper No. 83-1560, ASAE St. Joseph, MI 49085.

Worthington, W. H. 1949a. Evaluations of Factors Affecting the Operating Stability of Wheel Tractors. Agricultural Engineering 30(3): 119-123.

Worthington, W. H. 1949b. Evaluations of Factors Affecting the Operating Stability of Wheel Tractors. Agricultural Engineering 30(4): 179-183.

Wulfsohn and S. K. Upadhyaya 1986. Tractive Characteristics of Radial Ply and Bias Ply tires, ASAE Paper No. 86-1057.

Yong, R. N., P. Boonsinsuk and E. A. Fattah 1980. Journal of Terramechanics, Vol. 17, No. 1. pp. 43-58.

Yong, R. N., E. A. Fattah and N. Skiadas 1984. Vehicle Traction Mechanics. Development in Agricultural Engineering, Vol. 3, Elsevier Science Publishing Co. New York.

Yong, R. N. and G. L. Webb 1969. Energy Dissipation and Drawbar Pull Prediction in Soil-Wheel Interaction. Proc. 3rd Int. Soc. in Terrain Vehicle Systems Essen, Vol. 1, pp. 93-142.

Young, R. E. and R. L. Schafer 1977. Autotraction: How Automation Can Improve Traction. Agricultural Engineering 58(2): 15-18.

Zhang, N., J. V. Perumpral and R. K. Byler 1985. Automatic Control System for Optimizing Diesel Engine Performance. Paper No. 85-1582 ASAE St. Joseph MI.

Zhang, N., J. V. Perumpral and R. K. Byler 1986. Diesel Engine Control Based on an ARMA Model. ASAE Paper No. 86-1622.

Zhang, N. and J. V. Perumpral 1987. Engine and Slip Control for Improving Tractor Operating Efficiency. ASAE Paper No. 87-1062. ASAE St. Joseph MI.

Zoz, F. M. 1972. Predicting Tractor Field Performance. Transactions of the ASAE 15(2): 249-255.

Zoz, F. M. and W. W. Brixius 1979. Traction Prediction for Agricultural Tractors on Concrete ASAE Paper No. 79-1046 ASAE St. Joseph MI.